Magnetic Vortices in Closely Packed Cap Structures

Dissertation

zur Erlangung des akademischen Grades

Dr. rer. nat.

eingereicht an der

Mathematisch-Naturwissenschaftlich-Technischen Fakultät

der Universität Augsburg

von

Dennis Nissen

Augsburg, Oktober 2016

Erstgutachter:	Prof. Dr. Manfred Albrecht
Zweitgutachter:	Prof. Dr. Jürgen Fassbender

Tag der mündlichen Prüfung: 29. November 2016

Wir müssen unbedingt Raum für Zweifel lassen,
sonst gibt es keinen Fortschritt, kein Dazulernen.
Man kann nichts Neues herausfinden,
wenn man nicht vorher eine Frage stellt.
Und um zu fragen, bedarf es des Zweifelns.

-RICHARD P. FEYNMAN-

Bibliographic record

Nissen, Dennis:

Magnetic Vortices in Closely Packed Cap Structures

Dissertation

Universität Augsburg, Mathematisch-Naturwissenschaftlich-Technische Fakultät (2016)

Abstract

The present thesis deals with the investigation of magnetic cap structures showing a vortex. For this, commercially available spheres (silica or polystyrene) have been ordered in a two-dimensional arrangement by self-assembly processes. By deposition of soft magnetic films on top of the spheres, we achieved large arrays of densely packed magnetic cap structures characterized by a magnetic vortex.

The first part of this thesis focuses on the investigation of permalloy cap structures, with a diameter of about 330 nm. Here, mainly the magnetization reversal of the structures in a two-dimensional lattice was investigated. In particular, we present the dependence of the nucleation and annihilation fields as a function of permalloy thickness and temperature. We show that a critical thickness is required to stabilize a magnetic vortex in the cap structures. Furthermore, we could show that an increase of the film thickness is accompanied by an onset of exchange coupling of the cap structures due to emergence of bridges connecting them, caused by closely packing of the underlying particles. Surprisingly, for the coupled structures we observed a domain like nucleation process of vortex structures with domains showing the same circulation sense. Additionally, increasing film thickness results in spatially enlarged vortex cores.

Furthermore, we also investigated the response of a vortex to an external field. In particular, we investigated the vortex core switching in a lattice of closely packed cap structures by a global out-of-plane field. Furthermore, we could also show that individual cores can be switched by a local field pulse using a scanning magnetoresistive microscope.

The second part of this work concentrates on the investigation of exchange biased magnetic vortices in cap structures. Therefore, in addition to a soft magnetic layer promoting the formation

of a vortex, an antiferromagnetic layer has been deposited on the caps. In this study, we mainly investigated the magnetization reversal as a function of temperature and cooling field. Overall, we could show that zero field cooling results in the stabilization of the vortex structure due to imprinting of the vortex spin structure into the antiferromagnet. For samples with CoO as antiferromagnet, we found a strong athermal training effect after field cooling. Furthermore, the magnetization reversal occurs via formation of a distorted viscous vortex. We also investigated the effect of the blocking temperature. In particular, for IrMn as antiferromagnet, we could show that approaching the Néel temperature results in an increase in coercivity.

CONTENTS

Contents ..... **vii**

1 Introduction **1**

2 Theoretical Background **5**

2.1 Magnetic energy contributions in permalloy 5

2.1.1 Exchange energy 5

2.1.2 Zeeman energy 6

2.1.3 Magnetic anisotropy energy 7

2.1.4 Magnetic stray field / dipolar energy 7

2.2 The magnetic vortex 9

2.2.1 Flux-closure domain pattern 9

2.2.2 Anatomy of a magnetic vortex 11

2.2.3 Transition from single domain to vortex state 12

2.2.4 Magnetic hysteresis curve 14

2.2.5 The Rigid Vortex Model 16

2.2.5.1 Core profile and diameter 16

2.2.5.2 Vortex displacement introduced by an external field 17

2.3 Exchange bias 19

3 Experimental Techniques 21

3.1 Sample preparation 21

3.1.1 Particle self-assembly 21

3.1.2 Film growth using magnetron sputtering 24

3.2 Sample characterization 26

3.2.1 Structural characterization 26

3.2.1.1 Investigations by electron microscopy 26

3.2.1.2 X-ray reflectometry (XRR) 28

3.2.2 Magnetic characterization 29

3.2.2.1 Superconducting Quantum Interference Device (SQUID) 29

3.2.2.2 Magneto-optical Kerr effect 31

3.2.2.3 Magnetic force microscopy 34

3.2.2.4 Full-field soft X-ray transmission microscopy 36

4 Magnetic Vortices in Py Cap Structures 39

4.1 Experimental details 41

4.2 Investigation of vortex cores in a two-dimensional lattice 43

4.3 Coupling of vortices in a two-dimensional lattice 49

4.4 MTXM study on Py cap arrays 60

4.5 Conclusion 63

5 Exchange-Biased Cap Structures 67

5.1 Reversal modes in EB vortex structures 69

5.2 Sample preparation 71

5.3 Py/CoO caps: Results and discussion 73
5.4 Fe/IrMn caps: Results and discussion 84
5.5 Conclusion 91

6 Summary 95

7 References 99

8 Publications 115

8.1 Papers 115
8.2 Presentations 117

Acknowledgment 119

1 INTRODUCTION

In the recent years, nanostructures have attracted huge interest in almost all areas of science and technology [1]–[3]. Thanks to the advances of the last years, it is possible to engineer nanostructures with a wide range of physical properties. This makes them a prominent candidate for future products in the field of materials, electronics or even medicine [4]. Overall, due to their unique properties, magnetic nanostructures are an integral part in many state-of-the-art technologies as well as emerging technologies such as in the field of spintronic devices, magnetic microelectromechanical systems, magnetic recording or applications in biomedicine [5]–[8].

In general, all systems strive to minimize their total free energy. In particular, in ferromagnetic (FM) materials the free energy is given by a combination of exchange energy, Zeeman energy, anisotropy energy, and stray field energy [9]. It appears that it is impossible to find a minimum for all energy terms at the same time. The system, therefore, favors a local minimum of the total energy leading to a metastable magnetic configuration (c.f. section 2.1). As a result, magnetic domains are formed to minimize the magnetostatic energy of a ferromagnetic system. In this regard, as the size of a magnetic structure is reduced to the nanometer scale a multi domain state becomes energetically unfavorable, and as a result, the nanomagnets exhibit a single domain or an incoherent magnetization configuration [10]. As an example, in Figure 1.1 a calculated phase diagram for permalloy (Py: $Ni_{81}Fe_{19}$) disks is presented, showing the dependence of the thickness and radius of a disk structure on the preferred domain state without (a) and with (b) uniaxial magnetic anisotropy [11]. As can be seen, the phase diagram reveals a strong dependence on the material parameters, but also on the structure geometry [12]–[16]. Furthermore, for so-called cap structures, formed by film deposition onto nanospheres, additionally to single domain and vortex states, the so-called onion states exist [17]–[19].

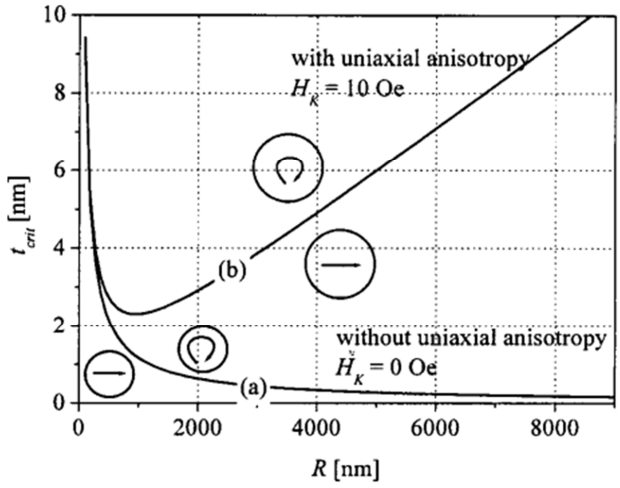

Figure 1.1: *Calculated phase diagram of permalloy disk structures showing the dependence of thickness and radius of a disk structure on the preferred domain state for (a) without and (b) with uniaxial anisotropy of permalloy. Taken from Hoffmann et al.* [11].

A particular domain configuration is the so-called magnetic vortex state favored in soft ferromagnetic disk or cap structures in the region between a single and a multi domain state. Here, due to the formation of a magnetic flux closure, in colloquial terms, the magnetization curls around and the magnetostatic energy is reduced to a minimum. In the center of the structure, the so-called core is formed due to exchange energy, favoring a parallel alignment of adjacent spins. Here, the magnetization is pointing out of plane and gives a contribution to the stray field. Thereby, in the vortex core the magnetization is pointing perpendicular to the vortex plane either *up* ($p = 1$) or *down* ($p = -1$) [20]–[22], whereas the sense of rotation can either be clockwise ($c = 1$) or counter clockwise ($c = -1$) [23]–[25]. Consequently, four different ground states of a magnetic vortex exist [26]–[28]. Furthermore, the product of polarity and sense of rotation is called chirality ($C = p * c$) or handedness of the magnetic vortex.

It has been reported recently that symmetry breaking can occur in the formation process of a magnetic vortex. This would be contrary to the previous assumption that a magnetic vortex has four different however degenerate ground states [26]. Im *et al.* have speculated that this effect might be a result of a so-called intrinsic Dzyaloshinskii - Moriya interaction, however, they also consider defects from the production process responsible for this effect [26].

Due to the individual properties, magnetic vortex structures have attracted much attention in

fundamental research in the recent years [29]–[33]. Thereby, amongst the static properties of vortex structures, dynamic properties have been studied. In particular, it has been shown that the dynamic properties of vortex structures strongly differ from flat films or even nanostructures with the same size revealing a single domain mainly due to the vortex core. In this regard, it has been shown that after excitation the magnetic vortex structures reveal a so-called gyrotropic mode arising from oscillations of the vortex core [34]–[36]. Furthermore, the magnetization reversal of the vortex core has been investigated in detail [37]–[40]. In this regard, it has been shown that the magnetization reversal can occur *e.g.* via formation of a so-called vortex-antivortex pair [41]–[43] or even via a Bloch point mediated process [44].

Additionally, the coupling of vortex structures has been investigated in detail [45]–[47]. Mainly, Landau patterns and disk structures consisting of two ferromagnetic layers separated by an interlayer have been studied [48]–[54]. In this regard, the influence of a variation of the interlayer on the exchange coupling is of particular interest. It has been shown that by changing the interlayer material and thickness, the coupling can be adjusted. In particular, for Cu as interlayer one can achieve a weak ferromagnetic, as well as a weak antiferromagnetic coupling of the vortex structures, which can be easily switched from one to another by an external field [53]. Whereas, for Ru and Rh one achieves a strong coupling of the in-plan flux direction. This coupling can be varied between antiferromagnetic and ferromagnetic by changing the interlayer thickness [53]. Additionally, the coupling of a soft magnetic layer preferring a magnetic vortex as ground state to a layer revealing a perpendicular anisotropy has been studied [55]–[57]. It has been shown that in this way it is possible to control the core polarization. Beyond, by tuning the interlayer coupling, the spin structure of the soft magnetic layer can be adjusted. For example, a vortex structure, donut type structures with various skyrmion numbers or even spiral configurations can be achieved in the soft magnetic layer.

Magnetic vortices start to find applications in various fields including data storage in a vortex based random-access memory device [27], [58], frequency-controlled magnetic vortex memory [59], as magnetic field sensor due to its hysteresis free part [60], for spintronic [37], ultra-fast circuits [61] or even biomedical applications [62]–[64].

However, typically, magnetic vortex states are stabilized in disk-shaped magnetic nanostructures fabricated by lithographic techniques [65]. Unfortunately, such top-down methods are slow,

expensive and therefore, uneconomical for large production figures. On the contrary, nanostructure fabrication by bottom-up approaches offers significant advantages and unique properties [66]. In particular, one of the approaches focuses on the manufacturing of large arrays of spherical particle monolayers by self-assembly processes acting as underlayer for further film depositions. In this way, it is possible to obtain magnetic cap structures on the particle monolayers forming vortex states by deposition of soft magnetic films on top. However, for a possible usage of cap structures, a fundamental understanding is strongly required.

The first part of this work is focused on cap structures with a diameter of about 330 nm in a two-dimensional lattice formed by permalloy film deposition onto large arrays of self-assembled densely packed spherical particles. In particular, the film thickness dependence, as well as the temperature influence on the vortex state are investigated. In this study, special attention is paid on the variation of the characteristic nucleation and annihilation fields of the vortex. Furthermore, also the possibility to influence the vortex core by an external magnetic field is investigated.

The remainder of this thesis focuses on the investigation of magnetic cap structures, showing a vortex, coupled to an antiferromagnetic layer. In particular, it is showed that by field cooling an exchange bias effect can be induced. This has been analyzed as a function of temperature, cooling field, and number of field cycles. In this study, particular attention was paid to the reversal mechanism of the cap structures.

2 THEORETICAL BACKGROUND

In this chapter, a brief summary of the theoretical background is given to understand the formation and behavior of magnetic cap structures referring to [9]. However, a more detailed overview of the basics in magnetism can be found in [67]–[70].

2.1 Magnetic energy contributions in permalloy

In general, systems strive to minimize their total free energy. In particular, the free energy of a magnetic material is divided into the exchange energy, Zeeman energy, anisotropy energy, and the stray field energy. However, it appears that it is impossible to find a minimum for all energy terms at the same time [9]. The system, therefore, favors a local minimum of the total energy leading to a stable magnetic configuration. Therefore, it is important to know how the various energy terms are contributing to this energy. In this section, the energy terms mentioned above are briefly introduced.

2.1.1 Exchange energy

Exchange interaction is a quantum mechanical phenomenon, describing the long-range magnetic ordering in magnetic materials, enabling ferromagnetism, antiferromagnetism, and ferrimagnetism. The exchange energy associated with this interaction can be written as:

$$E_{ex} = -2\, J_{12}\, \boldsymbol{S}_1 \boldsymbol{S}_2$$

In this equation, J denotes the so-called quantum mechanical exchange integral, and $\boldsymbol{S}_1$, $\boldsymbol{S}_2$ the directions of two neighboring spins. For J positive a parallel alignment of neighboring spins is favored (ferromagnetic material), while J negative favors an antiparallel alignment of the spins (antiferromagnetic-, ferrimagnet-material) [9], [71]. Hence, the exchange energy in ferromagnetic systems strives to align homogeneously the magnetization along a certain direction for energy minimization [72], [73].

Moreover, for a system with localized spins the exchange interaction can be expressed by the *Heisenberg model:*

$$E_{ex} = -2 \sum_{i<j} J_{ij}\, \boldsymbol{S}_1 \boldsymbol{S}_2$$

In this equation, the restriction $i < j$ in the sum avoids double counting of spins. However, by replacing the spins with the local magnetization M, it is possible to simplify the formula. Furthermore, the sum over all spins can be superseded by an integral over the sample volume and, therefore, the exchange energy can be written as:

$$E_{ex} = A \int_V (\nabla \boldsymbol{M})^2 dV$$

In this formula, A is the material specific exchange constant, which is directly related to the exchange integral J. For Py, which is mainly used in this thesis, A is about $1.3 * 10^{-11}$ *J/m* [74].

2.1.2 Zeeman energy

In an external field H_{ext}, the magnetic moments of a sample tend to align along the field to minimize the *Zeeman energy*. In total, the *Zeeman energy* is given by the equation [75]:

$$E_Z = \int_V H_{ext} * M(r) dV$$

2.1.3 Magnetic anisotropy energy

Magnetic anisotropy describes the occurrence of a preferred direction of the magnetization along the so-called magnetic easy-axis in magnetic materials. Its physical origin is the dipolar as well as the spin-orbit coupling. Hence, the so-called anisotropy energy is defined as the work required to switch the magnetization out of its preferred easy axis. By aligning the magnetization along the easy axis, the anisotropy energy can be minimized. However, as shown in chapter 5.2, the investigated Py structures grow polycrystalline and, therefore, any existing crystal anisotropy cancels out in average by the differently oriented crystallites.

2.1.4 Magnetic stray field / dipolar energy

Additionally to the interaction of the magnetic moments of a sample with an external field causing the *Zeeman energy* (mentioned above), there is an additional interaction of the magnetic moments in a specimen. The magnetic moments of a sample also interact via a dipolar field created by their adjacent moments. The sum over all dipolar fields in a sample is generally called the stray field H_S of the sample. Inside the sample, the so-called stray field is orientated opposite to the internal magnetization of the sample and, therefore, known as demagnetization field. In this regard, it should be noted that the stray field energy shows a strong dependency on the shape and volume of the magnetic sample. For example, the stray field of a sample can be significantly increased by changing the magnetization from in-plane to out-of-plane. In total the magnetic flux is given by the equation:

$$\boldsymbol{B} = \mu_0(\boldsymbol{H_S} + \boldsymbol{M})$$

However, from the *Maxwell equations,* in particular, *Gauss's law* it is possible to decompose the equation to:

$$\nabla \boldsymbol{H_S} = \nabla \boldsymbol{M}$$

With *Ampère's law* $(\nabla \times \boldsymbol{H_S} = 0)$ it is possible to convert the equation into a Poisson equation, and by solving it to calculate the stray field energy of a magnetic sample [9]:

$$E_S = -\frac{1}{2}\mu_0 \int_V \boldsymbol{H}_s(r)\boldsymbol{M}(r)dV$$

From here, the demagnetizing field energy can be calculated by an integral over the sample volume. This equation can be further simplified with the assumption that the stray field acts as an external field on the specimen. Therefore, the stray field energy of a magnetic sample can be calculated by integrating over the whole volume of the system [9]:

$$E_S = \int \boldsymbol{H}_s(r)^2 dV$$

2.2 The magnetic vortex

In the following, a description of the magnetic vortex will be given. Therefore, mainly the mechanism leading to the vortex formation, anatomy of a magnetic vortex, characteristic hysteresis curve, and the rigid vortex model will be discussed.

2.2.1 Flux-closure domain pattern

In ferromagnetic materials, neighboring magnetic moments are aligned parallel. However, measurements indicate an unexpected low total magnetic moment. This effect can be explained by the idea of Weiss *et al.* that in ferromagnetic materials, the magnetization distribution is broken into uniformly magnetized domains [9], also called *Weisssche Bezirke* named after the physicist Pierre-Ernest Weiss. Additionally, the magnetization vectors of neighboring domains are pointing in different directions and consequently, their magnetizations add up, on average, to zero. These domains are separated by domain walls in which the magnetization direction rotates from one direction to the other one. Their dimension is predicted by the so-called exchange length $l_{ex} = \sqrt{A/K}$. In this equation, A denotes the exchange stiffness constant, and K the magnetic anisotropy. The domain walls are mainly divided into Bloch, respectively Néel walls, besides many other kinds of domain walls exist. However, the Bloch (90°) and Néel (180°) walls differ in the rotation of the magnetization. Bloch walls are often present in thick magnetic layers. In this case, the magnetization is always parallel orientated to the wall plane and rotates helically [76]. In contrast, Néel walls are predominant in thin magnetic layers. In this case, the magnetization rotation is within the plane of the domain wall [77].

Moreover, by the formation of domains with a nearly closed magnetization flux the total energy can be further minimized. A typical example of such a configuration is the *Landau pattern*, also known as *Kittel square*. In particular, these domains are generated in such a way that a closed flux minimizes the stray field of the sample [78], [79]. In Figure 2.1 some typical flux closed domains are presented. In (a), a *Landau pattern* stabilized in a 50 nm thick Py square with equal sides of 3 µm is shown. The image has been taken by a scanning transition X-ray microscopy at the Ni L_3

edge (taken from Wohlhüter *et al.* [56]). The arrows indicate the direction of the local magnetization. Whereas, in (b) a simulation of a magnetic vortex stabilized in a cap structure is depicted, being probably the simplest flux-closure domain structure. Again, the arrows represent the magnetic configuration, whereas the colors additionally support the indication of the in-plane magnetization. In the center of the vortex, the magnetization is pointing *up* or *down*, forming the vortex core.

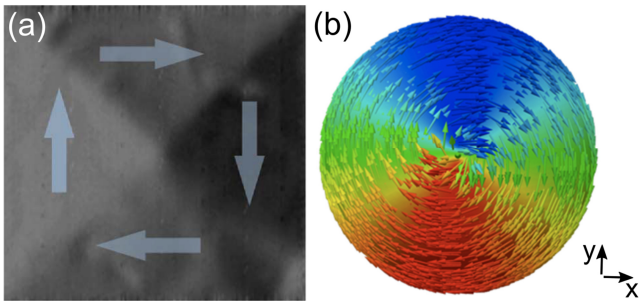

***Figure 2.1**: Examples of in-plane flux closure domain configurations. In (a) a picture of a Landau pattern of a Py square with a thickness of about 50 nm is shown, recorded at the Ni L_3 edge by scanning transition X-ray microscopy from Wohlhüter et al.* [56]. *In (b) a simulation of the spin structure (magnetic vortex) in a Py cap is presented. In both figures the arrows denote the direction of the local magnetization, in (b) red and blue represent the in-plane component of the magnetization (M_x).*

2.2.2 Anatomy of a magnetic vortex

As already mentioned, the magnetic vortex represents a simple domain configuration. It consists of a circularly symmetric in-plane magnetization distribution, which can rotate clockwise or counterclockwise, and a core in the center, which can point *up*, respectively *down*. In the following, the anatomy of a magnetic vortex will be briefly presented. In Figure 2.2 (a) a simplified scheme of a magnetic vortex state taken from N. Martin *et al.* [80] is shown. In this figure, the arrows indicate the main magnetic configuration, known as the in-plane curling magnetization, whereas, the color code indicates the z-component (out-of-plane component) of the magnetization, which can be found in the center region, revealing the magnetic vortex core. It originates from the fact that adjacent spins do not favor an antiparallel alignment and, therefore, the magnetization in the center is pushed out-of-plane. Here it should be noted that the first time a vortex core was confirmed experimentally was in 2000 by Shinjio *et al.* [22] using magnetic force microscopy (MFM). This is especially interesting due to the fact that magnetization distribution for the magnetic vortex was predicted by theorists long time ago [81], [82]. However, analytical calculations of the spin structure in Co and Py disk predicted that in a magnetic vortex besides to the core a second region exists where the spins are not perfectly aligned in the in-plane direction. In particular, close to the central region where the core is located, the spins are also readily turned out-of-plane, but in the opposite direction to the core [83], [84]. This region is commonly referred as *Sombrero dip*. In Figure 2.2 (b) the calculated out-of-plane magnetization component M_Z across a disk is shown taken from Guslienko *et al.* [83], [85]. Utilizing high-resolution spin-polarized scanning tunneling microscopy, it was possible to resolve the internal structure of a vortex core and experimentally prove the *Sombrero dip* [21]. In Figure 2.2 (c) the calculated (dots) and measured (gray lines) out-of-plane magnetization component M_z close to a vortex core are presented (taken from [21]).

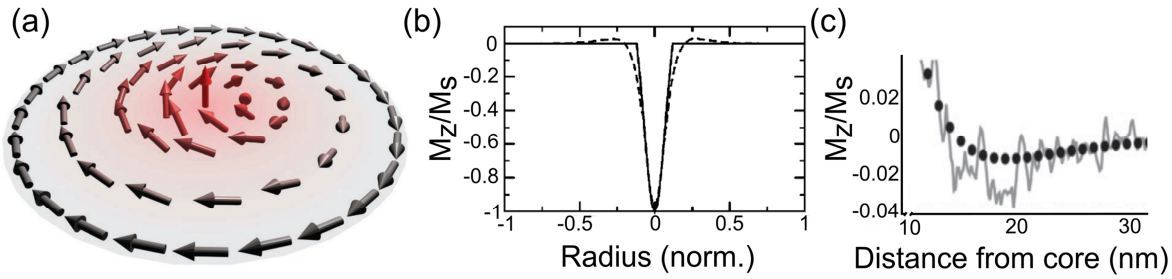

Figure 2.2: *Vortex state in a Py disk. In (a) a simplified scheme of the spin configuration of a magnetic vortex state taken from N. Martin et al.* [80] *is shown. The arrows indicate the magnetic configuration, whereas the colors act as a better illustration of the out-of-plane magnetization* M_Z *in the core. In (b) the profile of* M_Z *through the center of the disk is shown. The solid line represents the simplified rigid vortex model whereas the dashed line represents a more realistic vortex model based on finite element approximation, which also describe the effect of a readily turn of the out-of-plane magnetization close to the core (taken from* [83], [85]*). In (c) experimental determination of the out-of-plane magnetization component* M_Z *close to the vortex core is presented (from* [21]*).*

2.2.3 Transition from single domain to vortex state

In general, systems strive to minimize the total free energy. As discussed before, the free energy of a ferromagnetic material can be divided into various energy terms, and it appears that it is impossible to find a minimum for all energies at the same time. Especially for magnetic systems, a local minimum of the total energy is represented by a certain magnetization configuration. In this regard, it has been shown that ferromagnetic materials commonly form domain structures to reduce their magnetostatic energy [9].

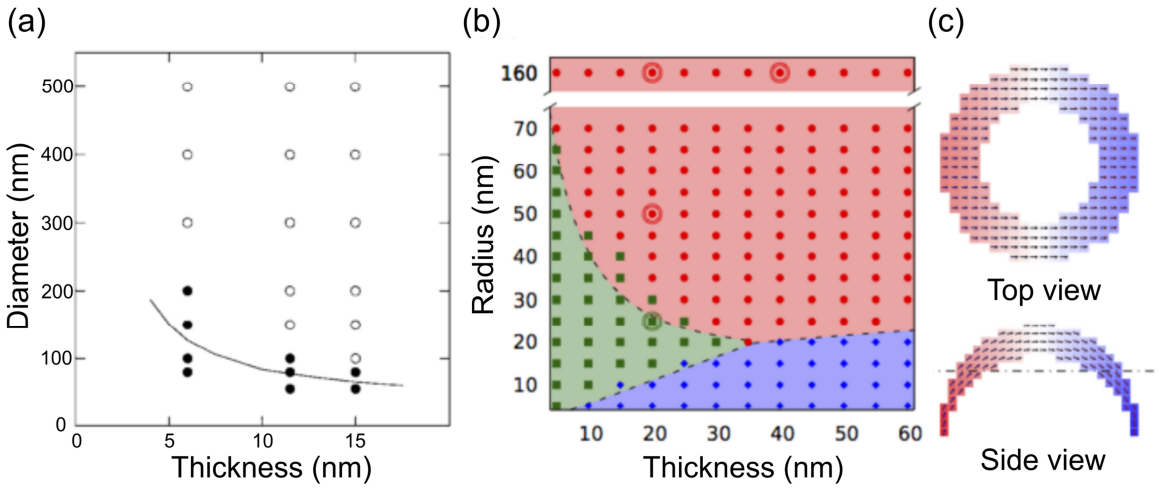

Figure 2.3: *Phase diagram of magnetic nano structures. In (a) an experimentally determined phase diagram of Py disks is shown. The circles indicate structures showing a vortex, whereas the dots represent disks in a single domain state (taken from* [86]*). In (b) a calculated phase diagram of Py caps is shown (blue - homogeneously magnetized state, green - onion state, and red - vortex state). A detailed view of the onion state is shown in (c). A top view and cross section of a Py cap with a radius of 30 nm and a thickness of 10 nm are depicted ((b) and (c) taken from* [17]*).*

However, in small soft ferromagnetic systems in the region between the multi domain and the single domain state a magnetic vortex is energetically favored. Through the formation of a circular magnetic structure, the magnetostatic energy is reduced to a minimum. In this way, only the vortex core provides a contribution to the stray field. Even though the exchange energy is increased due to the formation of a magnetic vortex, which is unfavorable, the vortex structure is stable because the total energy decreases. In Figure 2.3 typical phase diagrams of Py disks and cap structures are shown. In particular, they show the dependence of the magnetic domain state as a function of thickness and diameter. However, most works found in literature investigating the domain state of confined structures showing a magnetic vortex have been performed on disk structures in the micrometer range. Therefore, in (a) an experimentally determined phase diagram of small disk structures is presented (taken from Cowburn *et al.* [86]). In this figure, the solid dots indicate disks in a single domain state, whereas the open circles label disks revealing a magnetic vortex. The solid line indicates the theoretically predicted phase boundary between a magnetic vortex and a single domain state. It should be mentioned that the phase diagram can also strongly vary by changing the geometry of the microstructure. As an example, the phase diagram of a

magnetic cap structure shows significant changes [17]. In contrast to classical disk structures, besides a single domain state and a vortex state also the onion state can be formed. In this state the magnetization follows the curvature of the top surface but no perfect flux closure occurs. Furthermore, the characteristic annihilation and nucleation fields differ strongly between disk and cap structures. As an example, in Figure 2.3 (b) a phase diagram of a magnetic cap structure with the three ground states is shown (taken from Streubel *et al.* [17]). In this phase diagram, the blue region indicates the homogeneously magnetized state (single domain). In the green region the onion state is favored, whereas, in the red area the cap structures show a magnetic vortex state. For a better illustration of the *onion state*, in Figure 2.3 (c) a top view and a cross section of the magnetization configuration of a cap with a thickness of 10 nm and a radius of 30 nm are shown (also taken from [17]).

2.2.4 Magnetic hysteresis curve

The relationship between the strength of an externally applied magnetic field and the magnetization of a magnetic material is expressed in a hysteresis curve. However, there are considerable variations in the hysteresis curve, resulting from different magnetic properties, as well as of a structural nature *e.g.* for nanostructured materials. Figure 2.4 shows an example of a MOKE hysteresis loop of an array of closely packed Py caps with a thickness of 60 nm and a cap diameter of 330 nm. Please note that focusing optics were employed to reduce the diameter of the used laser beam spot to about 3 μm on the sample. Nevertheless, the signal is averaged over about 100 Py caps. As can be seen, the magnetization reversal occurs via nucleation and annihilation of a magnetic vortex, as characterized by the nucleation field H_{nu} and annihilation field H_{an}.

The internal spin configurations in an individual cap structure during the magnetization reversal under the applied in-plane magnetic field are sketched along the hysteresis curve based on the rigid vortex model, which will be introduced later. Considering the hysteresis curve in detail, the loop is starting from a single domain state in negative saturation field, followed by a vortex state in zero field, and the shifted vortex state in the positive field of about 150 Oe. In the final state the vortex switches back to a single domain state in a large positive field.

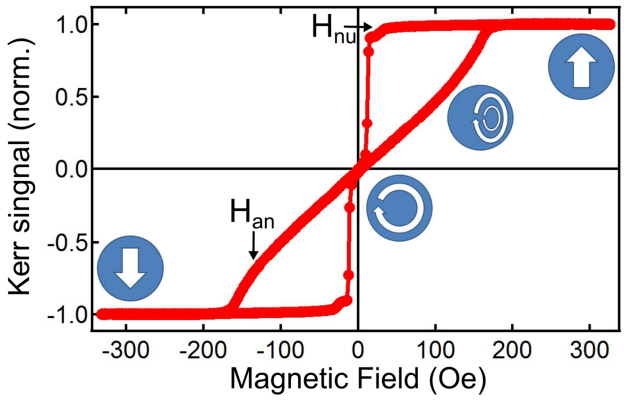

Figure 2.4: *MOKE hysteresis loop of Py caps with a thickness of 60 nm and diameter of 330 nm. The used layer stack is Ta(5 nm)/Py(60 nm)/Ta(2 nm)/silica-particles. For a better indication, the magnetic configurations along the hysteresis loop as well as the nucleation and annihilation fields are marked.*

2.2.5 The Rigid Vortex Model

An easy model that describes a vortex in which an external field does not influence the vortex shape is the so-called rigid vortex model (RVM). In the following section, a short analytical description of the core profile using the RVM, as well as the magnetization reversal in an external field will be given.

2.2.5.1 Core profile and diameter

A model for the analytical description of the magnetization distribution in a cylindrical structure in zero field was given by Usov and co-workers in 1993 [81]. In Figure 2.5 a simplified sketch of a magnetic disk with a thickness *L*, radius *R*, and core radius *a* is presented.

The magnetization at a point $r < a$ (inside the core) can be described in polar coordinates:

$$M_x = \frac{2ar}{a^2 + r^2}\sin(\Phi)$$

$$M_y = \frac{2ar}{a^2 + r^2}\cos(\Phi)$$

$$M_z = \sqrt{1 - \frac{2ar}{a^2 + r^2}}$$

On the other hand, the magnetization outside the core ($R \geq r > a$) is given by:

$$M_x = -\sin(\Phi)$$

$$M_y = -\cos(\Phi)$$

$$M_z = 0$$

By introducing the exchange length l_{ex}, the ratio $g = L/R$, and the numerical constant κ it is possible to specify an equation for the radius a of the core:

$$a = \left(\frac{l_{ex}^2 R}{12\kappa \frac{L}{R}} \right)^{\frac{1}{3}}$$

It should be noted that magnetic caps show a similar behavior as magnetic cylinders and therefore also the RVM can be applied.

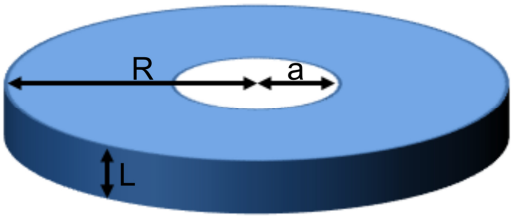

Figure 2.5: *Layout of a magnetic disk. In the sketch the characteristic dimensions of the disk, the core-radius a, disk radius R, as well as the thicknesses L are marked.*

2.2.5.2 Vortex displacement introduced by an external field

As mentioned above, the magnetization variation of a magnetic disk showing a vortex by applying an in-plane field and, particularly, the position of a magnetic vortex can be qualitatively described by the RVM. As depicted in Figure 2.6 (a) in remanence, the vortex is placed in the center of the structure. However, by applying small magnetic in-plane fields the magnetic vortex is shifted perpendicular to the field direction, as presented in Figure 2.6 (b). It should be noted that in this model, the vortex magnetization distribution is unaffected by an external field, as the name rigid implies.

Therefore, the changes in the magnetization just arise from the shift of the magnetization distribution with respect to the disk boundary serving as a limit. However, with increasing field, the center of the vortex is shifted to the boundary until the characteristic annihilation field is reached, as depicted in Figure 2.6 (c). By further increasing the field, the vortex annihilates and an in-plane saturated state can be found in the structure. In Figure 2.6 (d) a sketch of such a saturated

state is shown, it can be conceived as a vortex at infinite distance. By reduction of the external field after saturation, a vortex will start to nucleate and the reversed process occurs.

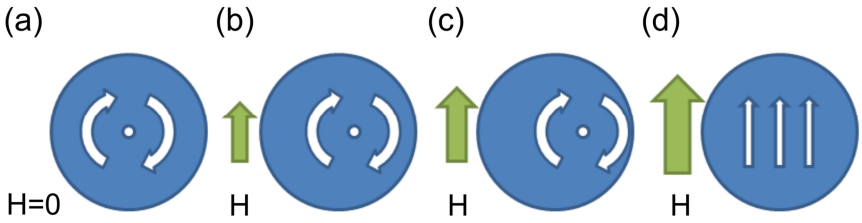

Figure 2.6: *Effect of an in-plane field on a magnetic vortex described by the RVM. In (a) the centered vortex in remanence is shown. It can clearly be seen in (b) that an increase of the field correlates with a displacement of the vortex perpendicular to the field. By further increasing the field, the center is pushed to the edge of the structure until the magnetization is close to vortex annihilation shown in (c). The saturated state is shown in (d); this configuration can be explained by a vortex with an infinite distance to the structure.*

2.3 Exchange bias

Spontaneous magnetic order not only appears for FM or ferrimagnetic (FI) materials, it is also known for anti-ferromagnetic (AF) materials. In contrast to FM materials, in an AF the individual magnetic moments are aligned antiparallel, and the total magnetization cancels out. The critical temperature at which the AF loses their order is known as Néel temperature (T_N). By bringing together an AF below T_N and a FM, the AF will influence the behavior of the FM resulting in the so-called exchange bias (EB) effect. Additionally, for an AF a blocking temperature exists defined as the temperature where the AF loses the ability to pin the FM. Classically, the EB effect has been known as a unidirectional anisotropy, arising from the coupling between a ferromagnet and antiferromagnet. It was first discovered by Meiklejohn and Bean in 1956 for a CoO/Co nanoparticle system [87] and has been widely studied in various FM/AF bilayers [88], [89].

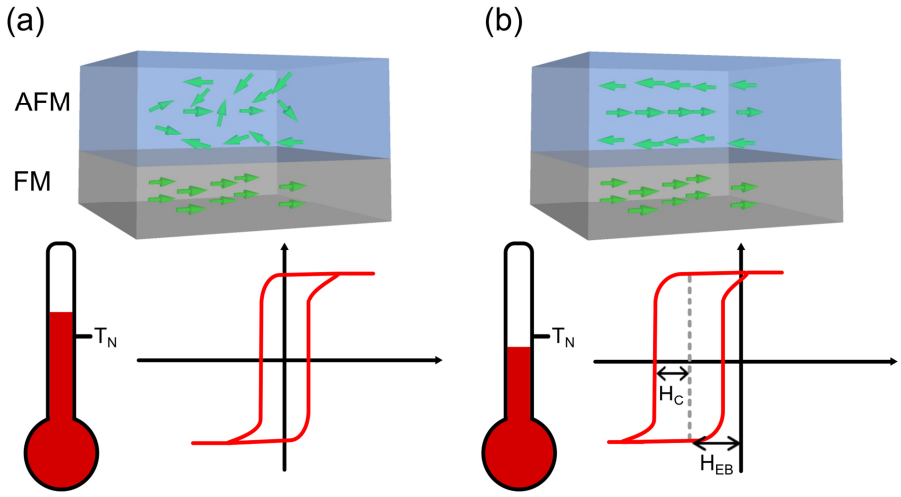

Figure 2.7: *Schematic picture of the exchange bias effect in an AF/FM bilayer after field cooling. In (a) the system is above the Néel temperature of the AF and below the Curie temperature of the FM, consequently only the FM order can be found. This configuration results in a symmetric hysteresis curve. By field cooling below the Néel temperature, strong interfacial exchange coupling is introduced, leading to an unidirectional anisotropy in the FM* [95]. *As a result, we observe a loop shift by H_{EB} and typically an increase in coercivity H_C.*

Today, however, the EB effect is also observed in different systems, *e.g.* in nanostructures [90], or even for FM/FI, and FI/FI bilayer systems, which can also exhibit an unidirectional exchange anisotropy [91]–[94]. The classical exchange bias effect, which occurs in FM/AF bilayers systems has attracted much attention due to its various industrial applications in the field of data storage [96]–[98], or sensor applications [99], [100]. It appears after field cooling, more precisely if an external magnetic field is applied in addition to the exchange field produced by the magnetic moments of the FM and the system is cooled below the Néel temperature of the AF. A sketch of an FM/AF pair above the Néel temperature (a) and after the field cooling procedure (b) is given in Figure 2.7. However, the EB effect can actively alter the magnetic behavior of the contributing layer in different ways. The most common characteristics are the shift and broadening of the hysteresis curve, as depicted in Figure 2.7, whereby, in this case, the loop shift is opposite to the cooling field (negative EB effect).

Another characteristic phenomenon in FM/AF bilayers is the so-called training effect [101]–[103]. In particular, it is observed that the exchange bias field can be strongly modified by loop cycling [104], [105]. As mentioned above, the EB effect also occurs in magnetic nanostructures and can be used to alter the magnetic properties. Below some examples will be given showing how the EB effect can be used to alter the properties of nanostructures revealing a vortex state. For NiFe/IrMn vortex structures it was shown that the exchange bias effect can be used to selectively influence a magnetic vortex. In particular, it is presented that by a zero field cooling process, the stability of the vortex state can be drastically enhanced, by imprinting of the vortex spin structure into the AF [106]–[108]. Here, both the nucleation and annihilation fields increase [109]. Additionally, it can be also used to influence directly the sense of rotation [110], [111]. Furthermore, it was also observed that exchange-biased vortices can reveal an asymmetric magnetization reversal process [112], which can be tuned by the cooling field [109], [113]–[115]. In this context, Guslienko *et al.* [115], [116] established an analytical model, explaining the magnetization reversal via nucleation and annihilation of a magnetic vortex with a tilted vortex core. In particular, the tilted core results in an asymmetry of the hysteresis loop in addition to the overall EB shift [115]. More recently, the so-called viscous vortex reversal was introduced by *Gilbert et al.* [117]. However, a more detailed description of the different reversal modes will be given in chapter 5.1.

3 EXPERIMENTAL TECHNIQUES

In the following, an overview of sample preparation and measuring techniques used in the framework of this thesis is given. In particular, the basic principles of fabrication, processing, as well as characterization of magnetic cap structures are discussed.

3.1 Sample preparation

An innovative approach to form magnetic nanostructures is to utilize film deposition on monolayers of self-assembled close-packed nanoparticles. In this way, so-called cap structures are formed, which can reveal a magnetic vortex. In this chapter, a brief overview of the primary methods, used for the fabrication of magnetic cap structures, is presented.

3.1.1 Particle self-assembly

One way to realize magnetic nanostructures is to use top-down lithography techniques [118]. Unfortunately, these methods are slow, expensive and therefore uneconomical for large production figures. In contrast, the so-called bottom-up approaches allow cheap and fast nanostructuring on larger areas enabling an alternative solution [119], [120]. In particular, one of the approaches focuses on the manufacturing of large arrays of spherical SiO_2-particle monolayers [121] employing self-assembly processes, which act as underlayer for further film depositions [122]–[124]. With the variation of the particle diameter, it is possible to tune the aspect ratio (diameter /thickness) of the nanostructures. Additionally, this attempt offers new

features like the possibility to introduce and to control coupling of neighboring structures by simple variation of the film thickness. Thereby, the thickness t of the cap decreases gradually along the surface of the sphere (see Figure 3.1 (d)), and should obey $t(\theta) = t_0 \cos(\theta)$ [125], [126]. By depositing soft magnetic materials on top, it is possible to obtain magnetic cap structures on the particles showing a vortex state [17], [18], [127]–[130].

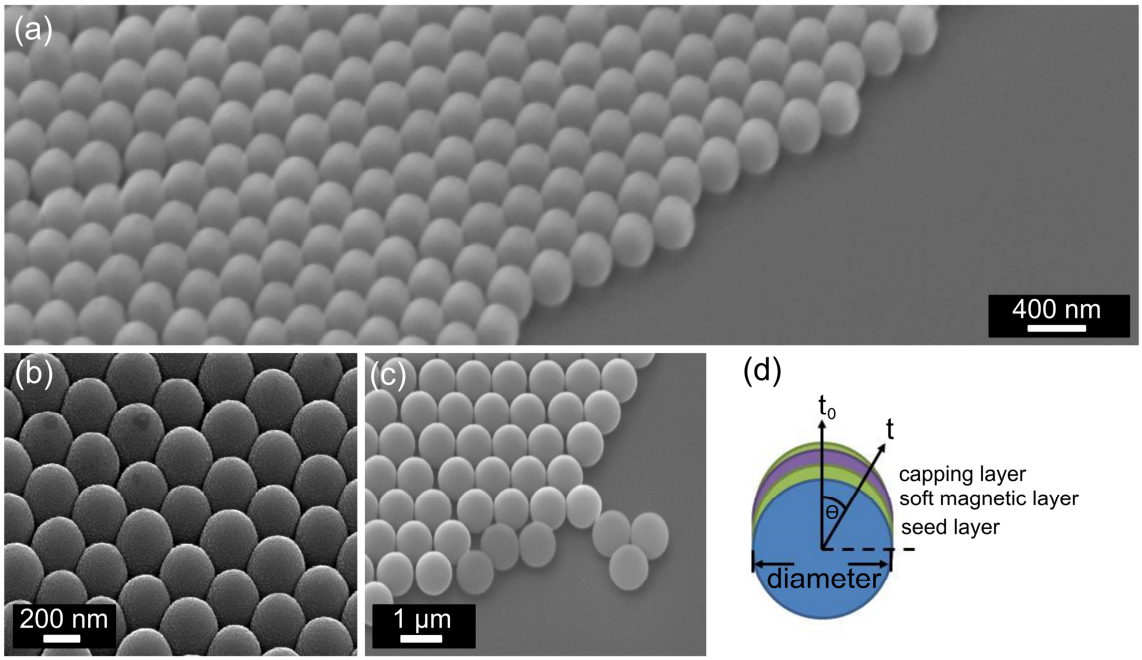

Figure 3.1: *Various SEM images of silica particles with a diameter of (a), (b) about 330 nm and (c) 900 nm, taken under an angle of 30°. In (d) the illustration of a cross section of a capped particle is shown.*

In this work commercially available SiO_2 colloidal solutions and polystyrene particles with diameters ranging from 4500 nm down to 100 nm have been used[1]. These solutions are further diluted with highly purified water, and the dispersion is applied on the substrate surface by drop coating. To improve and to control the wetting properties, the substrates (mainly silicon wafers) was first cleaned with highly purified water in an ultrasonic bath, and afterward exposed to oxygen plasma for 300 seconds before dropping the spheres on the substrate. Furthermore, with the variation of the tilt angle during the drying process, substrate temperature, as well as the droplet size, we had additional adjustment possibilities to promote the formation of closely

[1] Bangs Laborities, Inc. (http://www.bangslabs.com)

packed arrays. As an example, Figure 3.1 (a)-(c) shows SEM images of closely packed SiO_2-particle monolayers with different diameters produced with this technique. Afterward, the particle surfaces are used as a template to deposit a film onto the particle tops. A schematic illustration of a cross section of a cap structure is shown in Figure 3.1 (d). *Brombacher et al.* give more details about the preparation of silica particle monolayers [131], [132].

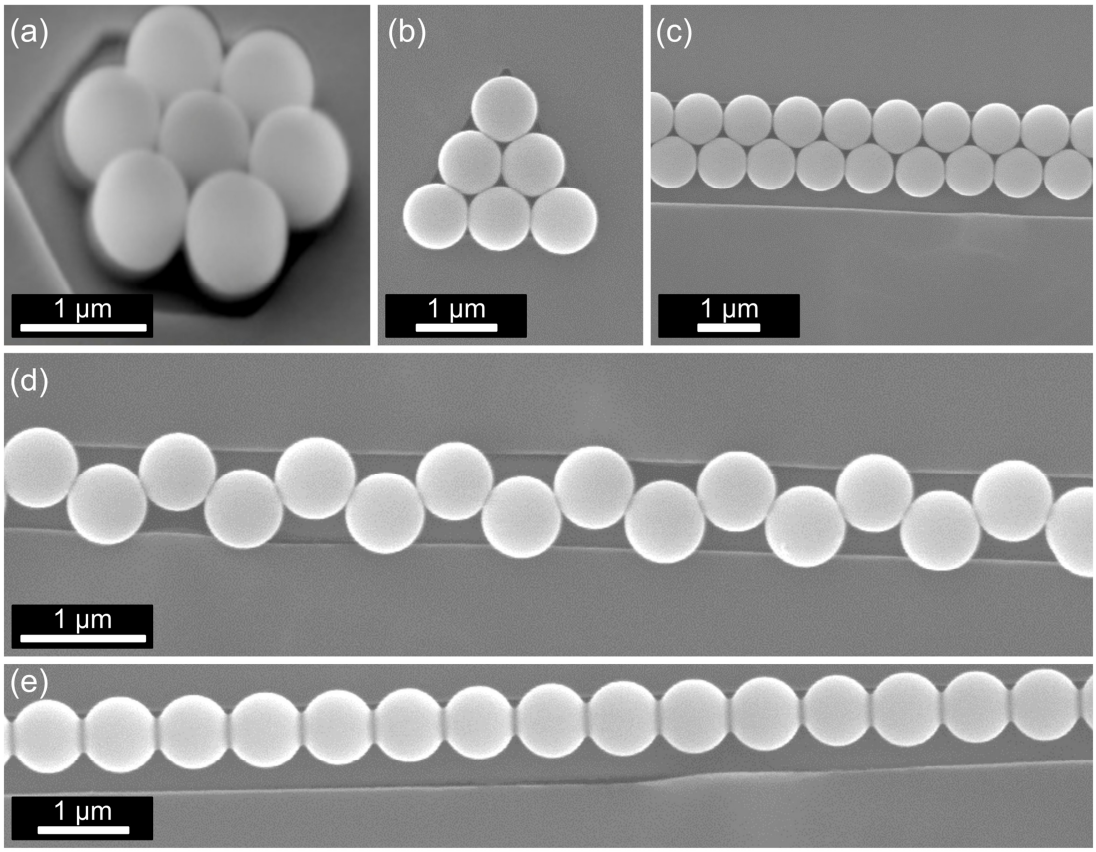

Figure 3.2: *SEM images of various templates filled with silica particles with a diameter of about 900 nm covered by a 50 nm Py film. As an example in (a) a hexagon filled with 7 particles, in (b) a filled triangle, in (c) a double chain out of particles, in (d) a single chain of particles, which are laterally staggered against each other, and in (e) a single chain of particles is shown.*

The preparation of large arrays of spherical monolayers of particles with diameters from 100 nm to 4500 nm is relatively well understood and is easily controlled in a way that it is possible to reproduce large arrays in the area up to several mm^2. Therefore, the bottom-up approach can be extended by the use of pre-structured substrates to achieve spherical particle monolayers in confined geometry. The used patterns were created by e-beam lithography on top of naturally

oxidized silicon wafers. First, a PMMA film with a thickness of about 50 to 100 nm was deposited on top of the silicon wafer by spin coating, and afterward, the required areas have been exposed to an e-beam writer. The PMMA of the exposed areas could afterward easily be removed in an ultrasonic bath of acetone. More details about the preparation of pre-patterns by e-beam lithography can be found elsewhere [133]–[135]. Then, the silica particles were floated onto the holes in a similar process as used to produce large arrays of monolayers (described above). By doing so, it was possible to achieve isolated hexagons, triangles, or chains filled with closely packed particles. Figure 3.2 shows SEM images of various particle assemblies prepared on templates covered by a 50 nm permalloy film.

3.1.2 Film growth using magnetron sputtering

Sputter deposition is a physical vapor deposition technique, used to grow homogenous thin films in the nm regime under UHV conditions [136], [137]. In the framework of this thesis, sputter deposition has mainly been used to deposit thin films on closely packed spherical particles to form large areas of cap structures.

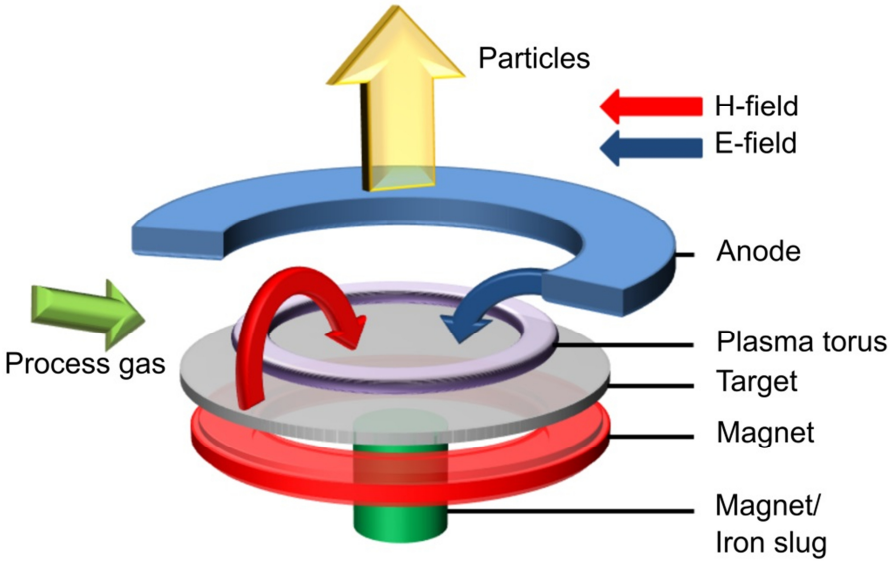

Figure 3.3: *Schematic drawing of a sputter gun used for magnetron sputtering, cf.* [95].

The mechanism of sputtering is based on the momentum exchange between an incident energetic particle and the atoms of a solid target, due to inelastic collisions. Therefore, single atoms or even whole clusters are knocked out of the target if the energy of the bombarding ions is higher than the binding energy of the target material. Most commonly, Ar is used as the process gas to generate ions as bombarding particles. The principle scheme of a magnetron sputter gun is depicted in Figure 3.3.

Ar plasma is generated by applying a voltage between the target, which acts as the cathode, and the anode, which is ring shaped around the target to obtain a localized electric field in an ambient argon gas atmosphere. In the so-called magnetron sputtering, a radially symmetric magnetic field is applied from below the magnets. The plasma electrons are confined on orbits above the target, and the probability for ionization of the argon atoms can be drastically increased. As a result, a torus-shaped plasma occurs. Consequently, varying the magnet configuration strongly influences the sputtering process. Exactly this effect has been used in the framework of this thesis to enable the deposition of soft magnetic Py. In particular, with a standard magnet configuration, it was not possible to ignite a plasma. This can be explained by the fact that the soft magnetic target makes a magnetic short cut, and the magnetic field lines could not cross the target. However, by replacing the center magnet by an iron slug, it was possible to revoke the magnetic short cut and ignite a plasma.

After plasma ignition, ions are accelerated towards the target and remove material from it. Those knocked out clusters of atoms condensate on the substrate, which is placed above the sputter gun. The thickness of the deposited film is obtained from the frequency shift of a quartz balance placed next to the substrate during the sputter deposition process.

Please note that the samples presented in this thesis were produced by keeping the Ar background pressure at 3.5 µbar, whereas the base pressure was about 5×10^{-7} mbar. The applied voltage was varied between 30 to 80 V. For these values the deposition rate scales rather linear with the applied voltage.

3.2 Sample characterization

In this chapter, a brief overview of the main methods used for the structural, as well as magnetic characterization of cap structures are presented.

3.2.1 Structural characterization

3.2.1.1 Investigations by electron microscopy

The physical resolution of a classical optical microscope depends on the wavelength of the used light. However, it is limited by the Abbe limit and in the best case, it is about 0.2 microns. In contrast, electron microscopes enables a higher resolution, since electron beams can have a much smaller wavelength than light [138].

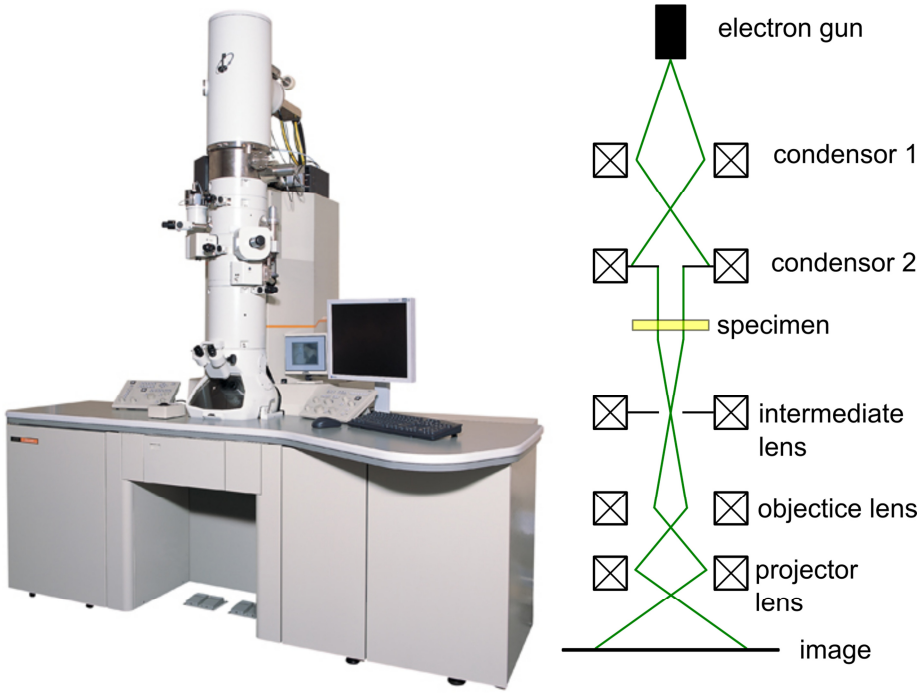

Figure 3.4: *On the left a photo of a TEM is shown taken from* [139] *whereas on the right the simplified beam path is shown, cf.* [140].

Since electron microscopy techniques are well described in literature mainly the measurement parameters will be given. Detailed information can be found elsewhere [141]–[143]. The design of a transmission electron microscope (TEM) is based on the design of the classical optical light microscope. However, in TEM electromagnetic lenses are used to focus the electron beam and form an image. These so-called electron optical lenses are analogous to the glass lenses of an optical light microscope. Moreover, it must be noted that the object under study must be very thin to ensure that the beam is able to pass through the sample. Afterward, the obtained image is detected by a CCD camera. A photo the used TEM with the associated beam path is shown in Figure 3.4. In this thesis, TEM was mainly used to investigate cross sections of cap structures to get a deeper understanding of the layer growth on top of silica particles. For the TEM investigations in this thesis, we used a *JEOL 2100F*. In this device the acceleration voltage for the electrons was adjusted to 200 keV. A typical cross section of a 70 nm thick Py layer is shown in Figure 3.5 (a).

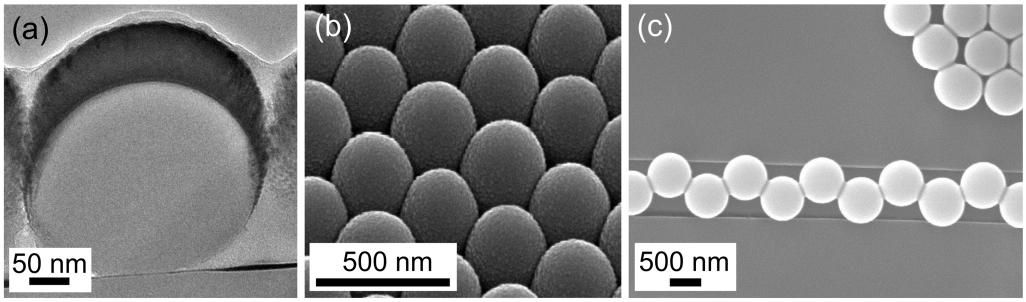

Figure 3.5: *Electron microscopy images of Py caps on silica particles. In (a) a cross section of an individual cap recorded by transmission electron microscopy is shown. In (b) and (c) scanning electron microscopy images of cap structures are presented. As an example, in (b) a closely packed monolayer, taken under 30°, and in (c) a chain of particles, which are laterally staggered against each other.*

In scanning electron microscopy (SEM) also electromagnetic lenses are used to focus an electron beam on the sample surface. Afterward, the sample is scanned with the focused electron beam. The interaction of electrons with the sample can be used to produce an image of the object [144]. In the framework of this thesis, SEM was used to image the arrangement of silica particles and cap structures on top of the particles. A typical SEM image of a large array of closely packed cap structures is shown in Figure 3.5 (b), taken at an angle of 30°. As a further example, a SEM image

of magnetic cap structures arranged in pre-patterns is shown in Figure 3.5 (c). Please note that for SEM investigations a conductive sample is required; otherwise, it leads to charging of the sample. However, in this study, this was no problem due to the metallic cap structures. The SEM investigations in this thesis were conducted on a *Nova 200 Nano SEM* from *FEI*. In this tool, the maximum acceleration voltage for the electron beam was about 18 keV.

3.2.1.2 X-ray reflectometry (XRR)

As mentioned above during the sputtering process, we used a quartz balance to monitor the deposited film thickness. However, the measured thickness differs from the real thickness on the substrate due to a deviation between the position of the sample holder and the quartz balance. This offset can be corrected by the so-called tooling factor. In order to determine the offset, we measured the film thickness by X-ray reflectometry (XRR) with an *XRD 3000 PTS* from *Seifert*. A detailed description of XRR can be found in [145]–[147]. Therefore, only a short overview will be given here. The basic idea of the analytical method is to reflect a beam of X-rays under small incident angles and to analyze the intensity of X-rays reflected in the specular direction. For small angles, we obtain a total reflection of the incident beam, in contrast to larger angles where the reflectivity drastically decreases. This decay of intensity is superimposed by the so-called Kiessig fringes *($\Delta\theta$)*, which become notable as oscillations of the intensity. From the period of the Kiessig fringes, the total film thickness t can be determined by taking into account the wavelength λ and the angle of incidence θ of the incident beam, using the following equation:

$$t = \frac{\lambda}{2\ sin\ \Delta\theta}$$

A sketch of a schematic *(θ - 2θ)* XRR measurement is given in Figure 3.6 (a), the corresponding reflectivity spectra for small angles with Kiessig fringes is depicted in (b).

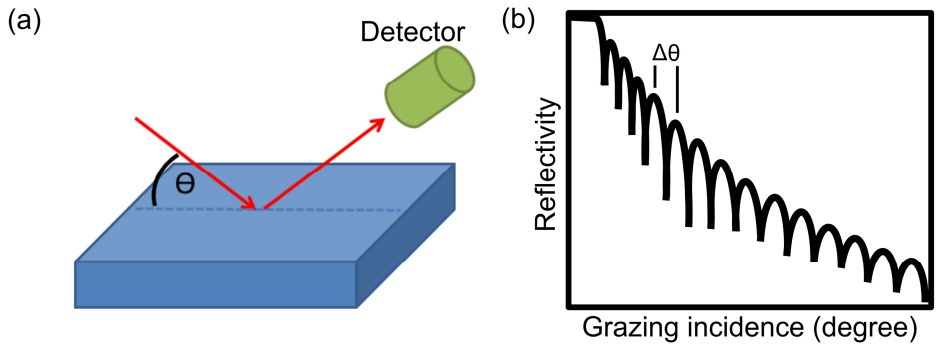

Figure 3.6: *(a) Schematics drawing of the (θ - 2θ) XRR geometry. (b) Sketch of the XRR pattern for small angles showing Kiessig fringes.*

3.2.2 Magnetic characterization

Various magnetometry and scanning imaging techniques have been used to determine the magnetic properties of individual caps as well as assemblies of closely packed caps. Therefore, a short summary of the most used methods will be given.

3.2.2.1 Superconducting Quantum Interference Device (SQUID)

A superconducting quantum interference device (SQUID) magnetometer is a very sensitive tool which allows measuring extremely small magnetic fields in the order of 10^{-12} G. An overview concerning SQUID magnetometry is given by R. L.Fagaly [148], therefore only as brief abstract is presented here:

In 1962 with the theoretical work of B. D. Josephson *et al.* [149], who proposed that electron pairs could tunnel between very closely spaced superconductors even with no potential difference the foundations were settled for the superconducting quantum interference device. However, the experimental confirmation of this effect was demonstrated two years later in 1964 by Anderson and Rowel [150].

For measuring the magnetization, SQUID uses a superconducting ring interrupted by Josephson junctions at one point in the case of a so-called AC-SQUID, and at two points for the DC-SQUID. These non-superconducting junctions are extremely thin and allow the superconducting charge

carriers, the so-called Cooper pairs, to tunnel through them. They will generate eddy currents in the ring, which are exactly a multiple of the elementary magnetic flux quantum $\Phi_0 = 2.07\times10^{-15}$ Vs. Now a change of an external magnetic field induces an electric circuit current in the superconducting ring, which increases or decreases the magnetic flux in the superconducting ring to a multiple of the flux quantum. These can be detected as they lead to a variation of the voltage, which is required to send a current through the Josephson junctions.

In this work, the measurements were obtained using an *MPMS 3 SQUID VSM* from *Quantum Design*, which archives a magnetic field control with $\leq 10^{-8}$ emu sensitivity at an external magnetic field of ± 70 kOe. It allows measuring the integral magnetic properties of a material sample in a temperature range from 1.8 up to 400 K on a standard sample holder, and in in-plane geometry up to 1000 K, while using a special sample holder containing a heater.

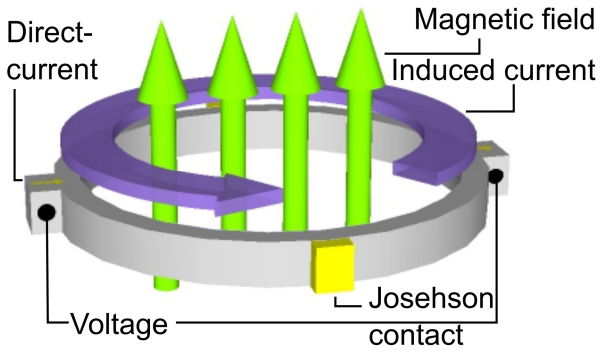

Figure 3.7: *Schematic drawing of a Superconducting quantum interference device (SQUID) placed in a magnetic field.*

A SQUID magnetometer does not only probe exclusively the properties of the magnetic layer, it also includes the substrate and parts of the sample holder, which are next to the investigated area. However, to achieve information about the in- and out-of-plane magnetization, two different geometries of sample holders are available. For out-of-plane measurements mainly a brass tube was used, which contains two quartz cylinders to clamp the sample. The cylinders are designed in a way that they are placed together being smaller than the distance between the pickup coils in the SQUID. However, by mounting the sample, a small gap remains between the quartz cylinders, which result in a paramagnetic background, which has to be subtracted. For in-plane

measurements, the specimen was fixed by *GE Varnish*[2] on top of a half cylindrical glass rod. Due to the fact that the size of the sample holder is larger than the distance between the pickup coils in the SQUID, the contribution from the sample holder to the measured signal can be neglected. But it should not be forgotten that also the used Si substrate and the *GE Varnish* give an additional diamagnetic contribution to the total measurement signal, which has to be subtracted.

However, in this work mainly in-plane measurements of nanostructures have been carried out. For this purpose a sample size in the range of 2×2 mm is required. For investigations of cap arrays, this can be provided by the large scale self-assembly fabrication process; the corresponding loop is an average over several millions of vortex structures.

3.2.2.2 Magneto-optical Kerr effect

The magneto-optical Kerr effect (MOKE) discovered in 1876 by John Kerr, describes the variation of polarized light through reflection from a magnetic surface [151]. In particular, MOKE describes a change of the polarization plane or intensity of light (electromagnetic wave) due to reflection from a specimen surface. In the process, the change of polarization plane or intensity change is proportional to the magnetization of the sample [152]. In this regard, it must be noted that the Kerr effect is a surface effect and has only a limited penetration depth, for typical metals it is $\leq$ 20 nm [152], [153]. The equivalent effect in transmission is the Faraday effect. Due to the limited penetration depth, MOKE is often used to probe thin magnetic layers. Therefore, a linear polarized beam is focused on the sample and the change of the axis of polarization, which is proportional to the magnetization, is measured of the reflected beam.

[2] also known as IMI 7031 from CMR-Direct

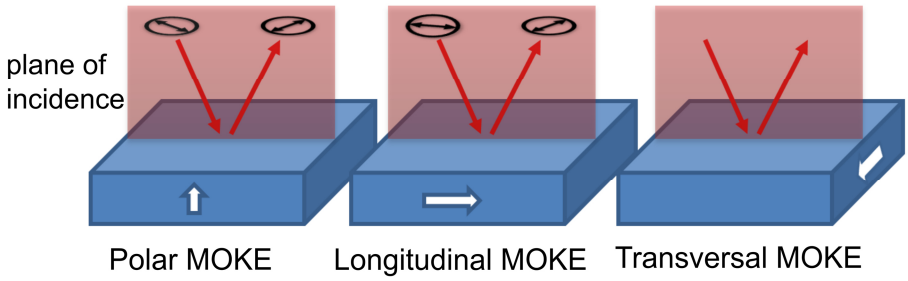

Figure 3.8: *The different geometries of the magneto-optic Kerr effect: (a) Polar MOKE, (b) Longitudinal MOKE, and (c) Transversal MOKE, cf.* [70].

This behavior can be explained by the fact that linear polarized light is a superposition of left- and right-handed circularly polarized light. The rotation of the polarization plane is based on the principle that left and right handed circularly polarized light show different propagation velocities in the specimen. Furthermore, the absorption also shows a dependency on the light intensity. Consequently, also the amplitude of the reflected electromagnetic waves varies resulting in elliptically polarized light [70].

As depicted in Figure 3.8, the MOKE effect can be divided into polar, longitudinal, and transversal MOKE effect due to the direction of the sample magnetization with respect to the plane of incidence of light.

- For the polar magneto-optical Kerr effect the magnetization vector is perpendicular to the specimen surface and parallel to the plane of incidence. In this case, the reflected beam undergoes a transition from a linear to an elliptical polarization. The change of the polarization plane is proportional to the magnetization of the sample.

- The longitudinal magneto-optic Kerr effect describes the situation where the magnetization vector is parallel to the sample surface and parallel to the plane of incidence. In contrast to the polar Kerr effect, it involves light reflected at an angle from the specimen surface and not normal to it. However, this effect also leads to rotation of the polarization plane of the reflected beam, like the polar Kerr effect. It should be noted that the in-plane MOKE curves, used in the framework of this thesis, are taken by means of the longitudinal Kerr effect.

- For the transverse magneto-optical Kerr effect the magnetization vector points parallel to the sample surface and perpendicular to the plane of incidence of the beam. It should be noted that this effect only occurs when the incident light is polarized in the incidence plane. In contrast to the above-mentioned effects where a variation of the polarity of the reflected light is measured, here the change in intensity of the reflected beam is detected. A significant disadvantage of this method is that the effect is typically an order of magnitude smaller than the longitudinal Kerr effect.

In order to probe local magnetic properties [154] of thin films or monolayer of densely packed caps, and video monitor the probed area at the same time, we used the *NanoMOKE2* setup from *Quantum Design*. Importantly, the laser spot can be focused down to 3 µm. Furthermore, with this setup measurements could be carried out in longitudinal configuration (field applied in-plane) with a maximum applied field of 4 kOe in a temperature range from 10 K - 600 K. A photo of the setup is shown in Figure 3.9.

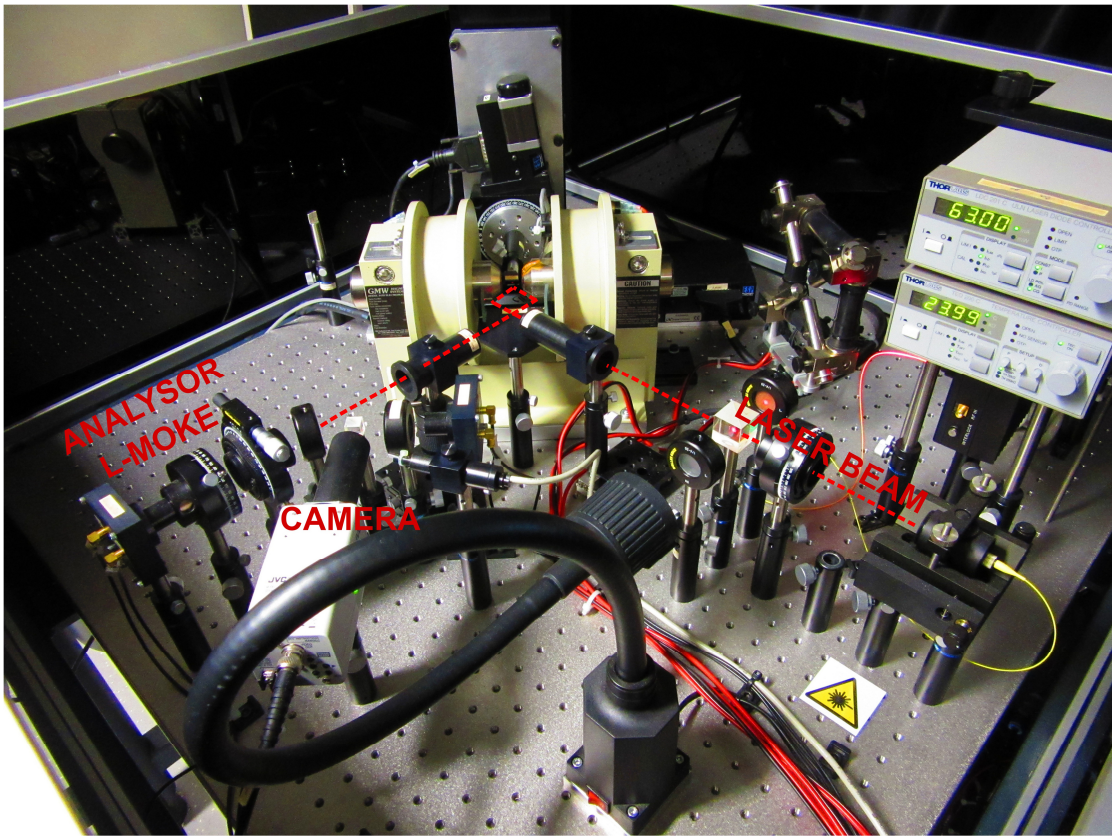

Figure 3.9: *Photo of the NanoMOKE 2 used in this work. For a better understanding the beam path for measuring longitudinal MOKE (L-MOKE), lenses and the camera for positioning of the sample are marked. At the sample stage also a flow-cryostat can be mounted to perform temperature dependent measurements in a temperature range between 5-600 K.*

3.2.2.3 Magnetic force microscopy

Magnetic force microscopy (MFM) is a special type of atomic force microscopy (AFM) based on the idea of scanning probe microscopy (SPM). It can be used to depict magnetic structures, also individual domain motion in an external field can be imaged, for instance, the motion of a vortex core by applying an in-plane field [83], [86], [155]. However, the concept is based on the idea of mapping the forces between the tip mounted at the end of a cantilever and the specimen.

Using a classical non-magnetic AFM tip, the atoms on the specimen surface interact with the tip via van der Waals, capillary, adhesion and contact forces. More precisely, the effective acting force depends on the distance between tip and specimen surface, and can be detected by the sag of

the cantilever. By using a magnetized tip in addition to the aforementioned forces, magnetic interactions contribute.

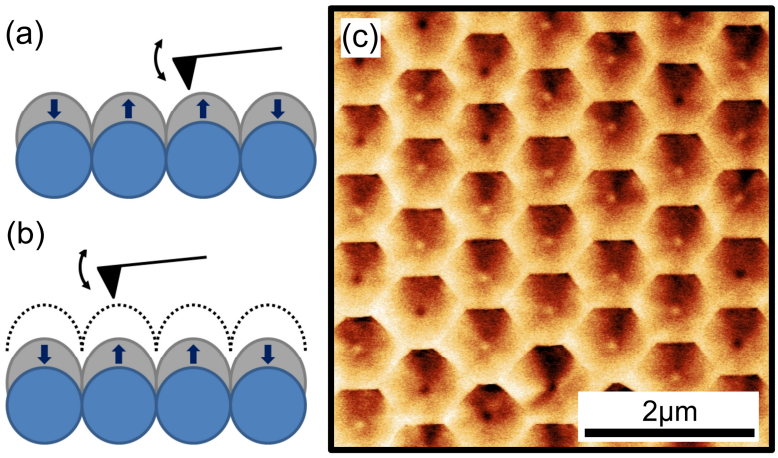

Figure 3.10: *Magnetic force microscopy (MFM). In (a) a schematic drawing of the first line scan is shown. Here the so-called Lift Mode is used to measure a height profile of the specimen. In (b) a schematic drawing of the second line scan is shown, which follows the topology in a constant height to the sample surface to detect the magnetic signal* [95], [132]. *As an example, in (c) an MFM measurement of densely packed silica particles with diameters of 330 nm covered by a 70-nm-thick Py layer is shown. The vortex cores are clearly visible by dark and bright contrast.*

The principle of mapping the magnetic structure works since the van der Waals forces decay faster than the magnetic forces with increasing the tip-sample distance [156]. To reconstruct only the magnetic contribution, in a first scan, a height profile is recorded using the *tapping mode*. Therefore, the cantilever is oscillating near its eigenfrequency and scanned over the surface. In Figure 3.10 (a) a sketch of the scan in the *tapping mode* of magnetic caps is shown. Afterward, the tip is lifted up from the surface, and at a constant height, a second scan was performed in the so-called *Lift Mode*, as depicted in Figure 3.10 (b). In this work, the imaging was realized with a *Dimension 3000* microscope from *Veeco Instruments*. In Figure 3.10 (c) a typical MFM image of an array of densely packed silica particles with diameters of 330 nm covered by a 70-nm-thick Py layer forming a vortex is shown in the demagnetized state, as an example. The vortex cores are clearly visible by dark and bright contrast.

3.2.2.4 Full-field soft X-ray transmission microscopy

Full-field high-resolution magnetic transmission X-ray microscopy (MTXM) is a powerful technique to image element specific local magnetic moments with a spatial resolution of better than 15 nm [157].

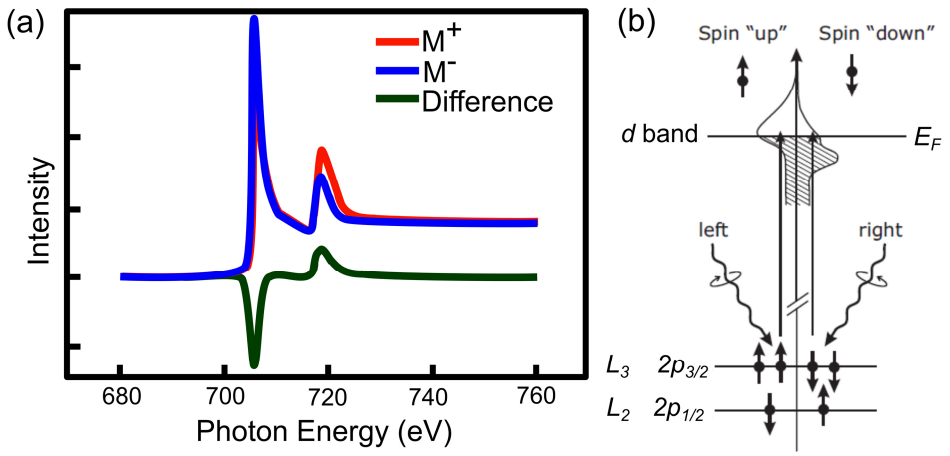

Figure 3.11: *In (a) a sketch of the X-ray absorption spectra of iron for left (blue) circularly polarized light and for right (red) circularly polarized light is shown. The difference spectrum (dichroism) is plotted in green. In (b) a sketch of a two step model for XMCD is shown. Taken from* [158].

The technique is based on the X-ray magnetic circular dichroism (XMCD) effect [159]–[161]: The absorption of X-rays by an atom with magnetic moment is dependent on the polarization of the X-rays. In particular, the difference spectrum between left- and right-handed circularly polarized X-rays can be used due to the fact that it is proportional to the magnetization. Furthermore, element specificity can be achieved by adjusting the X-ray energy to the absorption edge energy characteristic for each element. A sketch of typical XMCD spectra for both polarizations of iron at the $L_{2/3}$ edge, including the differential spectrum, is shown in Figure 3.11 (a). The two peaks result from transitions from $2p_{3/2}$ and $2p_{1/2}$ electrons into unoccupied *3d* states, showing a maximum directly above the Fermi level. In particular, the L_2 edge results from the $2p_{1/2}$ into *3d* transition, and the L_3 edge from a $2p_{3/2}$ into *3d* transition. However, the magnetic properties of transition metals are mainly determined by the *d* electrons. Therefore, to explain the circular X-ray dichroism at the $L_{2/3}$ edge of *3d* transition metals, a two step model from Stöhr and Wu can be used [162]. In the first step, spin polarized electrons are

generated by excitation of core electrons from the *p* shell by circularly polarized X-rays, as can be seen in Figure 3.11 (b). For a non-magnetic material, the total number of transitions is the same for both polarizations. In the second step of the model, the electrons are detected by the unoccupied *3d* states in dependence of their polarization.

A sketch of the used MTXM setup at the ALS beamline 6.1.2 in Berkeley (USA) is depicting in Figure 3.12. This instrument focuses a beam of circularly polarized X-rays using a zone plate to achieve a standard spatial resolution of better than 15 nm. In this experiment, synchrotron radiation impinges on a condenser zone plate, which together with a pinhole placed close to the sample, provides a hollow cone illumination of the sample and acts as a linear monochromator due to its wavelength-dependent focal length [157].

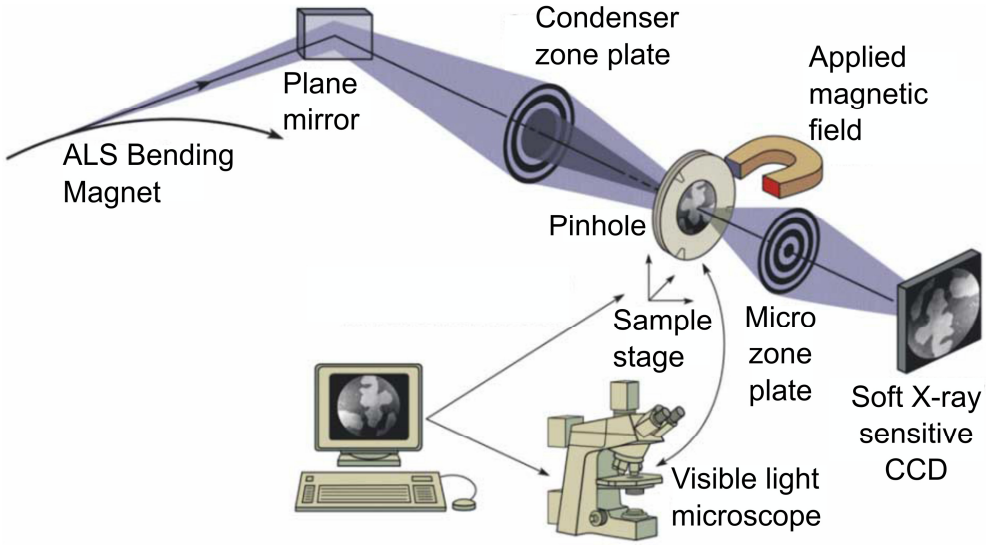

Figure 3.12: *Sketch of the optical setup of the full-field high resolution soft X-ray microscope at the ALS (Berkeley, USA). Taken from Fischer et al.* [157].

Afterward, the micro zone plate (MZP), downstream the specimen images, and transmits the photons onto a 2D CCD [157]. Moreover, it should be noted, the end station can be operated in a typical energy range between 500 - 1300 eV.

Additionally, external magnetic fields up to 5 kOe in the beam direction and 2 kOe along the sample plane can be applied during the measurement. To take an image of the in-plane

component, the sample can be mounted under a tilt of about 30° relative to the incident beam. Since MTXM operates in transmission, we used assemblies of closely packed polystyrene particles on Si_3N_4 membranes for X-ray transmission experiments. In particular, for these experiments, we used Si_3N_4 membranes with a window size of 1.5 x 1.5 mm and a thickness of 200 nm from *Norcada.*

4 MAGNETIC VORTICES IN PY CAP STRUCTURES

Magnetic nanostructures have attracted large interest due to their unique properties. In this regard, as the size of a magnetic structure is reduced, the multi domain state becomes energetically unfavorable, and either a single domain or an inhomogeneous magnetization configuration is formed. In particular, for soft ferromagnetic disks in the micron size range a so-called vortex state is favored, where the magnetization is forming an in-plane flux closure structure to minimize the magnetostatic energy [12], [21], [41], [81], [86], [163].

This magnetic in-plane configuration can rotate clockwise (CW) or counter clockwise (CCW). In the center, a vortex core occurs where the magnetization is pointing perpendicular to the plane as a result of minimizing the exchange energy [21], [22].

For our study, we prepared magnetic vortex structures in a two-dimensional lattice by permalloy (Py) film deposition onto large arrays of self-assembled spherical particles with different diameters. A detailed description of the manufacturing process is presented in chapter 3.

In the first part, we focus our investigations on the cores of magnetic vortex structures stabilized in cap structures with various thicknesses and with a diameter of about 330 nm. In this study, particular attention is paid on the reversal characteristics of the core by applying an out-of-plane field.

In the second part, we present the dependence of the nucleation and annihilation fields of the vortex structures on the Py layer thickness (aspect ratio) and on temperature for cap structures with a fixed diameter of about 330 nm. Here, special attention is paid on the onset of strong

exchange and magneto-static coupling between adjacent caps. These couplings arise due to the emergence of bridges of at the contact area between particles.

Furthermore, a full-field magnetic soft X-ray microscopy study on Py cap structures with a thickness of 130 nm and a diameter of 900 nm will be presented.

4.1 Experimental details

We use a simple bottom-up approach to realize arrays of magnetic vortex structures. This approach is based on self-assembly of spherical silica particles [121] with a diameter of 330 nm followed by deposition of a magnetic permalloy thin film onto the particle array forming Py cap structures [18], [128], [129]. Here we focus on the influence of magnetic coupling on the magnetic properties induced by varying the Py film thickness between 20 - 130 nm. All films were deposited by DC magnetron sputter deposition in a chamber with a base pressure of about 5×10^{-7} mbar. During deposition, the Ar pressure was adjusted to 3.5×10^{-3} mbar and the thickness was monitored using a quartz balance crystal. The Py layer was grown on a 5 nm thick Ta layer, to improve the growing conditions, and covered by a further 5 nm thick Ta layer to prevent oxidation.

The morphology and the structure of the samples were characterized by SEM and by investigation of cross section via TEM, respectively. In order to probe the magnetic properties of the Py caps, MOKE magnetometry in longitudinal configuration was used to measure in-plane magnetic hysteresis loops. In this case, focusing optics were employed to reduce the diameter of the diode laser (λ = 670 nm) beam spot to about 3 μm on the sample, thus the signal is averaged over about 100 Py caps. For temperature dependent measurements, additionally a liquid nitrogen cryogenic sample stage was used allowing measurements in the temperature range between 77 K and 500 K. Furthermore, direct observation of vortex structures was carried out using full-field magnetic transmission soft X-ray microscopy at the Advanced Light Source (beamline 6.1.2.) in Berkeley (CA, USA), enabling real-space magnetic imaging with spatial resolution down to 20 nm [157]. In this experiment, the magnetic contrast is given by XMCD, caused by the X-ray absorption coefficients as a function of the orientation between the sample magnetization and the X-ray helicity [157]. The magnetic imaging of Py caps was performed at a photon energy corresponding to the Fe L_3 (707 eV) X-ray absorption edge. To record images of in-plane magnetizations, specifically the circulation in the Py caps, the sample was mounted at 60° angles with respect to the X-ray propagation direction. To subtract the nonmagnetic background of the images taken at particular magnetic fields, we normalized them to the picture recorded in saturation. Within an exposure time of only a few seconds, an area of 30 × 30 caps can be imaged.

In a further study, the vortex cores were investigated by an in-field scanning magnetoresistive microscope (SMRM) [164]–[166]. This device uses a standard magnetic recording head of a hard disk drive containing a tunneling magnetoresistive (TMR) read element sensitive to the perpendicular component of the magnetic stray field of a vortex structure. Please note that this method allows magnetic imaging without influencing the magnetization state of the specimen. In this setup, the sample is fixed on a *xy* stage controlled by piezoelectric drivers providing the possibility to scan the sample with a velocity up to 25 μm/s with a resolution of about 0.2 nm, while the sample is in physical contact with the recording head. The obtained spatial resolution is better than 30 nm in down-track direction and 65 nm in the cross-track direction. Thus, individual vortex cores can be imaged and their lateral displacement, when an in-plane field is applied can be evaluated. A detailed description of the device is given by Mitin *et al.* [165].

4.2 Investigation of vortex cores in a two-dimensional lattice[3]

As already discussed, the magnetic vortex is characterized by the chirality or handedness of the vortex. This is the product of the in-plane flux closure, the so-called circulation, and the out-of-plane component, the so-called polarity of the vortex, which can point either *up* or *down*. However, for possible specific applications, it is required to control individually the sense of rotation, which can be either clockwise or counter clockwise, as well as the polarity.

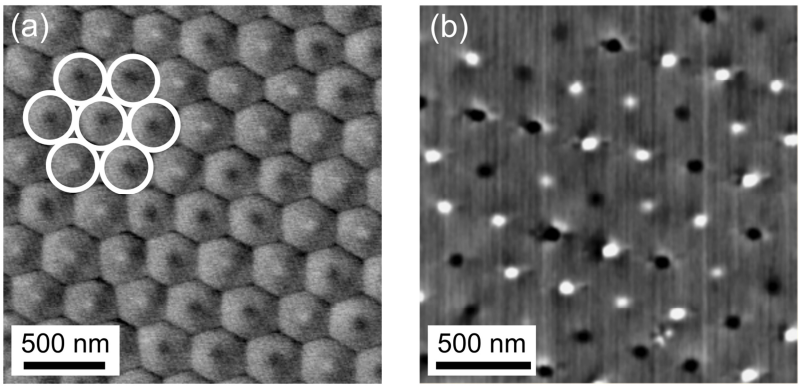

Figure 4.1: *Images of a densely packed particle array (particle diameter: 330 nm) covered by a 30 nm thick Py layer recorded in the demagnetized state. (a) MFM image, where the vortex cores are clearly visible by dark and bright contrast. In the upper left corner the underlying particles are marked by circles, cf.* [167]. *(b) SMRM image, here also the cores can be easily recognized, cf. Mitin et al.* [164].

It has been shown that the sense of rotation can be selectively modified by dipolar interactions induced by two rhomboid nanomagnets with predetermined magnetization directions [168], by using exchange bias [110], [111], or even in structures with broken rotational symmetry by applying in-plane fields in a specific direction [23], [25], [169]. The polarity can be controlled, for

[3] Please note that the presented results have been obtained in a close cooperation with D. Mitin. The results presented in this section are partially published: D. Mitin, **D. Nissen**, P. Schädlich, S. S. P. K. Arekapudi and M. Albrecht, J. Appl. Phys. **115**, 063906 (2014).

instance, by global magnetic fields [40], [170], [171]. However, these mechanisms result in the dilemma that it is not possible to control individually the polarity of magnetic vortex structures, and therefore they are not suitable for closely packed cap structures.

However, to gain a better understanding of the switching process of the polarity in a cap lattice, we investigated a lattice of magnetic vortices by in-field MFM that allows applying global out-of-plane fields, and compared the results to those obtained by SMRM [164]–[166]. This device offers the opportunity of applying a local out-of-plane magnetic field pulse to specific areas.

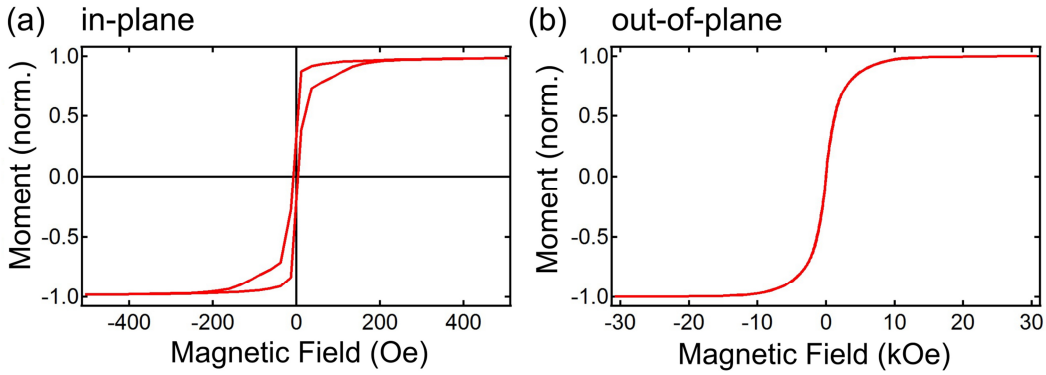

Figure 4.2: *SQUID measurements of cap array of densely packed Py caps with a thickness of about 30 nm and a diameter of 330 nm recorded at 300 K. The measurements have been performed in the in-plane geometry (a) and out-of-plane geometry (b), cf. Mitin et al.*[164].

As can be seen in Figure 4.1, in a first study, we compared an MFM image (a) with an SMRM image (b) of a sample with the same layer stack. The cap array with a Py thickness of about 30 nm was produced by DC°magnetron sputtering and afterward demagnetized. Consequently, the core polarization should be randomly distributed.

In (a) a typical MFM image is shown where the cores of the vortices are clearly visible by the bright and dark contrast. For a better indication, in the upper left corner, the underlying particles are marked by circles. Therefore, the formation of vortex states in the array was clearly confirmed, cf. [167]. In (b) an SMRM image of a cap array with the same Py thickness is shown. Here also the cores of the vortex can be clearly seen, again indicated by a bright and dark contrast. By comparing of individual vortex cores in (b), we found a small dispersion in brightness.

We assume that this originates from a slight size distribution of the underlying closely packed silica particles. We also assume that the non-perfectly round shape of the cores can be caused by surface defects arising during the scanning process taking place in direct contact [164]. In order to confirm the magnetic vortex state, we also performed SQUID measurements. In Figure 4.2 the hysteresis curves obtained from in-plane (a) and out-of-plane (b) measurements are presented. The in-plane measurements clearly reveal a magnetization reversal via formation of a magnetic vortex. Here the typical nucleation and annihilation field of the vortex state can be recognized, as expected. In the out-of-plane measurements at remanence only the cores of the vortices are contributing. Consequently, coming from saturation one would expect a small remanence magnetization and hysteretic behavior corresponding to the magnetization of the vortex core. This could not be observed, due to the overall small contribution of the cores in comparison to the total magnetization compared with the limited sensitivity of the measurement device, which is in line with the literature [170].

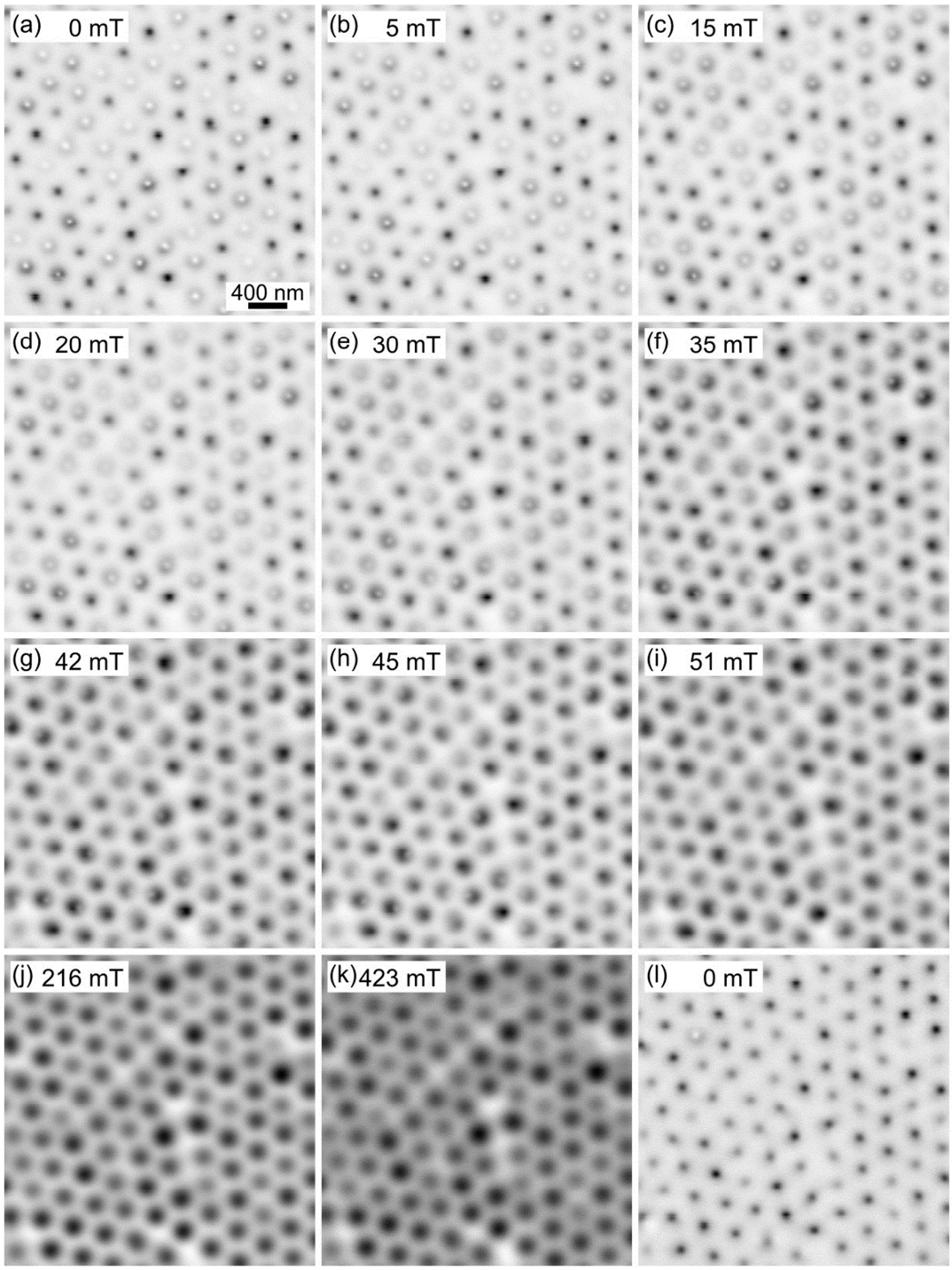

Figure 4.3: *In-field out-of-plane MFM images of densely packed silica particles with diameters of 330 nm covered by a 70 nm thick Py layer. The vortex cores are clearly visible by dark and bright contrast. In (a) the sample is shown at remanence after demagnetization, (b)-(k) show images taken in a rising out-of-plane field, and (l) an image at 0 mT after saturation.*

As already mentioned, the polarity of a vortex structure can be controlled by global magnetic fields [170], [171]. Therefore, as shown in Figure 4.3, we performed an in-field out-of-plane MFM study on an array of densely packed silica particles with diameters of 330 nm covered by a 70 nm thick Py layer. As shown in (a), the magnetic vortex state of the cap structure was confirmed after demagnetization. The light and dark regions originate from the vortex cores, and we detect a quite equally distribution. Afterward, an out-of-plane field has been applied and successively increased, see (b)-(k). It seems that by increasing the field the cores pointing *up* are getting simply enlarged. Whereas for cores pointing *down* (bright) also an enlargement with increasing field can be detected. However, it seems that in this case the elongation is composed of a shift of the cores to the edge of the particle and an additional growing region pointing in the opposite direction (dark). One could assume that the achieved shifting is a result of an interaction of the in-plane circulation with the applied field in combination with the special topology of a cap structure. However, at around 51 mT nearly all caps have switched, and a further increase of field only induces minor changes. As shown in (l), after reducing the field to zero, the polarization remains pointing *up*, as expected. A closer look reveals that one core in the upper left corner has switched back. We assume that this is due a defect in the cap structure promoting this polarity.

As already mentioned, the SMRM device also enables the possibility to apply local magnetic field pulses raising the question if it is possible to switch a vortex core in a lattice of closely packed cap structures. In Figure 4.4 the sequential switching of individual vortex cores in a lattice of closely packed Py caps with a thickness of 30 nm and diameter of about 330 nm is demonstrated. For this, a current of approximately 1.2 V has been applied for 10 ns on the coil in the read/write head. This results in a local magnetic out-of-plane field pulse of about 7.3 kOe, which is applied to the individual cores of the structures. As can be seen, the field is sufficient to change the polarity, and we obtain a sequentially switching from black to white.

However, a more detailed investigation of the switching event carried out by Mitin *et al.* reveals a threshold in the writing voltage for a successful switching event [164]. Surprisingly, for an *up*-to-*down* (bright to dark) reversal a voltage higher than 0.78 V, corresponding to a local field of about 3.8 kOe, has to be applied, in contrast to the *down*-to-*up* (dark to bright) reversal where a voltage of about 0.71 V, resulting in a local field of 3.3 kOe, was necessary for an efficient switching.

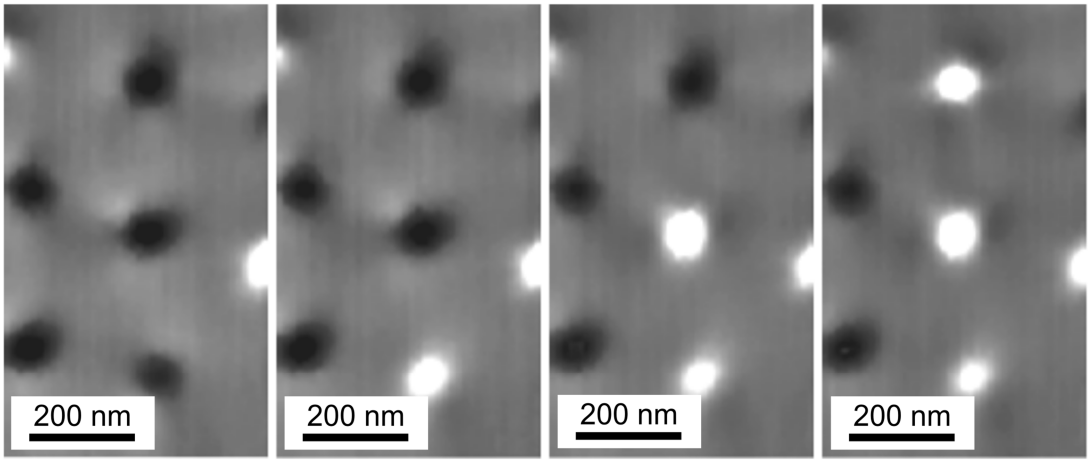

Figure 4.4: *Sequential switching of vortex cores (clearly visible by dark and bright contrast) in a lattice of closely packed Py caps with a thickness of 30 nm from dark (down) to bright (up), reproduced from Mitin et al.* [164].

This is in agreement with a recent report from Steubel *et al.* [18], who investigated the polarity of a Py cap lattice (diameter 330 nm; thickness 40 nm) by frequency-modulated MFM and showed slight differences in the maximum intensity for different core polarities. However, up to now, we found no final physical explanation for the asymmetric switching behavior. However, one can argue that the asymmetry occurs either due to the particular topology of a cap structure or due to a unique magnetic environment built by the neighboring caps. Nonetheless, it has been shown that magnetostatic coupling can influence the in-plane circulation [172], [173], and maybe also the polarity and, therefore, the switching behavior. Additionally, one must reflect upon simply direct exchange coupling of neighboring caps due to the closely packing, which could influence the switching behavior [18], [128].

4.3 Coupling of vortices in a two-dimensional lattice[4]

As explained in detail in chapter 3, we use a simple bottom-up approach to realize arrays of magnetic vortex structures. For this study we used self-assembly of spherical silica particles [121] with a diameter of 330 nm followed by deposition of soft magnetic permalloy film onto the particle array forming Py cap structures [17], [55], [127], [128], [130]. However, by increasing the film thickness coupling of neighboring structures occurs due to the closely packing. In this chapter, the influence of magnetic coupling on the magnetic properties induced by varying the Py film thickness from 20 nm up to 300 nm will be discussed. A typical image of closely packed particles covered with 70 nm Py is shown in Figure 4.5. In (a) a cross section bright field TEM image of two neighboring particles is shown confirming the growth of a cap structure on top. A closer look at the connecting area, however, reveals that both particles have a small shifted arrangement due to the closely packing, and therefore suggest that the connecting area is larger. In (b) an enlargement of an individual cap with its connecting area is shown. As can be clearly seen, neighboring caps are interconnected at the contact areas resulting in direct magnetic exchange coupling. A corresponding SEM image taken at an angle of 30° with respect to the sample normal confirming the closely packing is shown in (c). Please note that the coupling strength will show strong thickness dependence. Therefore, we expect that for a critical Py film thickness the caps are fully connected (full coupling) and no longer behave like individual structures. Furthermore, we assume that at the onset of coupling, at a film thickness of several tens of nanometer, the coupling of neighboring caps might influence the in-plane circulation orientation of connected caps, showing a vortex. This could lead to frustration of the in-plane circulation in a hexagonal cap array or even, as recently reported for a chain of disks, showing a vortex, to the formation of anti-vortices at the connecting area when the circulations are rotating in different directions. It should be noted that due to the curved surface of a cap structure, the thickness of the Py layer in radial direction decreases from the top center of the film cap towards the rim. In particular, the thickness t of the cap decreases gradually along the surface of the sphere and should obey

[4] Please note that most part of the results presented in this section are already published in: **D. Nissen**, D. Mitin, O. Klein, S. S. P. K. Arekapudi, S. Thomas, M.-Y. Im, P. Fischer, and M. Albrecht, *Magnetic coupling of vortices in a two-dimensional lattice*, Nanotechnology **26**, 465706 (2015) [128].

$t(\theta) = t_0 \cos(\theta)$ [125], [126], as already discussed in Figure 3.1. Consequently, due to the curved surface of a cap structure, we expect an enlarged core area in comparison to *classically* magnetic vortices formed in disk structures.

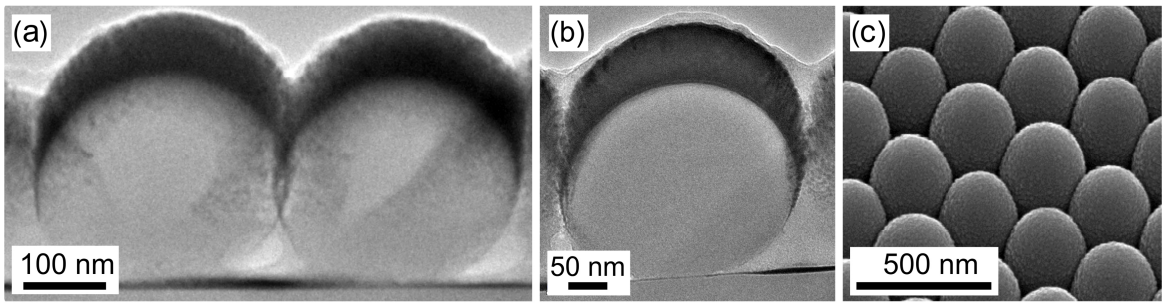

Figure 4.5: *(a, b) Cross section TEM image SEM image of an array of densely packed silica particles with diameters of 330 nm covered by a 70 nm thick Py layer. (c) SEM image, taken under an angle of 30° with respect to the sample normal.*

By increasing the film thickness, coupling of neighboring structures occurs at the connection points due to the closely packing. For a detailed investigation, we measured in-plane longitudinal MOKE hysteresis loops for various Py thicknesses at room temperature. In particular, we probed the local magnetic properties of an array of closely packed cap structures with our *NANO*-MOKE setup (see chapter 3). The measurements are shown in Figure 4.6. Surprisingly, for thicknesses up to 30 nm, no typical vortex hysteresis curve could be observed. This result is in contrast to calculations from Streubel *et al.*, who predicted a magnetic vortex already at a cap thickness of about 5 nm for Py [17].

However, the shown hysteresis curves of the caps with a Py thickness of about 40 nm already reveal characteristic nucleation and annihilation fields. Surprisingly, it seems that for thicknesses smaller than 60 nm the remanent magnetization is almost one, and a reverse field has to be applied to nucleate the vortex, whereas MFM investigations confirm a vortex core. A detailed discussion of the nucleation- and annihilation-field as a function of film thickness will follow later. Further increase of film thickness indicates no longer a typical vortex hysteresis. In particular, it seems that for a cap thickness of about 100 nm strong coupling occurs indicated by a transition to a different magnetic configuration, however still containing a vortex.

A detailed discussion will be done later. A further increase of the film thickness results in stronger coupling of the cap structures and, consequently, the typical vortex characteristics are more difficult to recognize. However, SMRM measurements, as will be discussed later, verify the vortex core even for cap thicknesses of about 130 nm. At a film thickness of about 300 nm, which is close to the diameter of the caps, the hysteresis loops of a flat film deposited on a silicon substrate and the cap structures are difficult to distinguish, meaning that the caps are fully coupled.

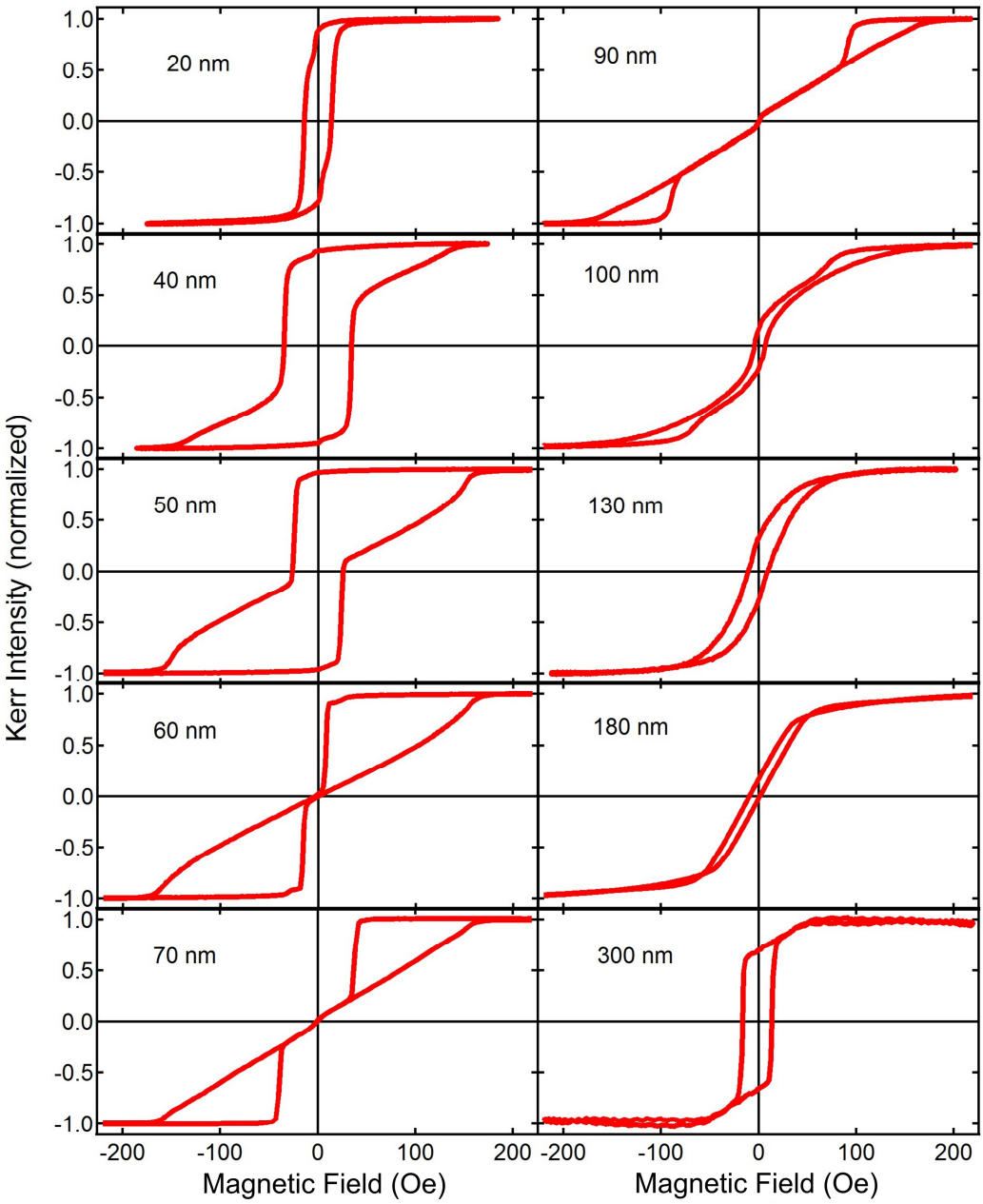

Figure 4.6: *Longitudinal MOKE hysteresis loops of Py caps with thicknesses varying from 20 nm up to 300 nm measured at room temperature by focusing on a particle monolayer.*

As mentioned above, caps with a thickness between 30 and 100 nm reveal a magnetic vortex, therefore for these samples, it was possible to extract the nucleation as well as the annihilation field from the hysteresis curves. As summarized in Figure 4.7, the nucleation field reveals strong thickness dependence, while the annihilation field shows only a small variation. In particular, for

a cap thickness smaller than 50 nm, after saturating the sample, an opposite magnetic field is required to nucleate a magnetic vortex. As can be seen, the nucleation field increases with film thickness and for Py thicknesses between 50 nm and 60 nm a transition from negative to positive nucleation field results. We expect that in this process the continuous increase of the nucleation field with film thickness is linked to the increasing magnetic moments of the caps which is expected to be the main driving force for the formation of a magnetic vortex. Here, it should be mentioned that also other effects can influence the nucleation process. In particular, the exchange coupling due to the magnetically connected cap structures, or as shown by Mejía-López *et al.* inter-cap dipolar interactions opposing the vortex nucleation process [174].

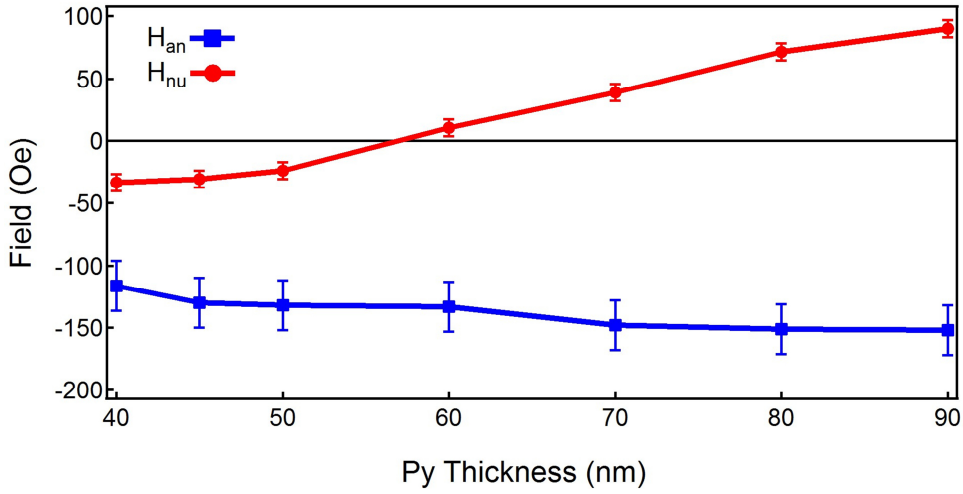

Figure 4.7: *Thickness dependence of the nucleation field H_{nu} and annihilation field H_{an} for Py caps with a diameter of about 330 nm extracted from MOKE measurements recorded at room temperature, cf.* [128].

As can be seen in Figure 4.6, Py caps with a thickness of about 70 nm show a magnetic vortex at remanence. Therefore, it was possible to investigate the temperature dependence of the nucleation, as well as the annihilation field. In detail, we investigated the magnetization reversal in a temperature range from 100 K up to 500 K. In Figure 4.8 the nucleation and annihilation fields as a function of temperature are presented. Overall, we found a stabilization of the vortex state with decreasing temperature. Accordingly, for the nucleation field presented in Figure 4.8 (a), we detect a slight increase with decreasing temperature, indicating vortex stabilization. Here it should be noted that the nucleation field extracted from measurements at

room temperature exhibit a slight difference compared to the nucleation fields at room temperature from the Py thickness series, presented on page 53. This can be explained by the fact that these measurements were performed on a different but comparable sample prepared under similar conditions. The temperature dependence of the annihilation field is depicted in Figure 4.8 (b). Here, we detect a lowering of the annihilation field with decreasing temperature, also indicating the stabilization of the magnetic vortex state.

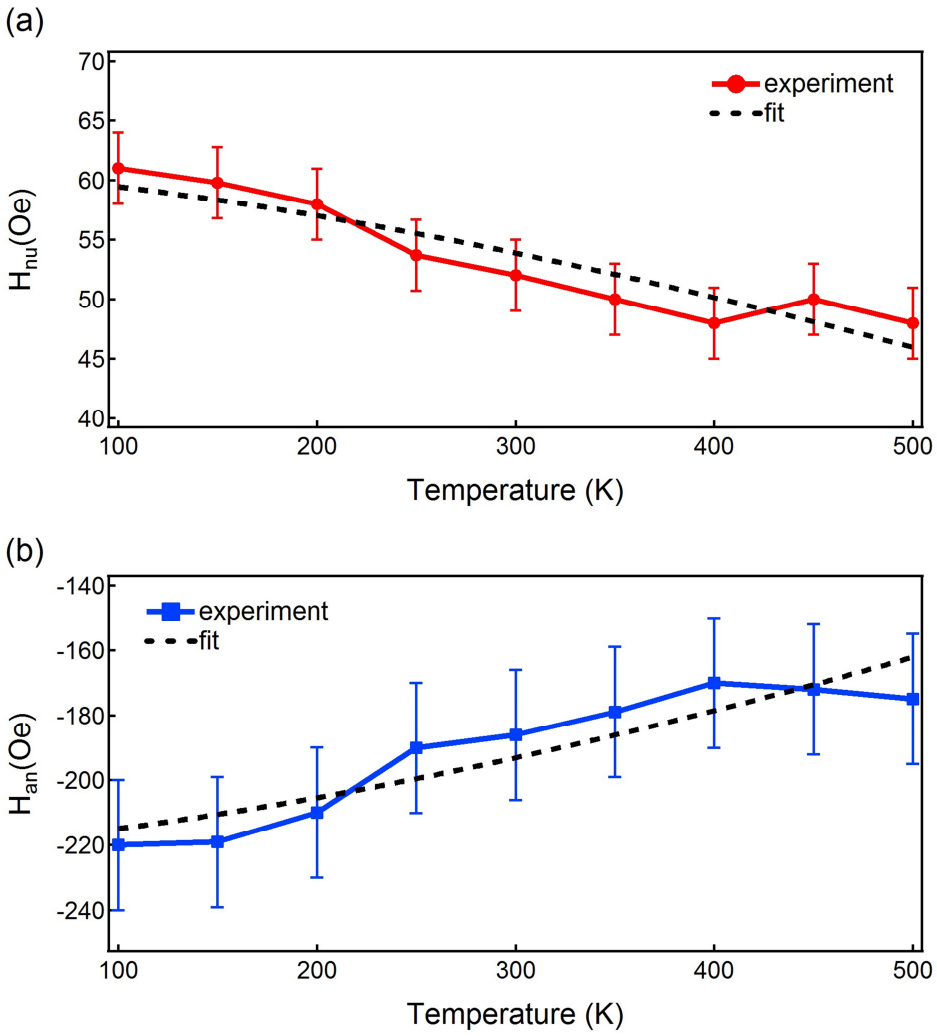

Figure 4.8: *Temperature dependence (a) of the nucleation field H_{nu}, and (b) the annihilation field H_{an} for Py caps with a diameter of about 330 nm and a thickness of 70 nm cf.* [128].

It is well known that the nucleation and the annihilation fields are proportional to the saturation magnetization [175]–[177]. According to Mihajlović *et al.*, the temperature dependence of the nucleation and annihilation fields can be described by the following relationship [175]:

$$H_{an,\,nu}(T) = H_{(an,\,nu)0}\left(1 - \alpha_{an,\,nu} T^{3/2}\right)$$

The fits are also shown in Figure 4.8 (dashed lines) with the corresponding fit parameters:

$$\alpha_{an} = (2.35 \pm 0.35) \times 10^{-5}\, K^{-3/2}, \text{ and } \alpha_{nu} = (2.18 \pm 0.29) \times 10^{-5}\, K^{-3/2}.$$

They are in accordance with reports from Mihajlović *et al.* who presented a comparable temperature behavior for vortices prepared on Py disks with a diameter of about 526 nm and a Py thickness of 50 nm.

As already mentioned, exchange coupling or even dipolar coupling between neighboring structures due to the dense packing of cap structures might influence the stability and consequently the nucleation process of magnetic vortices. Therefore, a correlation of the sense of rotation of the in-plane magnetization between neighboring caps in a lattice might be expected. To answer this question, we performed an investigation using full-field soft X-ray transmission microscopy of Py caps with a thickness of 50 nm under varying in-plane magnetic fields. Please note that the experimental technique works in transmission and, therefore, only materials that ensure a transition of a soft X-ray beam have been used [157]. In particular, the SiO_2 spheres have been replaced by polystyrene spheres with a comparable diameter of about 350 nm, and the substrate has been replaced by a silicon-nitride membrane with a thickness of about 100 nm for a sufficient transmission of the X-rays. In section 3.2.2.4 a short overview of the used MTXM setup is given. In this context, it should be underlined that due to the variation of the cap diameter, a variation of the nucleation and annihilation fields can be expected. In Figure 4.9 a series of magnetic images is presented, obtained under an angle of 30° relative to the projection of the in-plane magnetization. Here, the sample was first saturated in in-plane direction in a field of about 130 Oe, and afterward, several measurements have been carried out after gradual reduction of the field.

As can be seen, even after reducing the field to 120 Oe, we detect the onset of magnetic vortex nucleation. It should be noted that the bright respectively dark contrast on the caps result from the

projection of the Fe magnetization along the propagation direction of the circularly polarized light [128]. Thus, after vortex nucleation, it is possible to distinguish the sense of rotation of the in-plane magnetization. By further reducing of the field, more and more vortices start to nucleate.

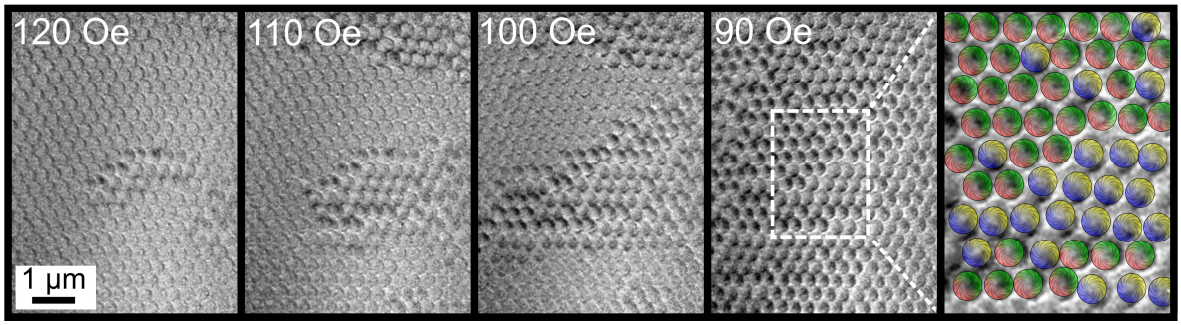

Figure 4.9: *High resolution MTXM images of a closely packed vortex lattice of permalloy caps formed by film deposition of a 50 nm thick Py film on polystyrene particles with a diameter of 350 nm. The images have been recorded at the Fe edge. On the right side a zoom in of the image recorded in a field of 90 Oe, revealing domain like areas with the same rotation sense of the in-plane magnetization. For a better distinction, the rotation sense is color coded (taken from* [128]*).*

Surprisingly, we do not detect individual and randomly distributed nucleation events over the whole sample, as might be expected. It seems that the nucleation process occurs mostly by domain wall propagation, which does not depend on the sense of rotation of the vortex. As can be seen, at a field of 90 Oe magnetic vortices have been nucleated in all cap structures and the magnetization does not change by further reducing the field up to the annihilation field. Therefore, it was possible to investigate the sense of rotation in detail. On the right image of Figure 4.9, a zoom in is shown for a better distinguishability, the different senses of rotations are color coded. It is easy to recognize that large connected areas exist exhibiting the same rotation sense.

In a further study of the coupling with increasing film thickness, we investigated a lattice of closely packed magnetic vortices by SMRM. As described in detail by Mitin *et al.* with an SMRM it is possible to image the perpendicular magnetic component in the vortex structure represented by the cores [165]. Furthermore, it is possible to apply a magnetic in-plane field and therefore it is possible to evaluate the sense of the in-plane rotation by using the rigid vortex model introduced in section 2.2.5. In particular, by comparing the remanence state where the cores are located in the

center of the particles with an image taken under an applied in-plane field (displaced cores), and extracting the difference in lateral core displacement the sense of rotation (circulation) of the in-plane magnetic moment configuration can be determined.

For this propose, we choose a field of about (160 ± 10) Oe, which is large enough to displace the core, however still far from the annihilation field of the vortex. As shown in Figure 4.10, we investigated a set of two samples, for which the diameter was kept constant to 330 nm and only the Py thickness was varied. The first investigated sample had a Py thickness of about 45 nm, which should be more or less comparable to the caps used for the MTXM study (reported above), and should clearly show magnetic vortices. To ensure a vast influence of the coupling between neighboring caps, we choose a Py thickness of about 130 nm for the second sample (see hysteresis curve presented in Figure 4.6). First, the samples were demagnetized, resulting in a randomly distributed polarity. The bright and dark regions located at the cap centers reveal directly the vortex cores, meaning a magnetization pointing *up* respectively *down*. As expected, no contrast is seen from the circulating in-plane magnetization. For a better understanding, the boundaries of some particles are marked, and the evaluated sense of rotation is color coded (Figure 4.10 (a) and (c)). In this study, we also analyzed if the samples show a preferred chirality caused by a polarity-circulation coupling expressed in a preferred polarity orientation for vortices. In that respect, we have found no evidence of a preferred chirality. However, to formulate a final statement better statistics are required. As shown in Figure 4.10 (b) and (d) we also evaluated the absolute core displacement resulted from a field of about (160 ± 10) Oe, including their directions of the displacement, as can be seen in the polar plot. The applied field direction was along the 0° direction. For the caps with a thickness of 45 nm, we detect a rather homogeneous distribution perpendicular to the applied field direction, shown in Figure 4.10 (b). For the caps with a Py thickness of about 130 nm, we found a much broader distribution with larger displacements. However, we assume that the stronger displacement can be traced back to the exchange coupling, which is much stronger for caps with a thickness of 130 nm in comparison to the 45 nm thick ones. Furthermore, the broader distribution of the displacement for the 130 nm caps can be explained due to strong exchange coupling, and therefore the displacement now also depends on the displacement of neighboring caps affecting each other. Furthermore, it must be taken into account that for the 130 nm Py caps, the magnetostatic coupling is increased as well.

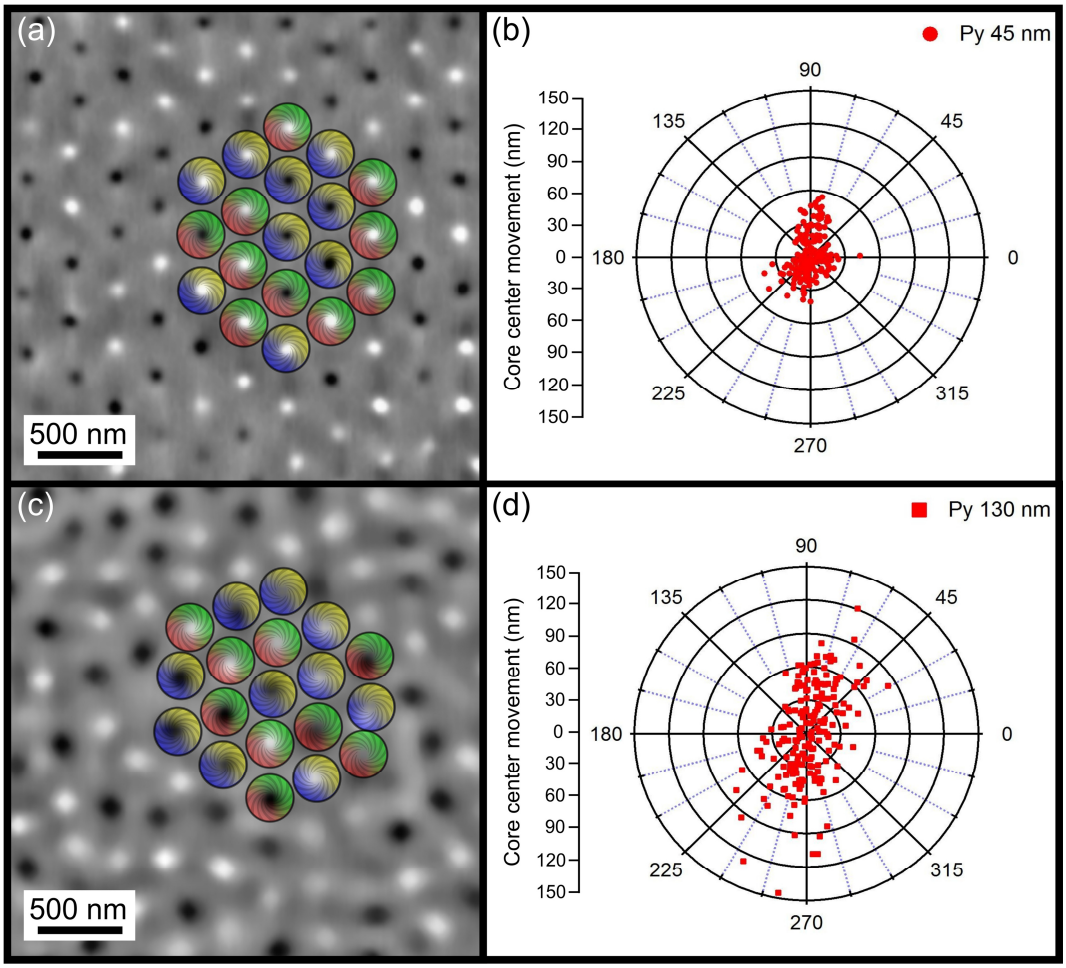

Figure 4.10: *SMRM investigations of closely packed Py caps with a diameter of about 330 nm and a thickness of (a) 45 nm and (c) 130 nm recorded in the demagnetized state. The bright and dark spots correspond to the magnetization orientation of the vortex. For a better indication the boundaries of some caps are marked and the sense of rotation is color coded. By comparing the lateral core positions with and without an external in-plane field of 160 ± 10 Oe, a pole-diagram was created for both samples (b, d), showing the lateral displacement of the cores mainly perpendicular to the applied field direction (along 0 degree direction), cf.* [128].

Furthermore, a comparison of Figure 4.10 (a) and (c) clearly reveals much larger cores for caps with a Py thickness of about 130 nm. We suppose that simply the increase of the thickness of the magnetic material is one reason for this. On the other hand, the lateral expansion of the core might be further caused by the specific geometrical surface of the cap. In particular, due to the geometric relation, the curvature of the Py surface will scale with the Py thickness.

However, also, the presence of more aligned *C* states might result in the weak contrast visible on some caps (see Figure 4.10 (c)). As mentioned above, we were not expecting pure vortex structures when looking at the corresponding hysteresis loop (cf. Figure 4.6). It seems that after saturating the sample in the in-plane direction and then reducing the field, a nucleation of out-of-plane vortex cores is initiated. Perhaps, the vortex structures occur in combination with some *C* states. This would also explain the obtained loop shape, and is in line with micromagnetic simulations reported recently by Sapozhnikov *et al.* [178].

4.4 MTXM study on Py cap arrays

In a further study, we investigated the magnetization reversal of closely packed Py caps with a thickness of 130 nm and a diameter of about 850 nm by MTXM. In this experiment, the images have been recorded at the Fe L_3 X-ray absorption edge. For the measurement, the sample has been mounted in out-of-plane geometry, while an in-plane field was applied. Consequently, in the vortex structures, the magnetic contrast only results from the vortex cores of the structures. In Figure 4.11 a series of images is shown. Starting from positive saturation at a field of 1500 Oe (Figure 4.11 (a)) all moments are aligned in the in-plane direction and no magnetic contrast can be seen. By reducing the field from 200 Oe to 100 Oe (Figure 4.11 (b), (c)), a displaced vortex core can be observed. For a better identification of the vortex cores, the dark cores, which correspond to a magnetization pointing up, are marked by red dotted lines, and the bright dots, corresponding to a magnetization pointing down, are indicated by white dotted lines. At remanence the cores are located in the center of the cap structures (Figure 4.11 (d)), as can be better seen in the line scan through the core of a vortex, shown in the inset of Figure 4.11 (d).

As expected, the cores are moving perpendicular to the applied in-plane field direction, as discussed in chapter 2.2.5. From the movement, the sense of rotation has been extracted and was visualized by adding an arrow.

In a further experiment, we measured several field cycles from positive to negative saturation and back to positive saturation. In Figure 4.12 a set of images is shown taken at saturation (a), (c), and (e). Here no magnetic contrast is obtained. Additionally, the corresponding images taken at remanence (Figure 4.12 (b), (d), and (f)) are shown, where vortices have been nucleated and appear in the center of the cap. Surprisingly, after the annihilation of the magnetic vortex and saturating the sample in the opposite in-plane direction, at remanence the vortices reveal a reversed polarity and sense of rotation, preserving its chirality, indicating a possible coupling of the polarity and sense of rotation. We observed this behavior for all vortices imaged on a large area (100 x 100 μm^2), whereas overall no preferred orientation of polarity and sense of rotation was found.

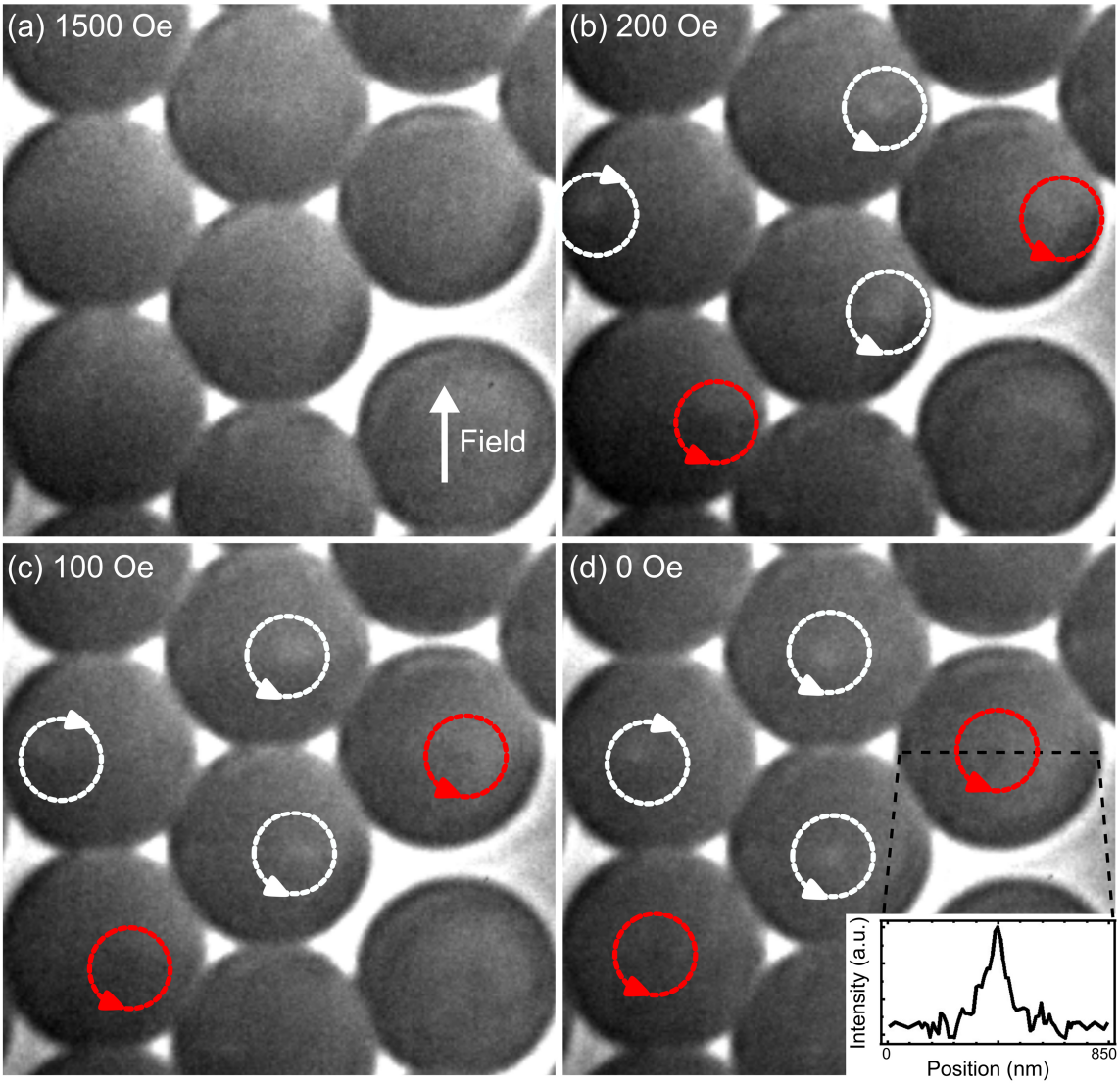

Figure 4.11: *MTXM images of 130 nm permalloy caps on polystyrene particles with a diameter of 850 nm measured in the out-of-plane geometry by applying an in-plane field. The images have been recorded at the Fe L_3 X-ray absorption edge. The inset in (d) shows a line scan through the core of a vortex.*

Up to now, we did not find an explanation for this behavior. One could argue that this behavior is due to direct exchange coupling of the individual cap structures with their neighbors as the Py film is rather thick.

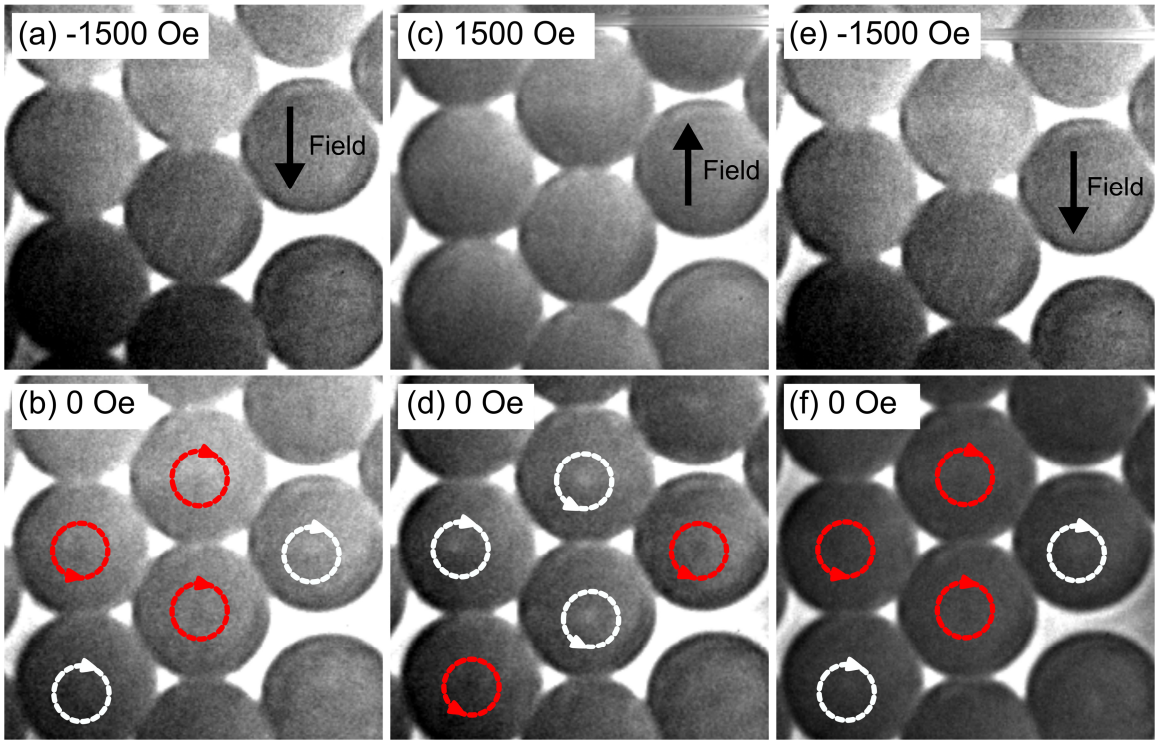

Figure 4.12: *Series of MTXM images measured, in out-of-plane geometry of permalloy caps formed by film deposition of a 130 nm thick Py film on polystyrene particles with a diameter of 850 nm. Recorded at saturation (a), (c), and (d), and afterward at remanence at the Fe L_3 edge.*

4.5 Conclusion

In conclusion, we have investigated Py cap structures formed on arrays of densely packed particles showing a magnetic vortex, where the magnetization is forming an in-plane flux closure structure to minimize the magnetostatic energy. In addition, in the center, a vortex core occurs where the magnetization is pointing perpendicular to the disk plane as a result of minimizing the exchange energy.

In the first study, we focused on the out-of-plane component of the vortex structure, the so-called core of the magnetic vortex. We showed that it is possible to influence the core polarity by applying an out-of-plane field for various Py thicknesses. In particular, we performed an in-field out-of-plane MFM study on Py caps with a thickness of 70 nm and a diameter of about 330 nm in the demagnetized state (core polarization randomly distributed). We showed that by applying a global out-of-plane field the cores pointing parallel to the applied field are getting simply enlarged. Whereas, for the cores pointing antiparallel with an increasing field an enlargement can also be detected, but it seems that in this case the elongation is composed of a shift of the cores to the edge of the particle, and an additional growing region pointing in the direction of the applied field. One could argue that the archived shifting is a result of an interaction of the in-plane circulation with the applied field in combination with the particular topology of a cap structure. However, we demonstrated that after removing the field the polarization remains, meaning that the polarity of the vortices had successfully been switched. Furthermore, we showed for a lattice of closely packed Py caps with a thickness of 45 nm and a diameter of 330 nm that it is possible to switch the polarity of a vortex individually by applying a local out-of-plane field pulse, using SMRM. Here, we observed a field threshold for a successful switching event. Surprisingly, for a successful *up*-to-*down* reversal a higher field of about 3.8 kOe had to be applied, in contrast to the *down*-to-*up* reversal where only a field of 3.3 kOe had to be applied for a successful switching was required [164].

One could argue that the difference results from magnetostatic coupling due to the magnetic environment given by the dense packing of the cap structures [172], [173], or even due to direct exchange coupling via the contact point between touching neighboring caps. As discussed by

Streubel *et al.* in detail the magnetic exchange coupling can result in frustration in the lattice of vortex structures [127] also affecting the vortex cores [164].

In the second study, we investigated the coupling of magnetic cap structures with a diameter of about 330 nm. The structures couple via the in-plane components of the magnetization at the contact area of neighboring cap structures. In the first part, we investigated the magnetization reversal of a magnetic lattice for various Py thicknesses by MOKE magnetometry. We could show that a minimum Py thickness of about 30 nm is required to stabilize a magnetic vortex in the cap structures. Surprisingly, below a thickness of 60 nm, a reverse field is needed to nucleate a vortex. It is demonstrated that by increasing the Py thickness up to a critical thickness of 90 nm the nucleation and annihilation field increases, and the vortex is stable over a broader field range. It seems that above 90 nm strong coupling occurs indicated by a transition to a different magnetic configuration, however still containing a vortex core. At a Py thickness close to the diameter of the caps, the hysteresis loops of a flat film, and of the cap array are difficult to distinguish, meaning that caps are fully coupled, and the curvature has only a minor influence. Furthermore, it is demonstrated for caps with a Py thickness of 70 nm that lowering the temperature results in a further stabilization of the vortex structures.

One could argue that the increase of the nucleation field gives an indication of the onset of exchange coupling between adjacent caps. Therefore, in a lattice of closely packed cap structures the nucleation process itself was directly imaged by means of MTXM. The study clearly confirmed that nucleation does not occur by individual and randomly distributed nucleation events but arises via domain wall propagation, due to exchange coupling of the caps [128]. Furthermore, we also investigated the rotation sense of the reversed areas. Surprisingly, we found rather large domain like areas with the same in-plane rotation sense, but no individual particles surrounded by particles with the opposite rotation were observed. Additionally, we found no indication of frustration as assumed by Streubel *et al.* [127].

In a further study, the coupling of the Py cap structures with increasing Py thickness and the possible influence of the magnetic vortex state was investigated by SMRM to image the lateral core displacements under an in-plane field of about 160 Oe. Surprisingly, caps with increased Py layer thickness reveal spatially enlarged vortex cores and a broader displacement distribution. We believe that the expansion of the cores is simply caused by the specific geometrical surface of the

spheres. Therefore, the specific curvature of the cap scales with the Py thickness resulting in an enlarged core. However, here it should be mentioned that the displacement distribution depends on the displacement of neighboring caps, which are affecting each other. In addition, the presence of some mixed states, vortices and *C* states, is indicated for the array with the thickest Py layer [128].

In a further study, we could show by MTXM that for rather thick Py caps with a thickness of about 130 nm and a diameter of about 850 nm a chirality coupling in the individual structures exist. In particular, we found, that all vortices show an individual coupling of their polarity to their individual rotation sense, whereas overall no preferred coupling of a polarity to the sense of rotation was found. However, up to now, we found no final explanation for this phenomenon, one could only argue that it results from the special magnetic environment or a possible direct exchange coupling of the cap structures with their neighbors.

5 EXCHANGE-BIASED CAP STRUCTURES[5]

As already discussed in chapter 1, magnetic vortices are a hot topic in current research partly because they are promising building blocks in spintronic devices, ultrafast circuits, high-performance memories or for sensor applications. However, for a certain application, it might be required to control the polarity and circulation of a vortex. It has been shown that in a vortex lattice the core can be switch individually by a magnetic recording head of a hard disk drive [164]. The rotation sense can be restricted for instance by the shape of the structure [169], [179], [180]. However, an elegant approach to systematically modifying the magnetic properties of a nanostructure, showing a magnetic vortex, is based on the exchange bias (EB) effect [181].

In this regard, magnetization reversal of exchange biased permalloy FM (Py)/AF (IrMn) disk structures was investigated in detail by several groups [109], [114], [115]. It has been shown that by zero field cooling (ZFC), a circular exchange bias is induced as a result of imprinting the vortex configuration of the ferromagnet into the AF IrMn [107], [111], [114], [130].

By doing so, the nucleation and annihilation fields of the magnetic vortex could be drastically enlarged. For field cooling of a magnetic disk structure, it has been shown that the magnetization reversal can occur via formation of a spread vortex structure with a shifted hysteresis loop [111]. Furthermore, it was reported that the EB effect can also be utilized to systematically influence the rotation of the in-plane circulation direction in asymmetric FM/AF/FM ring structures [110], [111].

[5] Please note that the results presented in this section are already published: S. Thomas, **D. Nissen**, and M. Albrecht, *Temperature dependent magnetization reversal of exchange biased magnetic vortices in IrMn/Fe microcaps,* Appl. Phys. Lett. **105**, 022405 (2014) [130], and **D. Nissen**, O. Klein, P. Matthes, and M. Albrecht, *Magnetization reversal in exchange-biased Py/CoO vortex structures, Phys. Rev. B (accepted)*

Beyond, it has been shown that the magnetization reversal shows a strong dependency on the direction of the applied cooling field relative to the measurement geometry [109], [113]–[115]. In particular, for different measurement angles with respect to the applied cooling field the magnetization reversal occurs either via the formation of a vortex state or even by coherent rotation. Furthermore, this angle can be adjusted by the applied cooling field [109]. Thereby, the rough guideline holds that for a measurement direction perpendicular to the direction of the applied cooling field, the magnetization reversal occurs via coherent rotation, whereas for a parallel measurement geometry a magnetization reversal takes place via formation of an exchange biased vortex [106], [107], [109], [114]. However, in the present study the applied cooling field was always parallel to the measurement direction, therefore a reversal via formation of a vortex is expected. In the following section, some models describing the magnetization reversal in exchange biased ferromagnetic / antiferromagnetic structures will be discussed. Furthermore, the temperature can also be used to influence the magnetization reversal of exchange biased magnetic vortex structures. In this regard, it should be mentioned that the temperature dependence of exchange biased disk structures has been investigated intensively. For instance, the magnetization reversal of Fe/FeF_2 structures has been measured at different temperatures [182]. In this work, it was shown that the vortex state formation leads to a smaller exchange bias when compared to that observed in continuous thin films [130]. Recently, Mihaijlovic *et al*. investigated the temperature dependence of the magnetization reversal of Py structures, suggesting that at rather low temperatures the vortex nucleation, as well as the annihilation processes are governed by thermal activation processes [175], whereas, most probably at elevated temperatures the magnetization reversal is determined by the temperature dependence of the saturation magnetization [183], [184].

Of special interest is also the distribution of the blocking temperature of the AF. In particular, we showed that in exchange biased IrMn/Fe caps, the vortex spin configuration at zero magnetic field destabilizes as the temperature approaches the blocking temperature of the AF [130]. Whereas, by further increasing the temperature, the antiferromagnetic ordering deteriorates and a restabilized vortex state was found. Surprisingly, for our Py/CoO system, we observe a different behavior.

5.1 Reversal modes in EB vortex structures

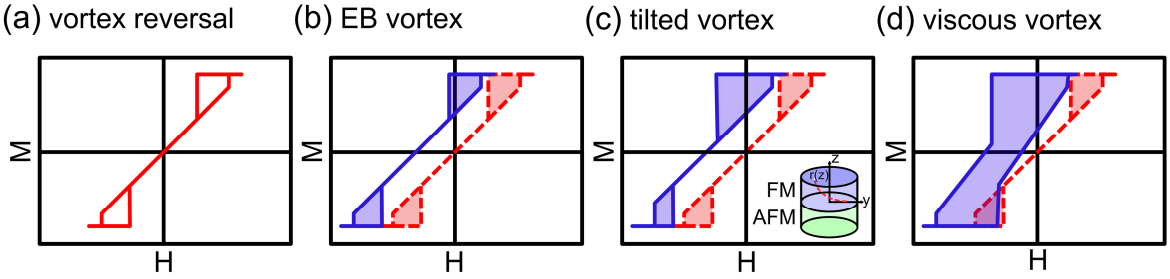

Figure 5.1: *Schematic sketch of a hysteresis loop of an (a) unbiased vortex, (b) classically exchange biased vortex, (c) tilted vortex plus a sketch of an EB disk system including the tilted core in the inset* [115]*, and (d) a viscous distorted vortex inspired from* [117].

As shown in Figure 5.1, there are mainly three reversal modes of EB vortex structures, which have to be distinguished, [117]: The exchange biased vortex, the titled vortex, and the viscous vortex. In Figure 5.1 (a) a sketch of a classical symmetric vortex hysteresis curve is shown. A description of the magnetization reversal process via formation of a magnetic vortex is given by the rigid vortex model (cf. section 2.2.5). In Figure 5.1 (b) a sketch of a so-called EB vortex structure is depicted (blue line) together with the shape of an unbiased vortex structure (red dashed line) for comparison. Characteristic for this case is an equal biasing of the nucleation (H_{NU}) and annihilation fields (H_{AN}), resulting in a shifted exchange bias field (H_{EB}) but a still symmetric hysteresis curve. By defining the variables $\Delta H_{NU} = H_{NU}^{+} + H_{NU}^{-} - 2H_{EB}$, and $\Delta H_{AN} = H_{AN}^{+} + H_{AN}^{-} - 2H_{EB}$, it is possible to formulate specific requirements for an EB vortex [117]:

$$\Delta H_{NU} = \Delta H_{AN} = 0, \text{ and } H_{EB} \neq 0$$

Figure 5.1 (c) shows a schematic hysteresis loop for a ferromagnetic structure without EB (red dashed line) and for EB structures (blue line) where the magnetization reversal takes place via formation of a tilted vortex [115]. It has been shown that contrary to classically exchange biased

vortices, where a straight core is assumed, in this case, the cores are tilted along the film thickness [117].

In particular, for the biased loop, the shifts of the annihilation fields are different for each branch, resulting in asymmetries of the irreversible parts of the hysteresis in addition to the overall displacement due to exchange bias [115]. This reversal behavior can be explained under the assumption of nonuniformity of the magnetization along the FM film thickness, whereby the EB is represented as a strongly localized interfacial exchange field. In particular, the competition between different magnetic energies enables the core position to vary throughout the layer (depth dependence), resulting in a tilt of the vortex core [115]. A schematic of the exchange biased vortex system is shown in the inset of Figure 5.1 (c); here the red dashed line denotes the depth dependence of the vortex core position r(z), cf. Gusilenko *et al.* [115]. Consequently, for the magnetization reversal via formation of a tilted vortex, it can be concluded:

$$\Delta H_{NU} = 0, \Delta H_{AN} \neq 0, \text{and } H_{EB} \neq 0$$

More recently for exchange biased AF/FM disks with a rather thick FM layer the reversal via formation of a so-called distorted viscous vortex was introduced by Gilbert *et al.* [117] (see Figure 5.1 (d)). In contrast to the previously discussed magnetization reversal mechanisms, the vortex is distorted at the immediate surroundings of the FM/AF interface and additionally dragged due to uncompensated spins of the AF layer. This promotes an asymmetry of the characteristic nucleation and annihilation fields [117]. The effect is particularly favored for thin AF layers due to the weak magnetic anisotropy, therefore the observed spin dragging results in an enhanced coercivity but without loop shift [117], [185]. However, for larger AF layer thicknesses, the anisotropy is large enough for the spins to maintain their orientation during the reversal [89], [117]. For an intermediate layer thickness, a mixture of spin dragging with an overall EB effect is expected. However, the whole reversal process leads to a strongly asymmetric hysteresis curve. For the reversal via formation of a distorted viscous vortex, it can be concluded:

$$\Delta H_{NU} \neq 0, \Delta H_{AN} \neq 0, \text{and } H_{EB} \neq 0$$

5.2 Sample preparation

As already mentioned in chapter 3.1, for nanostructuring large arrays of spherical SiO_2 particle monolayers were prepared by a self-assembly process [121]. For these studies, we used particles with a diameter of about 900 nm. Afterward, the closely packed silica spheres act as a template for the deposition of soft magnetic materials. On top, Fe or Py layers were grown by DC magnetron sputtering, forming cap structures, which exhibit a magnetic vortex [17], [18], [127]–[130]. On top of the FM cap, an AF was deposited. Thus a, rather complex exchange bias system is formed, due to the fact that the cap thickness decreases gradually along the surface of the sphere, obeying $t(\theta) = t_0 \cos(\theta)$ [125], [126] (see Figure 3.1).One could argue that this will have some influence on the EB effect as it scales inversely with the FM thickness and also depends on the thickness of the AF layer.

In one study, we produced cap structures consisting of Fe(4 nm)/IrMn (5 nm) bilayers. In another study, we used CoO as AF. Here, on top of the Py caps with a thickness of 50 nm, a 1 nm thick Co layer was deposited followed by oxidation to CoO under ambient conditions at room temperature for 3 hours. This procedure has been repeated to increase the CoO thickness. On top, a 5 nm thick capping layer was deposited to protect the systems from further oxidation. For the Fe/IrMn system, we utilized a thin Pt layer, and for the Py/CoO system, we used Ta.

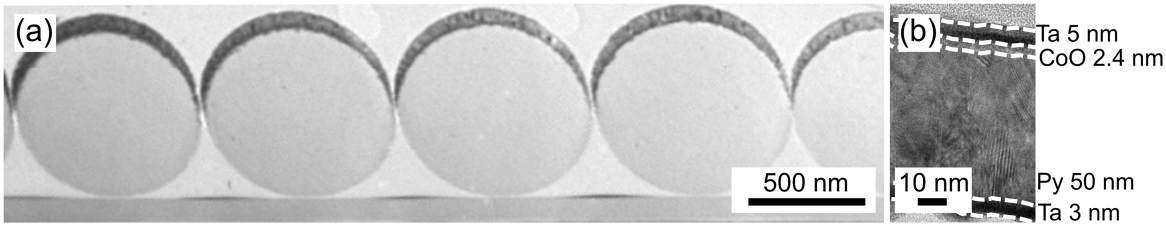

Figure 5.2: *(a) TEM bright field image (cross section) of Py(50 nm)/CoO(2.4 nm) caps formed on a densely packed monolayer of 900 nm silica particles. (b) Corresponding high resolution TEM image of an individual cap structure clearly revealing the deposited layer stack on top of the particle.*

In Figure 5.2 (a) a typical bright field TEM cross section image of a closely packed particle array capped by a Ta(3 nm)/Py(50 nm)/CoO(2.4 nm)/Ta(5 nm) system is shown. A corresponding high-resolution section of an individual cap structure is presented in Figure 5.2 (b), clearly revealing rather sharp interfaces and the polycrystalline structure of the Py layer.

5.3 Py/CoO caps: Results and discussion

In a first study, we investigated the magnetization reversal of Py/CoO cap structures for various CoO thicknesses. Figure 5.3 shows SQUID hysteresis loops of a Py(50 nm)/CoO(1.3 nm) cap array taken at 300 K (red line), respectively at 2 K (blue line) after zero field cooling (ZFC). At 300 K, which is above the Néel temperature of CoO, we achieved symmetric loops, revealing the nucleation (H_{NU}) and annihilation fields (H_{AN}) of the vortex state without any indication of an influence of the AF. We assume that the sharp reversal process close to remanence might result from direct magnetic exchange coupling of neighboring structures, this would be in line with recent reports from Hernandez *et al.* who obtained similar loop shapes for chains of connected disks showing a vortex [186]. A comparison of the two loops shows at 2 K an increase of the nucleation and annihilation fields while no loop displacement is observed. In particular, the behavior can be explained by imprinting the spin structure of the Py into the AF CoO while lowering the temperature to 2 K and crossing the Néel temperature [108], [111]. For a magnetic vortex as ground state, this spin structure will be imprinted into the AF and consequently lead to the stabilization of the vortex configuration.

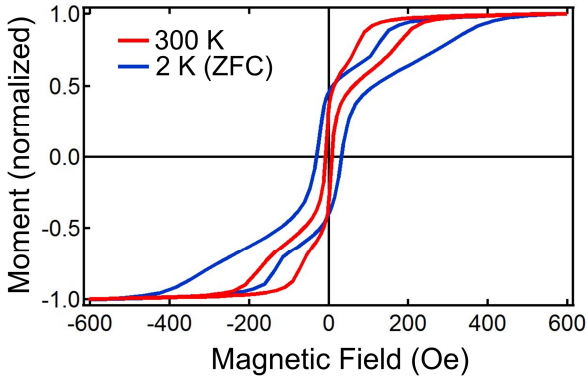

Figure 5.3: *In-plane SQUID hysteresis curves of a Py(50 nm)/CoO(1.3 nm) cap array measured at 300 K, as well as at 2 K after zero field cooling.*

As shown in Figure 5.4, an entirely different behavior is observed for the hysteresis curves of the same sample recorded at 2 K after field cooling in a field of 1 kOe (see Figure 5.4 (a)), respectively -1 kOe (Figure 5.4 (b)). Here, the expected shift of the hysteresis curves opposite to the cooling field direction is observed [89], [90]. Additionally, the first hysteresis loop shows a

strong asymmetry. In particular, the first descending branch, coming from saturation, reveals a remanence of almost full magnetization, indicating a magnetization reversal via formation of a single domain state or *C* state [83]. We assume that a single domain like configuration is imprinted into the CoO layer during the cooling process. Nevertheless, by loop cycling the sample, a strong training effect is observed. The strongest effect is already visible in the second loop, where the decreasing branch already indicates a reversal via formation of a magnetic vortex. For a better visualization, black arrows are included in the figures. The training brings the system back to a more symmetric loop shape, indicating a reversal via formation of a vortex. Therefore, the loops after cycling are very similar to the one obtained by ZFC (see Figure 5.3), although a small loop shift remains. However, it is widely recognized that the exchange bias effect is based on pinned uncompensated spins at the FM/AF interface, giving rise to a loop shift [34]. It is likely that due to the cooling field, which is larger than the annihilation field of the vortex, these uncompensated spins orientate along the direction of the cooling field. Due to loop cycling, most of these spins get rearranged following the spin configuration of the vortex, which results in a displaced vortex state. However, it should be noted that, even after training, the loop still reveals a small horizontal loop shift opposite to the cooling field direction.

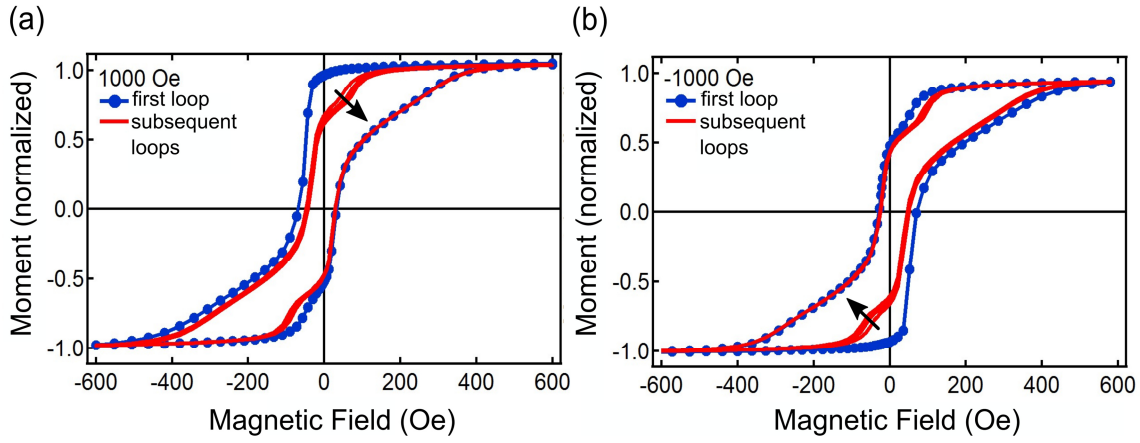

Figure 5.4: *In-plane SQUID hysteresis curves of a Py(50 nm)/CoO(1.3 nm) cap array recorded at 2 K after field cooling in a field of 1 kOe (a), and -1kOe (b). The arrows highlight the asymmetry in the first loop.*

The reversal mechanism was further investigated as a function of the applied cooling field, and additionally in dependence of the CoO layer thickness. In Figure 5.5 a set of SQUID hysteresis loops are presented also taken at 2 K after field cooling from room temperature in various fields,

for Py/CoO samples with various CoO layer thicknesses. We assume that for cooling fields larger than the vortex annihilation field, the spins of the ferromagnetic Py cap are following the applied in-plane field direction and therefore during the field cooling procedure a single domain spin structure is imprinted into the antiferromagnetic CoO. This effect was indeed observed for all samples.

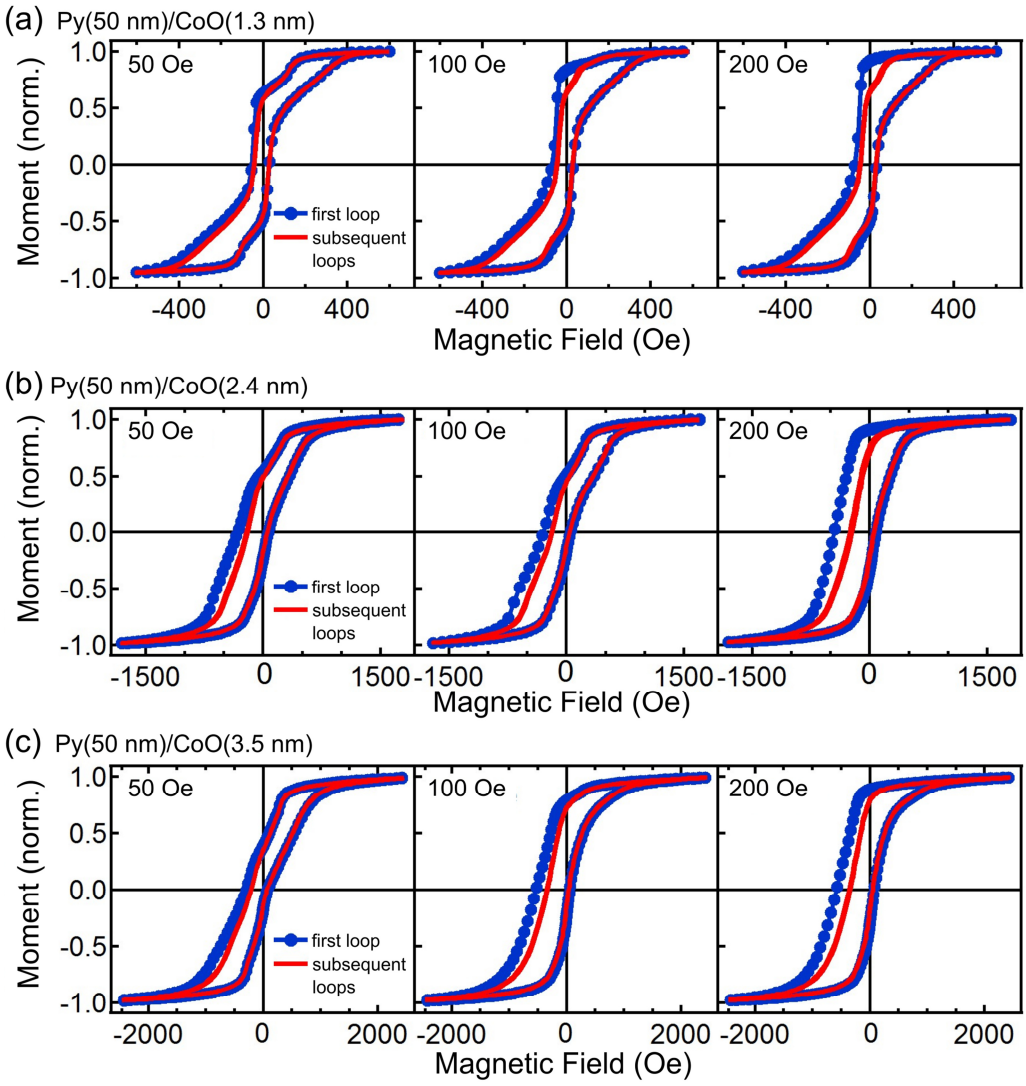

Figure 5.5: *In-plane SQUID hysteresis curves of Py(50 nm)/CoO(1.3 nm (a); 2.4 nm (b); 3.5 nm (c)) cap, measured at 2 K after FC in external fields of (50 Oe; 100 Oe; 200 Oe) from 300 K. The first loop (blue dots) and subsequent loops up to the fifth cycle (red lines) are presented.*

Surprisingly, the shape of the hysteresis loops is quite different for these samples. In particular, a

strong AF thickness dependency is observed. For cooling fields of 200 Oe for cap structures with a CoO thickness of about 1.3 nm a vortex like reversal can be primarily observed, which gets even more pronounced after training. However, for CoO thicknesses of 2.4 and 3.5 nm a strong training effect is also observed with no change of the overall loop shape and no reversal via formation of a magnetic vortex.

In general, it seems that during the field cooling procedure the initially imprinted single domain state is further stabilized for thicker CoO layers. For field cooling in an applied field of about 100 Oe, a displaced vortex should be imprinted into the AF and a different reversal behavior is expected. As can be seen for all samples, a drastically reduced remanence magnetization is already observed in the first loop, mostly visible for the caps with a CoO thickness of about 2.4 nm (Figure 5.5 (b)). With a cooling field of 50 Oe, it was possible to imprint only slightly displaced vortices into the antiferromagnetic CoO. Consequently, for all thicknesses, we detect a magnetization reversal via nucleation and annihilation of a magnetic vortex displaced opposite to the cooling field direction. Please note that for all CoO thicknesses a strong training effect even after the first loop is found, which is closely linked to a reduction of the loop shift.

However, by further loop cycling no significant change of the EB field could be observed. Contrary to the so-called “thermal” training, where thermally activated magnetization processes take place during loop cycling [101], this effect is referred to as “athermal” training [187], [188]. For more detailed analysis, the exchange bias field has been evaluated as function of cooling field and thickness of the antiferromagnetic CoO layer for trained and untrained loops; the results are shown in Figure 5.6 (a)-(c). As expected, we achieve a maximum EB field for cooling fields larger than the annihilation field of the magnetic vortex.

However, no significant changes of H_{EB} could be detected between cooling fields of 200 Oe, which is very close to the annihilation field of the magnetic vortex at 300 K, and cooling fields of about 1 kOe. This can be explained by the fact that after annihilation all spins are already aligned in the in-plane direction during field cooling and this configuration is imprinted into the AF, consequently higher fields do not change the spin configuration further during field cooling.

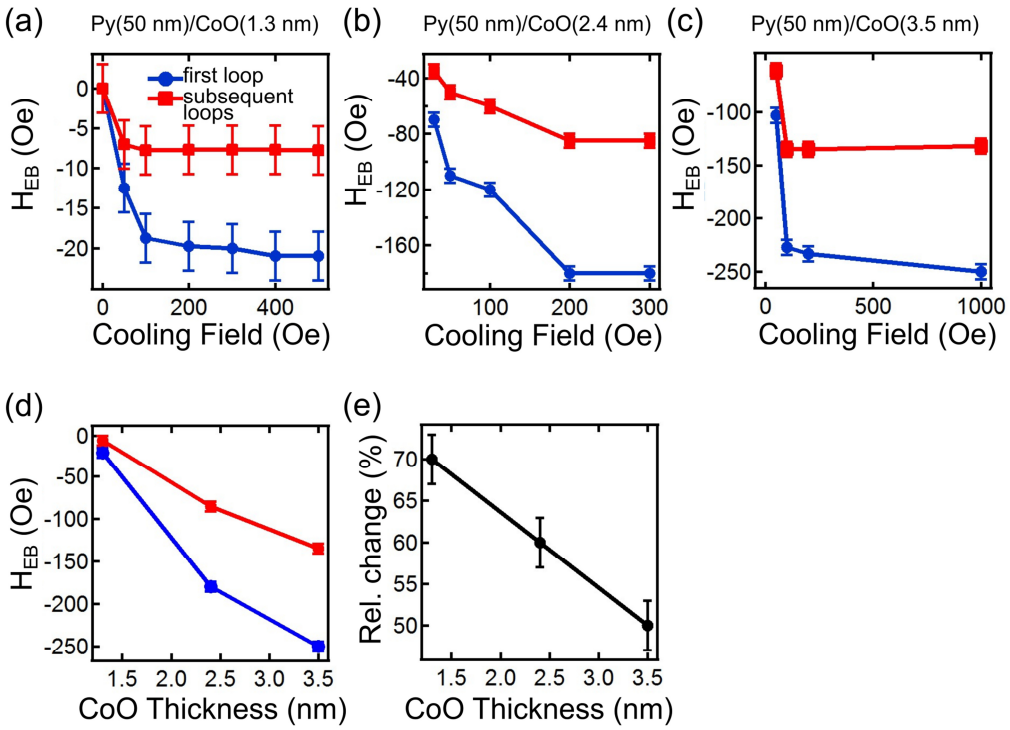

Figure 5.6: *(a-c) Cooling field dependence of the exchange bias field H_{EB} for Py(50 nm)/CoO(1.3; 2.4; 3.5 nm) samples. (d) Corresponding H_{EB} as function of CoO layer thickness extracted at 2 K after field cooling in an external field of 200 Oe. H_{EB} was extracted from the first loop (blue), and from a trained loop after the fifth cycle (red). (e) Calculated relative change of H_{EB} as function of CoO layer thickness.*

Furthermore, a detailed analysis of the exchange bias field as function of CoO layer thickness after field cooling in saturation (200 Oe) has been performed. For this, H_{EB} has been extracted from the first loop, as well as after training. As shown in Figure 5.6 (d), we observed an obvious increase of H_{EB} with increasing AF film thickness. Additionally, we also evaluated the relative change of H_{EB} due to the training effect (see Figure 5.6 (e)). Here, we observed that the relative change increases with decreasing CoO thickness. One assumption to explain this effect is that thicker CoO layers offer more thermal stability to the domain structure formed in the antiferromagnetic CoO and consequently we get a smaller training effect. However, this behavior is in conformity with other experimental results [189]–[193], as well as theoretical predictions based on an atomistic model [194].

Following this approach for cooling fields of 50 Oe, a slightly displaced vortex core is imprinted

into the AF. Therefore, in the following, the magnetization reversal of such systems will be discussed for all CoO thicknesses, determined from magnetometry measurements at 2 K after training. It is well accepted that after loop cycling (training process) pinned uncompensated spins are aligned along the cooling field direction, in contrast to the unpinned spins, which might follow the vortex configuration given by the FM. Furthermore, one can assume that the influence of the EB, which is acting on the interface between the FM and AF, gets much weaker with distance in the FM layer. As a result, for EB structures showing a vortex, it can be assumed that the vortex core gets centered more further away from the interface, resulting in a tilted vortex core.

This effect of a vortex core tilt in exchange biased disks has already been analytically described by Guslienko and Hoffmann [115], [116] (cf. section 5.1). Moreover, the so-called distorted viscous vortex reversal with characteristic asymmetries in the nucleation and annihilation fields was introduced very recently by Gilbert *et al.* [117] (see section 5.1). For this reason, ΔH_{NU} and ΔH_{AN} have been extracted and summarized in Figure 5.7 for various CoO thicknesses after field cooling in a field of 50 Oe. From here, the reversal mechanism can be clearly categorized to exchange biased vortices with magnetization reversal via formation of a distorted viscous vortex (see Figure 5.7). However, the effect is much more noticeable for thicker CoO layers, because thicker CoO layer provides stronger exchange coupling to the FM, resulting in a stronger tilt of the vortex core.

In this context, one should also consider the presence of a strong variation of the coupling strength along the curved cap structure. This effect will be particularly noticeable at the rim of the particle surface. However, here the vortex core nucleates and annihilates which makes it to a rather complex system. Consequently, this might have a large impact on the observed asymmetry in the magnetization reversal process.

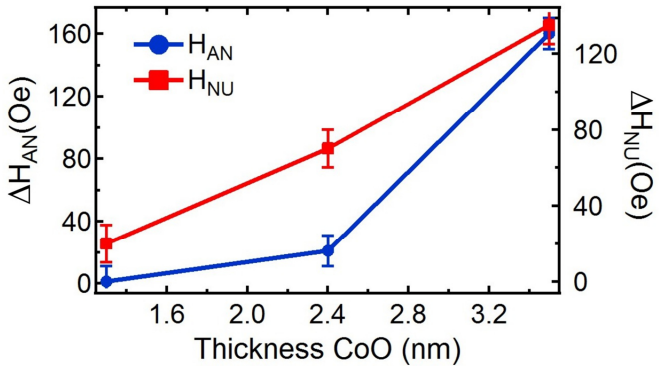

Figure 5.7: *ΔH_{NU} and ΔH_{AN} as function of CoO thickness for Py(50 nm)/CoO(1.3; 2.4; 3.5 nm) caps. The values are extracted at 2 K from trained loops after field cooling (50 Oe) from 300 K.*

As already mentioned, the highest effect appears for thick CoO layers. Therefore, in a further study, we investigated the temperature dependence of Py(50 nm)/CoO(3.5 nm) cap structures, providing a high thermal stability of the antiferromagnet. In particular, in Figure 5.8 we present hysteresis curves taken after field cooling from room temperature in a field of 1 kOe (left column) in comparison to curves taken after zero field cooling (right column), for various measurement temperatures. Please note that all presented curves are taken after loop cycling. For the field cooled structures, we observe a rather continuous transition from an in-plane state towards an imprinted *C* state and further to an imprinted displaced vortex state with increasing temperature. As presented, the onset of exchange bias starts below 160 K followed by an increase of H_{EB} with decreasing temperatures (see Figure 5.9 (a)). Whereas, as expected after ZFC, we detect the stabilization of the vortex structure due to imprinting of the vortex spin structure into the AF. This effect is more pronounced at lower temperatures.

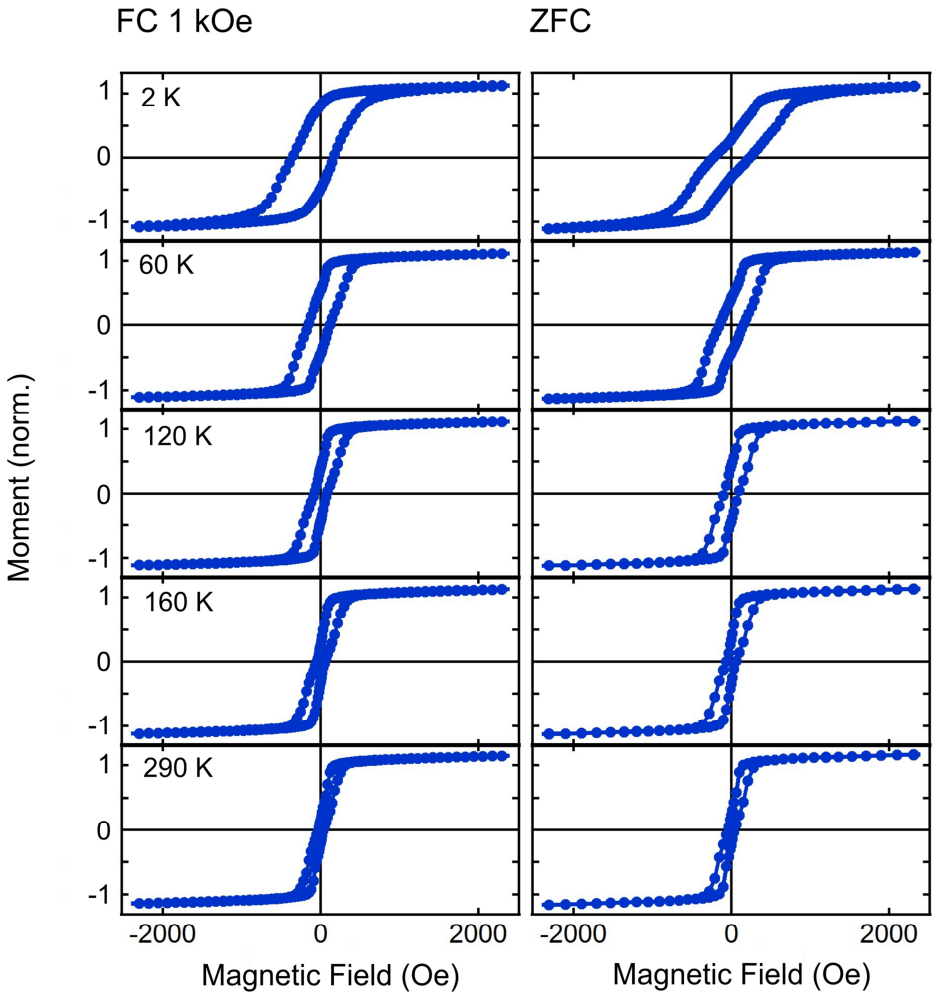

Figure 5.8: *In-plane SQUID hysteresis curves of Py(50 nm)/CoO(3.5 nm) caps recorded at different temperatures after field cooling in a field of 1 kOe (left column), and zero field cooling (right column).*

The obtained temperature behavior of H_{EB} (Figure 5.9 (a)) is directly linked to the grain size distribution and thermal stability of the AF. This would be in line with the recent work of Fernandez-Outon *et al.* [187], where the effect of a thermal instability in exchange biased materials is discussed in detail and attributed inter alia to the grain size distribution in the AF layer and its thermal stability. To obtain a deeper understanding of the thermal stability, we analyzed the blocking temperature distribution for all CoO thicknesses following a measuring procedure reported by Bollero *et al.*, and Guhr *et al.* [195], [196]. In this routine, the samples were first field cooled from 300 K down to 2 K in a field of - 200 Oe to set the exchange bias,

followed by a reversal of the field to + 200 Oe and heating up to a certain annealing temperature.

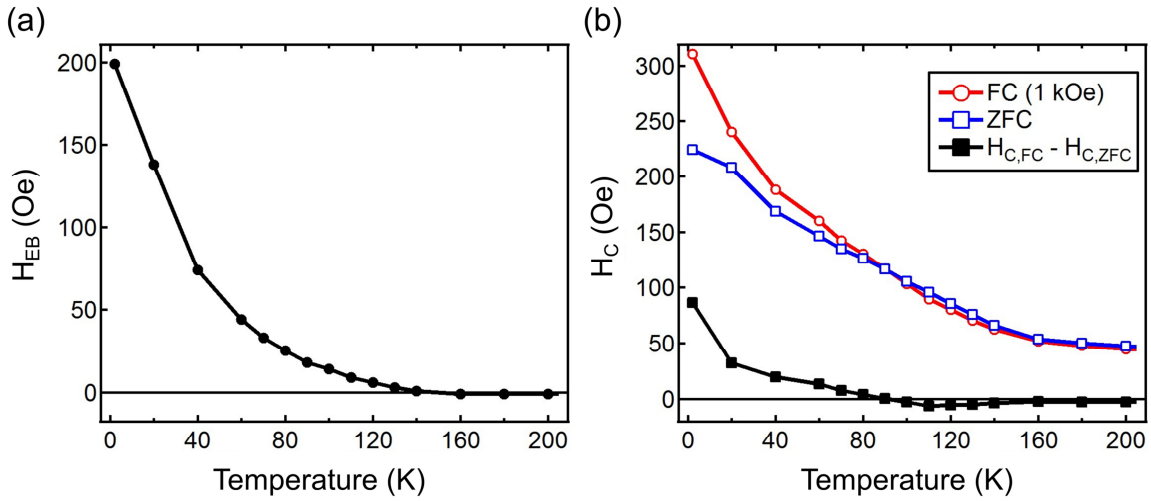

Figure 5.9: *(a) Temperature dependence of H_{EB} of Py(50 nm)/CoO(3.5 nm) caps extracted after field cooling from SQUID hysteresis curves. (b) Corresponding temperature dependence of the coercive field after zero field cooling (blue square) and field cooling (red dot). Additionally, the difference of these curves (black solid squares) is included. Please note that H_{EB} and H_c shown here have been extracted from trained loops after the third cycle.*

Afterward, the samples have been cooled down to 2 K in an applied field of + 200 Oe and hysteresis curves have been measured. From the obtained *M-H* loops, H_{EB} has been extracted. In Figure 5.10 (a) the dependence of H_{EB} on annealing temperature, normalized to the initial H_{EB} value taken at 2 K, is shown for all CoO thicknesses. As expected, we obtained a gradual reduction of H_{EB} with increasing annealing temperature up to a certain temperature where a loop shift could no longer be detected, and consequently, EB has vanished. This critical temperature is associated with the mean blocking temperature T_B. An evaluation of T_B for all CoO thicknesses is presented in the inset of Figure 5.10 (a). However, further increase of the annealing temperature leads to a negative shift and consequently a sign change of H_{EB}.

The transition proceeds over a rather broad temperature range, which can be attributed to the mean blocking temperature distribution of the AF layer. In this context, it can be noted that with increasing CoO layer thickness this distribution is getting even broader. The switching field distribution is shown in Figure 5.10 (b). However, a detailed look at the caps with a CoO

thickness of 3.5 nm reveals that for a temperature of about 160 K the exchange bias is entirely reversed, which is in line with the temperature series of H_{EB} presented in Figure 5.9 (a).

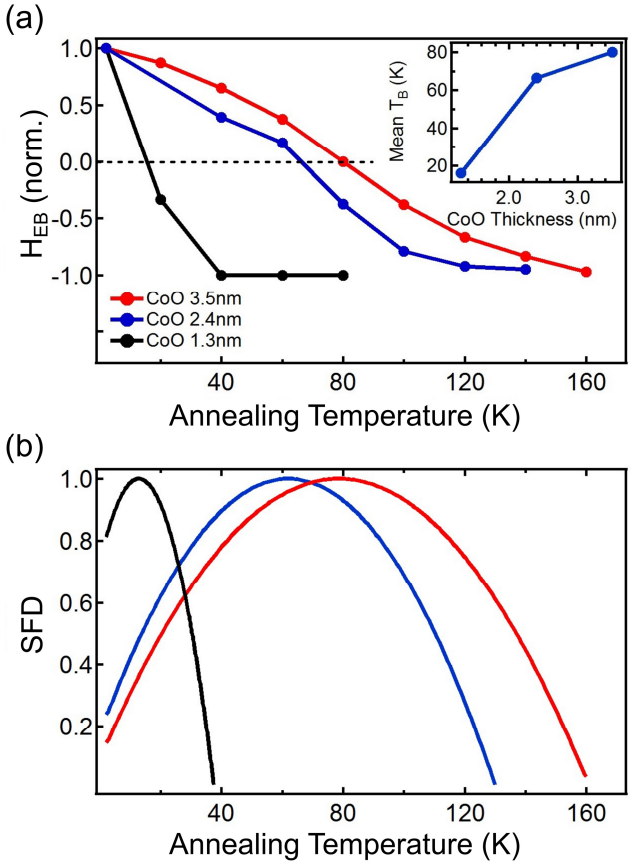

Figure 5.10: *(a) Blocking temperature distribution for Py(50 nm)/CoO(1.3; 2.4; 3.5 nm) cap structures, extracted from SQUID measurements. The inset shows the extracted mean blocking temperature T_B. H_{EB} has been extracted from trained loops (after the fifth cycle). (b) Corresponding switching field distribution (SFD).*

As already mentioned, we also compared H_C after FC in a field of 1 kOe and ZFC (see Figure 5.9 (b)). A detailed look at the difference between $H_{C,\,FC}$ and $H_{C,\,ZFC}$ (black solid squares) reveals that at the onset of EB at around 160 K differences in H_C appear. Surprisingly, in the range between 160 K and 80 K the coercivity of the zero field system seems to be slightly larger. In contrast to temperatures below 80 K, where we obtain a much larger coercivity for the field cooled configuration. This gets more pronounced with lowering the temperature. As already discussed, the uncompensated spins at the interface between the FM and AF give rise to a coercivity

enhancement, while the EB effect can be connected to uncompensated pinned spins at the interface. Referring to that, we assume that by field cooling (1 kOe), for temperatures below 80 K, gradually more spins get imprinted along the cooling field direction by lowering the temperature.

We can speculate that the ferromagnetic Py cap tends to form a vortex, while the EB prevents this configuration. We assume that this contest results in more and more unpinned spins in contrast to the zero field cooled case where this competition is not present (imprinted vortex structure).

5.4 Fe/IrMn caps: Results and discussion

In a second study, we investigated the magnetization reversal of exchange biased Fe(4 nm)/$Ir_{23}Mn_{77}$(5 nm)/Pt(5 nm) cap structures in a temperature range between 300 K and 450 K, and compared the results with Fe(4 nm)/Pt(5 nm) cap structures which do not show exchange bias. Please note that, by further increasing the temperature to 500 K, the magnetic properties were strongly deteriorating most probably due to interlayer diffusion. In Figure 5.11 in-plane SQUID measurements of Fe cap structures with a thickness of 4 nm are presented clearly revealing a magnetization reversal via formation of a magnetic vortex, taken in a temperature range between 300 K and 400 K. Magnetic vortex characteristic nucleation and annihilation fields can be easily recognized. Considering, for example, the measurement recorded at 300 K and starting from positive saturation, the vortices start to nucleate in a field of about 25 Oe whereas annihilation takes place at about -60 Oe.

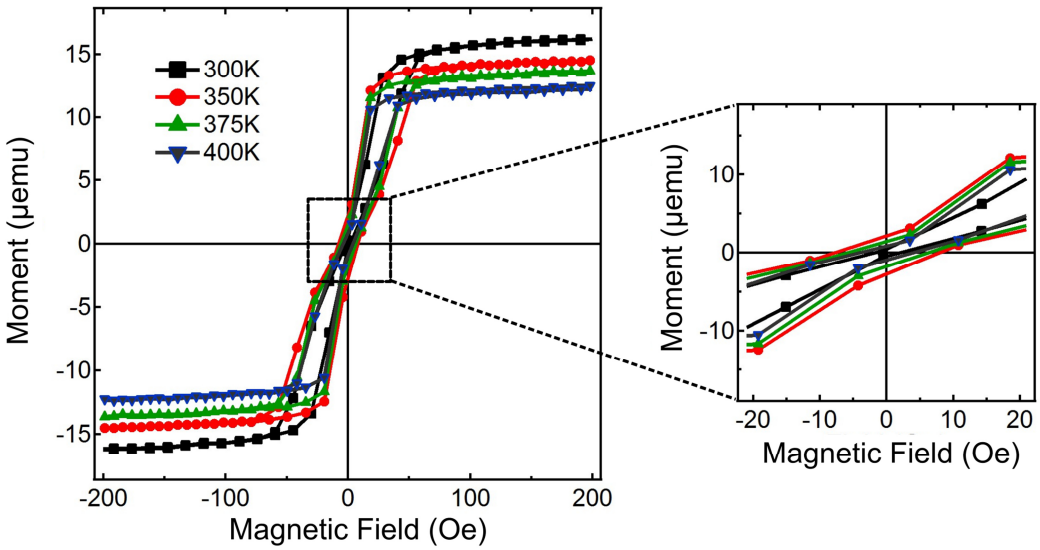

***Figure** 5.11: On the left hand side in-plane SQUID hysteresis loop of Fe caps with a thickness of 4 nm recorded at 300 K, 350 K, 375 K, and 400 K are shown. On the right hand side a zoom in of the central region is shown, revealing zero remanent magnetization (reproduced from Thomas et al.* [130]*).*

As can be seen, by increasing the temperature to 400 K the characteristic fields of the magnetic vortex remain. Whereas, for the saturation magnetic moment of the caps, we detect a decrease with increasing temperature.

In contrast, Figure 5.12 shows in-plane SQUID loops of Fe(4 nm)/IrMn(5 nm) cap structures recorded at 300 K after field cooling. Here, different in-plane cooling fields of 40 Oe, 70 Oe, and 1 kOe have been applied at 400 K, and afterward, the measurements have been recorded at 300 K. In this regard, it should be noted that 400 K used as starting temperature for the field cooling process is significantly below the Néel temperature for thick IrMn films of about 550 K, as reported in literature [197], [198]. However, as presented by Vallejo-Fernandez *et al.* this temperature should be high enough to control the setting process in IrMn based exchange bias systems [199]. At this temperature, the thermal activation of AF grains can be utilized to set the exchange bias despite the persisting AF order within each grain [130]. It seems that in cap structures a temperature of about 400 K is just enough for the majority of the AF grains to thermally overcome the energy barrier and align along the magnetization direction of the FM cap [130].

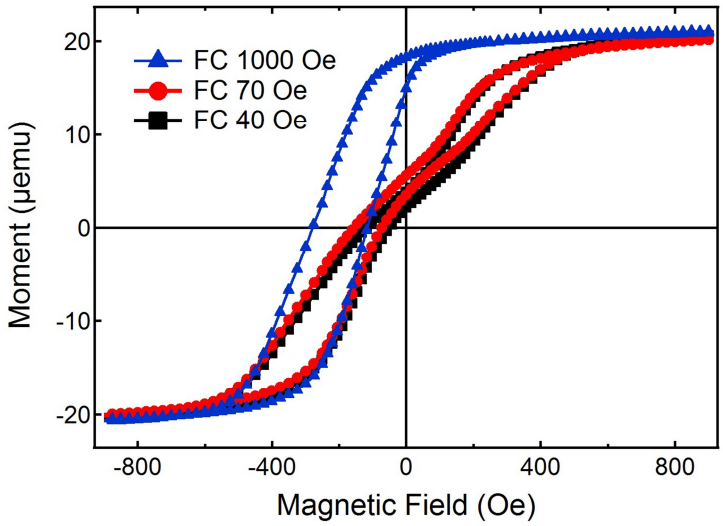

Figure 5.12: *In-plane SQUID measurements of Fe(4 nm)/IrMn(5 nm) caps taken at 300 K after field cooling in an in-plane field of 40 Oe, 70 Oe, and 1 kOe from 400 K (reproduced from Thomas et al.* [130]*).*

By passing the blocking temperature of antiferromagnetic IrMn, during ZFC, a circular exchange bias is induced by imprinting the vortex spin structure of the ferromagnetic Fe cap into the IrMn, similar effects have also been reported for flat structures [106], [111], [182].

However, applying small fields below the annihilation field of the vortex during the field cooling procedure results in an imprinting of a displaced vortex into the AF. In particular, the vortex core will be slightly off centered perpendicular to the applied field. The SQUID hysteresis loop taken after field cooling in an external field of 70 Oe is shown in Figure 5.12. Here, the loop becomes strongly asymmetric. This can be explained by the asymmetric motion of the vortex core as a function of external magnetic field, therefore, also a non-zero remanence is observed.

In this procedure, increasing the cooling field leads to an imprinting of a more displaced vortex structure, consequently also, the remanent magnetization increases. For cooling fields close to the vortex annihilation field, an onion state will be imprinted into the AF [74], [200]. For such a configuration in the AF, the formation of a magnetic vortex is no longer favorable during the magnetization reversal due to the dominance of the pinning energy induced by the exchange coupling between FM and AF [130]. Figure 5.12 shows SQUID hysteresis curves taken after field cooling in an external field of 1 kOe. We detect a drastic increase of coercivity to about 160 Oe and a horizontal loop shift of about -200 Oe. Further increase of the cooling field will promote an onion state without significant changes in the hysteresis loop.

We also investigated the temperature dependence of the exchange coupled cap structures in a temperature range between 300 K and 400 K, as shown in Figure 5.13. For this experiment, the samples have been first demagnetized at 400 K, consequently, a magnetic vortex should be formed, and cooled down to 300 K. In-plane measurements have been taken as a function of temperature. Surprisingly, we detect a small shift in the hysteresis curves. We assume that this effect originates from the superconducting magnet in the SQUID magnetometer, resulting in a weak remanent field in the magnets, which is large enough to displace the vortex core from the center of the caps [130].

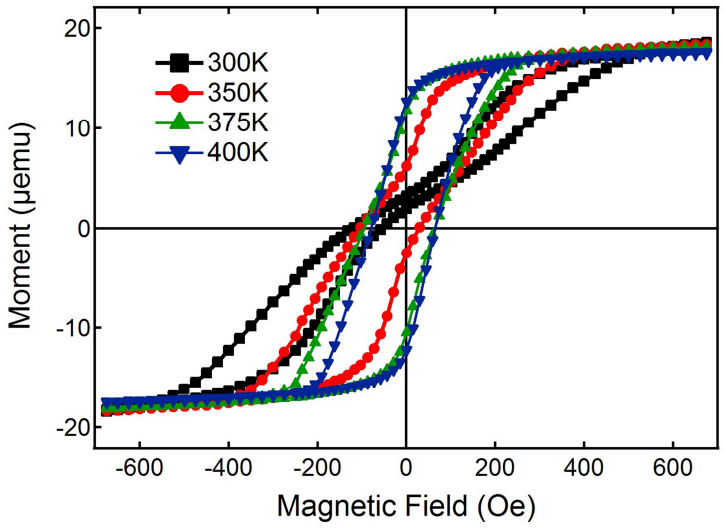

Figure 5.13: *Temperature dependent SQUID measurements of Fe/IrMn cap structures after demagnetization at 400 K and zero field cooling, reproduced from Thomas et al.* [130].

Nevertheless, at 300 K we detect a typical magnetization reversal via formation of a magnetic vortex with a loop shift H_{EB} of about 90 Oe (see Figure 5.13). As shown in Figure 5.14 (a), increasing the temperature leads to a linear decrease of H_{EB} due to the fact that more and more AF IrMn grains are getting thermally activated. For a better visualization, a dotted line is included, as a guide to the eye. The mean blocking temperature of 380 K of the AF on the caps could be extracted from the intersection of the dotted line with the abscissa [130], [201], [202]. However, at around 400 K the loops do not show any longer a loop shift.

Furthermore, we also investigated the corresponding temperature dependence of the coercivity, as shown in Figure 5.14 (b). As can be seen, increasing the temperature leads to a gradual increase of the coercivity. At around 375 K the characteristic vortex loop totally vanishes, and the coercivity reaches a maximum. This behavior is in contrast to the temperature dependent measurements of pure Fe cap structures presented in Figure 5.11. However, this effect can be explained by the blocking temperature of IrMn, which is very close to 375 K (Figure 5.14 (a)). One might conclude that the temperature stability of the vortex structures in exchange biased Fe/IrMn is directly linked to the magnetic properties of the antiferromagnetic IrMn layer.

One could argue that in the zero field cooling process a so-called circular exchange bias is introduced due to imprinting of the spin configuration of the Fe layer into the antiferromagnetic

IrMn layer. At 300 K, below the blocking temperature of IrMn, a sufficient number of antiferromagnetic spins are in a blocked state so that these spins do not rotate during a magnetization reversal of the cap structures [130]. This special configuration of the antiferromagnetic IrMn will result in a stabilization of the magnetic vortex structure [108], [109], [111].

However, the EB effect will vanish when the effective interfacial coupling J_{net} between the antiferromagnetic IrMn, and the ferromagnetic Fe approaches zero [130]. In any case, above the blocking temperature of IrMn, the antiferromagnetic spins will just rotate with the ferromagnetic spins during a magnetization reversal.

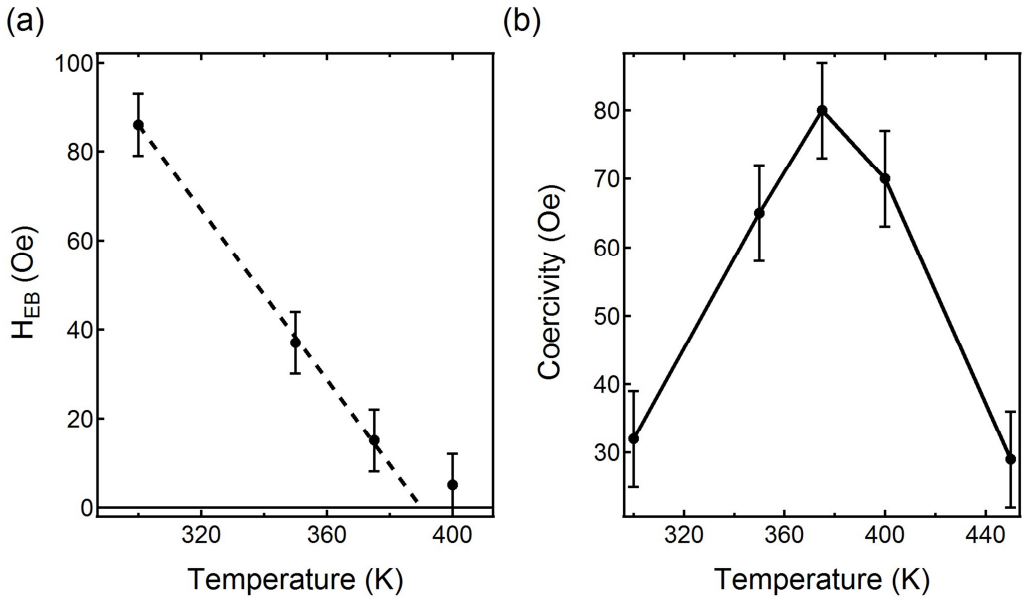

Figure 5.14: *Temperature dependencies of (a) exchange bias field H_{EB}, (b) and coercivity of Fe(4 nm)/IrMn(5 nm) cap structures after field cooling in a small field. The exchange bias field H_{EB} linearly decreases with increasing temperature. The dotted line can be used to extract the mean blocking temperature from the intersection with the abscissa (reproduced from Thomas et al.* [130]*).*

Therefore, it must be considered that in exchange coupled Fe/IrMn cap structures, the temperature dependence of the obtained hysteresis loops is strongly dependent on the ratio between the magnetic anisotropy of the antiferromagnet IrMn K_{AF} and the effective interfacial coupling J_{net}.

Thereby, K_{AF} as well as J_{net} exhibit a strong dependency on the antiferromagnetic sublattice magnetization M_{AF}. In particular, J_{net} will directly follow M_{AF} ($J_{net} \propto M_{AF}$), and $K_{AF} \propto [M_{AF}]^3$ [130], whereas, M_{AF} shows a strong temperature dependency $M_{AF} \propto [T_N - T]^{1/3}$ [203], [204].

Therefore, with increasing temperature, J_{net} and K_{AF} will decrease, and at the blocking temperature, a significant amount of antiferromagnetic spins will be thermally unstable on the time scale of the SQUID measurement [130]. During the magnetization reversal, some AF spins will be not rigid enough and dragged from the FM spins. As a result, we detect an increase of coercivity at the blocking temperature. Similar effects have also been observed for FM/AF bilayers [198], [205]–[208], and Co/Pd multilayers coupled to CoO on cap structures [196].

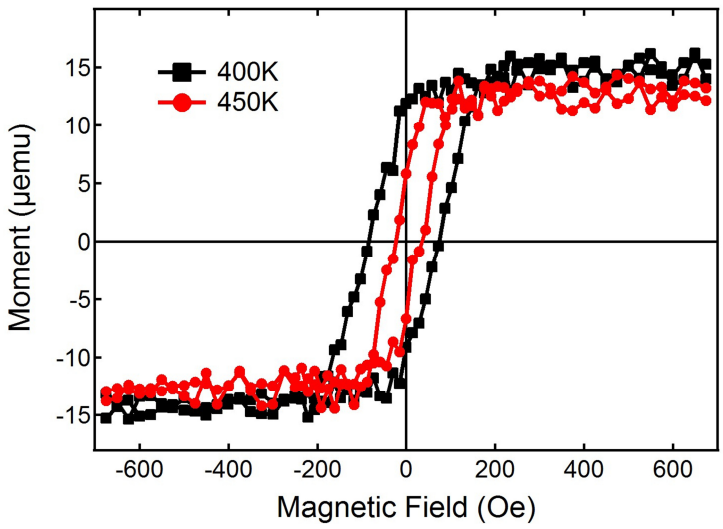

Figure 5.15: *In-plane SQUID loops of Fe/IrMn cap structures recorded at 400 K, respectively 450 K (reproduced from Thomas et al.* [130]*).*

However, reaching the Néel temperature, the antiferromagnetic IrMn will become paramagnetic, and additionally, the interfacial exchange coupling between the FM and AF will be strongly reduced. Therefore, the magnetization reversal of the cap structure will be controlled mainly by Fe. Consequently, in a temperature range between the Néel temperature of IrMn and the Curie temperature of Fe, which is above 1000 K for bulk Fe [209], one would expect a reformation of a magnetic vortex during magnetization reversal. Thus, we also performed in-plane SQUID measurements at 400 K and 450 K. It should be noted that it was not possible to further increase

the temperature due to interface diffusion and associated deterioration of the magnetic properties. As can be seen in Figure 5.15, the loop taken at 400 K shows no indication of a magnetic vortex formation, in contrast to the loop taken at 450 K. In this case, the magnetization drops around zero field, which indicates that at least partially the magnetization reversal occurs via the formation of a magnetic vortex.

5.5 Conclusion

We have investigated the magnetization reversal of exchange biased cap structures showing a magnetic vortex, which were formed by deposition of FM/AF films on arrays of densely packed silica particles.

In a first study, we investigated the magnetization reversal of Py/CoO vortex structures with a diameter of about 900 nm, for different CoO layer thicknesses. In particular, we investigated the dependence of the exchange bias effect on temperature, cooling field, and loop cycling (training). For all structures, the stabilization of a magnetic vortex after zero field cooling was observed due to imprinting of the vortex spin structure into the AF during the cooling process. Besides, we showed that the magnetization reversal can be strongly altered by inducing an exchange bias. As a result, we obtained a significant loop shift opposite to the cooling field direction, depending on the applied cooling field as well as CoO thickness. Furthermore, we showed that for cooling fields smaller than the annihilation field of a vortex, a displaced vortex can be imprinted during field cooling, whereas for larger fields a *C* state or even a single domain state can be observed. Beyond, after loop cycling the sample, a strong training effect was observed, known as “athermal” training, where the largest effect was already detected in the second loop.

By carefully analyzing the asymmetry of the nucleation and annihilation fields of the reversal loops, we could show that the magnetization reversal occurs via formation of a distorted viscous vortex. We assume that the reversal is favored due to the special topology of a cap structure. In particular, as the influence of the FM/AF interface gets weaker along the ferromagnetic film thickness, it enables the core position to vary throughout the layer. Consequently, the core of the vortex structure becomes tilted and centered further away from the interface between the ferromagnet and the antiferromagnet.

Therefore, one must consider if the curved surface of the cap even supports the magnetization reversal of a distorted viscous vortex. However, this magnetization reversal becomes even more favorable with increasing AF layer thickness due to stronger exchange coupling to the FM cap.

Furthermore, we compared the temperature dependence of H_C for ZFC and FC samples applying a

cooling field larger than the vortex annihilation field. We found that at the onset of EB at around 160 K strong differences in H_C appear. Surprisingly, for the temperature range between 160 K and 80 K the coercivity of the zero field cooled system seems to be slightly larger in comparison to the field cooled caps. In contrast below 80 K we obtained a much larger coercivity for the FC case. This behavior might be explained by the fact that below 80 K a higher number of unpinned spins are present after field cooling, giving rise to a coercivity enhancement. We assume that this behavior results from the competition at the FM/AF interface between pinned, uncompensated spins trying to align along the cooling field direction and unpinned spins, which try to follow the vortex spin structure. Additionally, we showed that the blocking temperature and its distribution increase drastically with increasing CoO layer thickness.

In a second study, we investigated the magnetization reversal of exchange biased Fe(4 nm)/IrMn(5 nm) cap structures and single Fe cap structures with a fixed diameter of about 900 nm at temperatures up to 450 K. As expected, for the single Fe caps we could show that the magnetization reversal occurs via formation of a magnetic vortex over the whole temperature range.

By adding an antiferromagnetic IrMn layer, an exchange bias effect occurs. As has been shown in the first study for Py/CoO caps, after zero field cooling the exchange coupling is observed by an imprinting of the spin configuration of the ferromagnet (vortex) into the antiferromagnet, resulting in a stabilization of the vortex structure.

Furthermore, we showed that field cooling can be used to alter the magnetization reversal by inducing exchange bias in the system. In particular, we presented that the remanent magnetization in Fe/IrMn caps increases with increasing cooling field. The evolution of the remanent magnetization with cooling field can be attributed to the progressive displacement of the imprinted vortex core with respect to the cap center during field cooling, as also obtained for field cooling experiments of Py/CoO caps.

We showed that approaching the blocking temperature of the antiferromagnetic IrMn is accompanied by a drastically increase of the coercivity and decrease of H_{EB}. A similar increase of coercivity has been reported for exchange biased caps, revealing perpendicular magnetic anisotropy, consisting of Pd/Co multilayers coupled to CoO [196], and various other exchange

bias thin film systems [105], [210]–[213], and also appears in theoretical models [214]. This effect is commonly known as *spin dragging*. It arises from low anisotropic, rotatable antiferromagnetic spins, which reverse along with the ferromagnetic reversal. Approaching the Néel temperature of IrMn, both the interfacial exchange coupling as well as the antiferromagnetic ordering deteriorate, resulting in a drastic decrease in coercivity [130]. Furthermore, around the blocking temperature no magnetization reversal via formation of a magnetic vortex was observed. By further increasing the temperature, we obtained a reoccurrence of a magnetization reversal process given by the formation of a magnetic vortex.

6 SUMMARY

Magnetic vortices have attracted huge interest in various areas of science and technology. Classically, magnetic vortex states are stabilized in magnetic disks fabricated by top-down lithographic techniques. On the contrary, nanostructure fabrication by so-called bottom-up approaches offers significant advantages and unique properties. In particular, utilizing particle self-assembly forming dense arrays of particle monolayers can serve as templates for the deposition of thin films. By depositing of soft magnetic films onto these particle assemblies, magnetic cap structures revealing a magnetic vortex can be formed. However, the investigation of magnetic vortices formed in cap structures represents a recent topic in the field of magnetism with only a few studies reported up to now.

Therefore, the purpose of this thesis was to gain a basic understanding of magnetic cap structures showing a vortex state. To do so, we investigated single FM layers and exchange coupled FM/ AF bilayers deposited onto closely packed particles using DC magnetron sputtering. For the characterization of magnetic properties superconducting quantum interference device magnetometry, magneto-optical Kerr effect magnetometry, magnetic force microscopy, magnetic transmission X-ray microscopy, and scanning magnetoresistive microscopy were used.

In the first part of the thesis, we demonstrated that it is possible to stabilize a magnetic vortex in cap structures prepared by permalloy deposition onto an array of densely packed particles with a diameter of 330 nm. To get a better understanding of the magnetic properties of permalloy caps, we investigated the influence of the permalloy layer thickness and temperature on the characteristic nucleation and annihilation fields of the vortex structure.

We could show that both increasing the film thickness and decreasing temperature lead to a stabilization of the vortex structure. Furthermore, we could show that increasing the film

thickness is accompanied by an onset of direct exchange coupling of adjacent cap structures, resulting in a nucleation process of the vortices, which arises via domain wall propagation and not randomly in individual structures. Additionally, we investigated the vortex cores of cap structures in a lattice of densely packed permalloy caps. In this regard, we showed that it is possible to switch the polarity of all vortex cores at the same time by applying a global out-of-plane field, or even the polarity of individual cores by applying a local field puls.

In regard to possible applications, it is strongly required to influence selectively the magnetic properties making such structures particularly interesting for sensor applications. An elegant way to do so, is to introduce exchange bias in the system.

Therefore, in the second part of the present thesis, we investigated the magnetic properties of exchange-biased cap structures with a diameter of 900 nm prepared by depositing an FM/AF bilayer onto an array of densely packed silica particles. In this system, the FM layer itself prefers to reverse via formation of a magnetic vortex. Overall, we were able to confirm that exchange coupling of both layers results in a stabilization of the vortex, due to imprinting of the spin structure of the FM, showing a vortex state, into the AF, resulting in a circular exchange bias, and that field cooling can be used to alter the magnetization reversal of these cap structures.

In particular, for rather thin Fe(4 nm)/IrMn(5 nm) bilayers, we could show that by increasing the cooling field, a more and more displaced vortex can be imprinted into the AF, and as a result, we obtain an increase of the remanent magnetization. Additionally, we also investigated the magnetization reversal for small cooling fields as a function of temperature. In this study, we found that with increasing temperature the exchange bias field decreases, whereas close to the blocking temperature of IrMn the coercivity increases and the magnetization reversal no longer occurs via vortex formation. We assume that the increase of coercivity is arising from rotatable, low anisotropic AF spins, which switch along with the FM reversal. Further increasing the temperature leads to a reoccurrence of a magnetization reversal via formation of a magnetic vortex.

For rather thick Py(50 nm)/CoO bilayer we could show that for cooling fields smaller than the annihilation field a displaced vortex is imprinted into the AF, whereas for larger cooling fields one imprints a *C* state into the AF. Whereas, in all samples we found a strong training effect after

loop cycling. In this system mainly the so-called athermal training takes place, where the strongest effect was already visible after the first loop. Furthermore, we could show for cooling fields smaller than the vortex annihilation field that the magnetization reversal occurs via formation of a distorted viscous vortex. One can argue that this effect is even promoted by the specific topology of a cap structure. The effect is more notable for thicker CoO layers.

Furthermore, for thick CoO layers, we found a huge difference in coercivity below 80 K between FC and ZFC. In particular, we observed much larger coercivities after FC. We assume that this behavior results from the competition at the FM/AF interface between pinned uncompensated spins trying to align along the cooling field direction and unpinned spins, which try to follow the vortex structure. Furthermore, we found a strong increase of the blocking temperature and of its distribution with increasing CoO thickness.

In conclusion, in this thesis, it has been shown that magnetic vortices can be stabilized in cap structures prepared by film deposition onto arrays of densely packed cap structures. This approach represents a real alternative to the production procedure by classical top-down approaches. We demonstrated that it is possible to switch the vortex core individually and use the film thickness and temperature to tune the characteristic fields of a magnetic vortex. Furthermore, it has been shown that by depositing of an additional antiferromagnetic layer an exchange bias can be introduced into the system. This effect can be used to influence selectively the magnetic properties making such structures particularly interesting for sensor applications.

However, for this, it needs to be clarified how to electrically contact individual cap structures. Another interesting question implies replacing the ferromagnet by a ferrimagnet. This material class would offer many new features, *e.g.* due to the high-temperature dependence of the magnetization of a ferrimagnet. Furthermore, one could also think about using a ferrimagnet to bias a ferromagnetic cap showing a vortex. However, these will be the aim of further investigations.

7 REFERENCES

[1] A. Scherzberg and J. Wendorff, *Nanotechnologie: Grundlagen, Anwendungen, Risiken, Regulierung*. Walter de Gruyter, 2008.

[2] D. J. Sellmyer and R. Skomski, *Advanced magnetic nanostructures*. Springer Science & Business Media, 2006.

[3] Y. Xia, P. Yang, Y. Sun, Y. Wu, B. Mayers, B. Gates, Y. Yin, F. Kim, and H. Yan, "One-Dimensional Nanostructures: Synthesis, Characterization, and Applications," *Adv. Mater.*, vol. 15, no. 5, pp. 353–389, Mar. 2003.

[4] A. Mnyusiwalla, A. S. Daar, and P. a Singer, "Mind the gap : science and ethics in nanotechnology," *Nanotechnology*, vol. 14, no. 3, pp. R9–R13, Mar. 2003.

[5] B. Azzerboni, G. Asti, L. Pareti, and M. Ghidini, Eds., *Magnetic Nanostructures in Modern Technology*. Dordrecht: Springer Netherlands, 2008.

[6] A. Akbarzadeh, M. Samiei, and S. Davaran, "Magnetic nanoparticles: preparation, physical properties, and applications in biomedicine," *Nanoscale Res. Lett.*, vol. 7, no. 1, p. 144, 2012.

[7] J. W. Lau and J. M. Shaw, "Magnetic nanostructures for advanced technologies: fabrication, metrology and challenges," *J. Phys. D. Appl. Phys.*, vol. 44, no. 30, p. 303001, Aug. 2011.

[8] J. Yan, S. C. Bae, and S. Granick, "Colloidal Superstructures Programmed into Magnetic Janus Particles," *Adv. Mater.*, vol. 27, no. 5, pp. 874–879, Feb. 2015.

[9] A. Aharoni, *Introduction to the Theory of Ferromagnetism*, Vol. 109. Oxford University Press, 2000.

[10] R. P. Cowburn, "Property variation with shape in magnetic nanoelements," *J. Phys. D. Appl. Phys.*, vol. 33, no. 1, pp. R1–R16, Jan. 2000.

[11] H. Hoffmann and F. Steinbauer, "Single domain and vortex state in ferromagnetic circular nanodots," *J. Appl. Phys.*, vol. 92, no. 9, p. 5463, 2002.

[12] K. L. Metlov, "Equilibrium large vortex state in ferromagnetic disks," *J. Appl. Phys.*, vol.

113, no. 22, p. 223905, 2013.

[13] K. L. Metlov and K. Y. Guslienko, "Stability of magnetic vortex in soft magnetic nano-sized circular cylinder," *J. Magn. Magn. Mater.*, vol. 242–245, pp. 1015–1017, Apr. 2002.

[14] X.-L. Liu, Y. Yang, J.-P. Wu, Y.-F. Zhang, H.-M. Fan, and J. Ding, "Novel magnetic vortex nanorings/nanodiscs: Synthesis and theranostic applications," *Chinese Phys. B*, vol. 24, no. 12, p. 127505, Dec. 2015.

[15] D. Kumar, P. Lupo, A. Haldar, and A. O. Adeyeye, "Unconventional spin distributions in thick Ni80Fe20 nanodisks," *Appl. Phys. Lett.*, vol. 108, no. 19, p. 192404, May 2016.

[16] Y. Nakatani, M. Hayashi, S. Kanai, S. Fukami, and H. Ohno, "Electric field control of Skyrmions in magnetic nanodisks," *Appl. Phys. Lett.*, vol. 108, no. 15, p. 152403, Apr. 2016.

[17] R. Streubel, V. P. Kravchuk, D. D. Sheka, D. Makarov, F. Kronast, O. G. Schmidt, and Y. Gaididei, "Equilibrium magnetic states in individual hemispherical permalloy caps," *Appl. Phys. Lett.*, vol. 101, no. 13, p. 132419, 2012.

[18] R. Streubel, F. Kronast, C. F. Reiche, T. Mühl, A. U. B. Wolter, O. G. Schmidt, and D. Makarov, "Vortex circulation and polarity patterns in closely packed cap arrays," *Appl. Phys. Lett.*, vol. 108, no. 4, p. 42407, Jan. 2016.

[19] R. Streubel, P. Fischer, F. Kronast, V. P. Kravchuk, D. D. Sheka, Y. Gaididei, O. G. Schmidt, and D. Makarov, "Magnetism in curved geometries," *J. Phys. D. Appl. Phys.*, vol. 49, no. 36, p. 363001, Sep. 2016.

[20] P. Fischer, M.-Y. Im, S. Kasai, K. Yamada, T. Ono, and A. Thiaville, "X-ray imaging of vortex cores in confined magnetic structures," *Phys. Rev. B*, vol. 83, no. 21, p. 212402, Jun. 2011.

[21] A. Wachowiak, J. Wiebe, M. Bode, O. Pietzsch, M. Morgenstern, and R. Wiesendanger, "Direct Observation of Internal Spin Structure of Magnetic Vortex Cores," *Science*, vol. 298, no. 5593, pp. 577–580, Oct. 2002.

[22] Shinjo, Okuno, Hassdorf, Shigeto, and Ono, "Magnetic vortex core observation in circular dots of permalloy," *Science*, vol. 289, no. 5481, pp. 930–2, Aug. 2000.

[23] M. Jaafar, R. Yanes, D. Perez de Lara, O. Chubykalo-Fesenko, A. Asenjo, E. M. Gonzalez, J. V. Anguita, M. Vazquez, and J. L. Vicent, "Control of the chirality and polarity of magnetic vortices in triangular nanodots," *Phys. Rev. B*, vol. 81, no. 5, p. 54439, Feb. 2010.

[24] M. Schneider, H. Hoffmann, and J. Zweck, "Magnetic switching of single vortex permalloy elements," *Appl. Phys. Lett.*, vol. 79, no. 19, p. 3113, 2001.

[25] S. Yakata, M. Miyata, S. Nonoguchi, H. Wada, and T. Kimura, "Control of vortex chirality in regular polygonal nanomagnets using in-plane magnetic field," *Appl. Phys. Lett.*, vol. 97, no. 22, p. 222503, Nov. 2010.

[26] M.-Y. Im, P. Fischer, K. Yamada, T. Sato, S. Kasai, Y. Nakatani, and T. Ono, "Symmetry breaking in the formation of magnetic vortex states in a permalloy nanodisk," *Nat.*

Commun., vol. 3, p. 983, Jul. 2012.

[27] S. Bohlens, B. Krüger, A. Drews, M. Bolte, G. Meier, and D. Pfannkuche, "Current controlled random-access memory based on magnetic vortex handedness," *Appl. Phys. Lett.*, vol. 93, no. 14, p. 142508, 2008.

[28] A. B. Butenko, A. A. Leonov, A. N. Bogdanov, and U. K. Rößler, "Theory of vortex states in magnetic nanodisks with induced Dzyaloshinskii-Moriya interactions," *Phys. Rev. B*, vol. 80, no. 13, p. 134410, Oct. 2009.

[29] V. S. Pribiag, I. N. Krivorotov, G. D. Fuchs, P. M. Braganca, O. Ozatay, J. C. Sankey, D. C. Ralph, and R. a. Buhrman, "Magnetic vortex oscillator driven by d.c. spin-polarized current," *Nat. Phys.*, vol. 3, no. 7, pp. 498–503, Jul. 2007.

[30] K. Yamada, S. Kasai, Y. Nakatani, K. Kobayashi, H. Kohno, A. Thiaville, and T. Ono, "Electrical switching of the vortex core in a magnetic disk," *Nat. Mater.*, vol. 6, no. 4, pp. 270–273, Apr. 2007.

[31] M.-Y. Im, K.-S. Lee, A. Vogel, J.-I. Hong, G. Meier, and P. Fischer, "Stochastic formation of magnetic vortex structures in asymmetric disks triggered by chaotic dynamics," *Nat. Commun.*, vol. 5, p. 5620, Dec. 2014.

[32] M. Noske, H. Stoll, M. Fähnle, A. Gangwar, G. Woltersdorf, A. Slavin, M. Weigand, G. Dieterle, J. Förster, C. H. Back, and G. Schütz, "Spin wave mediated unidirectional vortex core reversal by two orthogonal monopolar field pulses: The essential role of three-dimensional magnetization dynamics," *J. Appl. Phys.*, vol. 119, no. 17, p. 173901, May 2016.

[33] M. Coïsson, G. Barrera, F. Celegato, A. Manzin, F. Vinai, and P. Tiberto, "Magnetic vortex chirality determination via local hysteresis loops measurements with magnetic force microscopy," *Sci. Rep.*, vol. 6, no. July, p. 29904, Jul. 2016.

[34] S.-B. Choe, "Vortex Core-Driven Magnetization Dynamics," *Science (80-.).*, vol. 304, no. 5669, pp. 420–422, Apr. 2004.

[35] J. Ding, G. N. Kakazei, X. M. Liu, K. Y. Guslienko, and A. O. Adeyeye, "Intensity inversion of vortex gyrotropic modes in thick ferromagnetic nanodots," *Appl. Phys. Lett.*, vol. 104, no. 19, p. 192405, May 2014.

[36] S.-K. Kim, M.-W. Yoo, J. Lee, H.-Y. Lee, J.-H. Lee, Y. Gaididei, V. P. Kravchuk, and D. D. Sheka, "Resonantly exited precession motion of three-dimensional vortex core in magnetic nanospheres," *Sci. Rep.*, vol. 5, no. May, p. 11370, Jun. 2015.

[37] M. Kammerer, M. Weigand, M. Curcic, M. Noske, M. Sproll, A. Vansteenkiste, B. Van Waeyenberge, H. Stoll, G. Woltersdorf, C. H. Back, and G. Schuetz, "Magnetic vortex core reversal by excitation of spin waves," *Nat. Commun.*, vol. 2, p. 279, Apr. 2011.

[38] M. Noske, H. Stoll, M. Fähnle, R. Hertel, and G. Schütz, "Mechanisms for the symmetric and antisymmetric switching of a magnetic vortex core: Differences and common aspects," *Phys. Rev. B*, vol. 91, no. 1, p. 14414, Jan. 2015.

[39] R. Hertel, S. Gliga, M. Fähnle, and C. M. Schneider, "Ultrafast Nanomagnetic Toggle Switching of Vortex Cores," *Phys. Rev. Lett.*, vol. 98, no. 11, p. 117201, Mar. 2007.

[40] K. M. Lebecki and D. Legut, “Fast vortex core switching at high temperatures,” *J. Magn. Magn. Mater.*, vol. 411, pp. 7–11, Aug. 2016.

[41] B. Van Waeyenberge, A. Puzic, H. Stoll, K. W. Chou, T. Tyliszczak, R. Hertel, M. Fähnle, H. Brückl, K. Rott, G. Reiss, I. Neudecker, D. Weiss, C. H. Back, and G. Schütz, “Magnetic vortex core reversal by excitation with short bursts of an alternating field,” *Nature*, vol. 444, no. 7118, pp. 461–464, Nov. 2006.

[42] K. Y. Guslienko, K.-S. Lee, and S.-K. Kim, “Dynamic Origin of Vortex Core Switching in Soft Magnetic Nanodots,” *Phys. Rev. Lett.*, vol. 100, no. 2, p. 27203, Jan. 2008.

[43] Q. F. Xiao, J. Rudge, B. C. Choi, Y. K. Hong, and G. Donohoe, “Dynamics of vortex core switching in ferromagnetic nanodisks,” *Appl. Phys. Lett.*, vol. 89, no. 26, p. 262507, 2006.

[44] A. Thiaville, J. M. García, R. Dittrich, J. Miltat, and T. Schrefl, “Micromagnetic study of Bloch-point-mediated vortex core reversal,” *Phys. Rev. B*, vol. 67, no. 9, p. 94410, Mar. 2003.

[45] R. Hertel, “Magnetic nanostructures: Vortex states à la carte,” *Nat. Nanotechnol.*, vol. 8, no. 5, pp. 318–320, May 2013.

[46] T. Tanigaki, Y. Takahashi, T. Shimakura, T. Akashi, R. Tsuneta, A. Sugawara, and D. Shindo, “Three-Dimensional Observation of Magnetic Vortex Cores in Stacked Ferromagnetic Discs,” *Nano Lett.*, vol. 15, no. 2, pp. 1309–1314, Feb. 2015.

[47] R. Lehndorff, D. E. Bürgler, S. Gliga, R. Hertel, P. Grünberg, C. M. Schneider, and Z. Celinski, “Magnetization dynamics in spin torque nano-oscillators: Vortex state versus uniform state,” *Phys. Rev. B*, vol. 80, no. 5, p. 54412, Aug. 2009.

[48] S. Wintz, C. Bunce, A. Neudert, M. Körner, T. Strache, M. Buhl, A. Erbe, S. Gemming, J. Raabe, C. Quitmann, and J. Fassbender, “Topology and Origin of Effective Spin Meron Pairs in Ferromagnetic Multilayer Elements,” *Phys. Rev. Lett.*, vol. 110, no. 17, p. 177201, Apr. 2013.

[49] O. Heinonen, “Magnetization dynamics of coupled ferromagnetic disks,” *Phys. Rev. B*, vol. 92, no. 5, p. 54420, Aug. 2015.

[50] S. Wintz, T. Strache, M. Körner, C. Bunce, A. Banholzer, I. Mönch, R. Mattheis, J. Raabe, C. Quitmann, J. McCord, A. Erbe, K. Lenz, and J. Fassbender, “Control of vortex pair states by post-deposition interlayer exchange coupling modification,” *Phys. Rev. B*, vol. 85, no. 13, p. 134417, Apr. 2012.

[51] T. Li, S. Yi, and Y. Zhang, “Coupled spin-vortex pair in dipolar spinor Bose-Einstein condensates,” *Phys. Rev. A*, vol. 92, no. 6, p. 63603, Dec. 2015.

[52] S. Wintz, C. Bunce, A. Banholzer, M. Körner, T. Strache, R. Mattheis, J. McCord, J. Raabe, C. Quitmann, A. Erbe, and J. Fassbender, “Interlayer-coupled spin vortex pairs and their response to external magnetic fields,” *Phys. Rev. B*, vol. 85, no. 22, p. 224420, Jun. 2012.

[53] S. Wintz, T. Strache, M. Körner, M. Fritzsche, D. Markó, I. Mönch, R. Mattheis, J. Raabe, C. Quitmann, J. McCord, A. Erbe, and J. Fassbender, “Direct observation of antiferromagnetically oriented spin vortex states in magnetic multilayer elements,” *Appl.*

Phys. Lett., vol. 98, no. 23, p. 232511, 2011.

[54] S. Wintz, V. Tiberkevich, M. Weigand, J. Raabe, J. Lindner, A. Erbe, A. Slavin, and J. Fassbender, "Magnetic vortex cores as tunable spin-wave emitters," *Nat. Nanotechnol.*, no. July, pp. 1–7, Jul. 2016.

[55] R. Streubel, L. Han, M.-Y. Im, F. Kronast, U. K. Rößler, F. Radu, R. Abrudan, G. Lin, O. G. Schmidt, P. Fischer, and D. Makarov, "Manipulating Topological States by Imprinting Non-Collinear Spin Textures," *Sci. Rep.*, vol. 5, p. 8787, Mar. 2015.

[56] P. Wohlhüter, M. T. Bryan, P. Warnicke, S. Gliga, S. E. Stevenson, G. Heldt, L. Saharan, A. K. Suszka, C. Moutafis, R. V. Chopdekar, J. Raabe, T. Thomson, G. Hrkac, and L. J. Heyderman, "Nanoscale switch for vortex polarization mediated by Bloch core formation in magnetic hybrid systems," *Nat. Commun.*, vol. 6, p. 7836, Aug. 2015.

[57] G. Heldt, M. T. Bryan, G. Hrkac, S. E. Stevenson, R. V. Chopdekar, J. Raabe, T. Thomson, and L. J. Heyderman, "Topologically confined vortex oscillations in hybrid [Co/Pd]8-Permalloy structures," *Appl. Phys. Lett.*, vol. 104, no. 18, p. 182401, May 2014.

[58] S. K. Kim, K. S. Lee, Y. S. Yu, and Y. S. Choi, "Reliable low-power control of ultrafast vortex-core switching with the selectivity in an array of vortex states by in-plane circular-rotational magnetic fields and spin-polarized currents," *Appl. Phys. Lett.*, vol. 92, no. 2, 2008.

[59] B. Pigeau, G. de Loubens, O. Klein, A. Riegler, F. Lochner, G. Schmidt, L. W. Molenkamp, V. S. Tiberkevich, and A. N. Slavin, "A frequency-controlled magnetic vortex memory," *Appl. Phys. Lett.*, vol. 96, no. 13, p. 132506, 2010.

[60] R. P. Cowburn, "Magnetic nanodots for device applications," *J. Magn. Magn. Mater.*, vol. 242–245, pp. 505–511, Apr. 2002.

[61] W. L. Lim, R. H. Liu, T. Tyliszczak, S. G. Erokhin, D. Berkov, and S. Urazhdin, "Fast chirality reversal of the magnetic vortex by electric current," *Appl. Phys. Lett.*, vol. 105, no. 22, p. 222405, Dec. 2014.

[62] M. Goiriena-Goikoetxea, A. García-Arribas, M. Rouco, A. V Svalov, and J. M. Barandiaran, "High-yield fabrication of 60 nm Permalloy nanodiscs in well-defined magnetic vortex state for biomedical applications," *Nanotechnology*, vol. 27, no. 17, p. 175302, Apr. 2016.

[63] D.-H. Kim, E. A. Rozhkova, I. V. Ulasov, S. D. Bader, T. Rajh, M. S. Lesniak, and V. Novosad, "Biofunctionalized magnetic-vortex microdiscs for targeted cancer-cell destruction," *Nat. Mater.*, vol. 9, no. 2, pp. 165–171, Feb. 2010.

[64] E. A. Rozhkova, V. Novosad, D.-H. Kim, J. Pearson, R. Divan, T. Rajh, and S. D. Bader, "Ferromagnetic microdisks as carriers for biomedical applications," *J. Appl. Phys.*, vol. 105, no. 7, p. 07B306, 2009.

[65] Y. Xia, J. a. Rogers, K. E. Paul, and G. M. Whitesides, "Unconventional Methods for Fabricating and Patterning Nanostructures," *Chem. Rev.*, vol. 99, no. 7, pp. 1823–1848, Jul. 1999.

[66] R. E. Camley, Z. Celinski, and R. L. Stamps, *Magnetism of Surfaces, Interfaces, and*

Nanoscale Materials, vol. 5. Elsevier, 2015.

[67] A. H. Morrish, *The physical principles of magnetism*. Wiley-VCH, 2001.

[68] D. Jiles, *Introduction to magnetism and magnetic materials*. CRC press, 2015.

[69] J. Stöhr and H. C. Siegmann, "Magnetism," *Solid-State Sci. Springer, Berlin, Heidelb.*, vol. 5, 2006.

[70] S. Blundell and D. Thouless, *Magnetism in condensed matter*, vol. 18. Oxford university press New York, 2001.

[71] L. Néel, "Magnetism and Local Molecular Field," *Science*, vol. 174, no. 4013, pp. 985–992, Dec. 1971.

[72] W. Heisenberg, "Zur Theorie des Ferromagnetismus," *Zeitschrift für Phys. Phys.*, vol. 49, no. 9–10, pp. 619–636, Sep. 1928.

[73] W. Nolting, *Grundkurs Theoretische Physik 7: Viel-Teilchen-Theorie*. Springer-Verlag, 2014.

[74] J. K. Ha, R. Hertel, and J. Kirschner, "Micromagnetic study of magnetic configurations in submicron permalloy disks," *Phys. Rev. B*, vol. 67, no. 22, p. 224432, Jun. 2003.

[75] A. Hubert and R. Schäfer, *Magnetic Domains*. Berlin, Heidelberg: Springer Berlin Heidelberg, 1998.

[76] F. Bloch, "Zur Theorie des Austauschproblems und der Remanenzerscheinung der Ferromagnetika," *Zeitschrift für Phys.*, vol. 74, no. 5–6, pp. 295–335, May 1932.

[77] L. Néel, "Influence of thermal fluctuations on the magnetization of ferromagnetic small particles," *C.R. Acad. Sci*, vol. 241, pp. 533–584, 1955.

[78] L. Landau and E. Lifshits, "Classics in Magnetics A Phenomenological Theory of Damping in Ferromagnetic Materials," *Phys. Z. Sowjet Union*, vol. 8, no. 0, pp. 153–169, Nov. 1935.

[79] C. Kittel, "Physical Theory of Ferromagnetic Domains," *Rev. Mod. Phys.*, vol. 21, no. 4, pp. 541–584, Aug. 1949.

[80] N. Martin, N.-C. Bigall, I. Mönch, T. Gemming, A. Eychmüller, R. Mattheis, R. Schäfer, L. Schultz, and J. McCord, "Enhanced Nucleation of Vortices in Soft Magnetic Materials Prepared by Silica Nanosphere Lithography," *Adv. Funct. Mater.*, vol. 21, no. 5, pp. 891–896, Mar. 2011.

[81] N. a. Usov and S. E. Peschany, "Magnetization curling in a fine cylindrical particle," *J. Magn. Magn. Mater.*, vol. 118, no. 3, pp. L290–L294, Jan. 1993.

[82] A. Aharoni, "Upper bound to a single-domain behavior of a ferromagnetic cylinder," *J. Appl. Phys.*, vol. 68, no. 6, p. 2892, 1990.

[83] W. Scholz, K. Y. Guslienko, V. Novosad, D. Suess, T. Schrefl, R. . Chantrell, and J. Fidler, "Transition from single-domain to vortex state in soft magnetic cylindrical nanodots," *J. Magn. Magn. Mater.*, vol. 266, no. 1–2, pp. 155–163, 2003.

[84] L. D. Buda, I. L. Prejbeanu, M. Demand, U. Ebels, and K. Punadjela, "Vortex states stability in circular Co(0001) dots," *IEEE Trans. Magn.*, vol. 37, no. 4, pp. 2061–2063, Jul. 2001.

[85] K. Y. Guslienko, W. Scholz, R. W. Chantrell, and V. Novosad, "Vortex-state oscillations in soft magnetic cylindrical dots," *Phys. Rev. B*, vol. 71, no. 14, p. 144407, Apr. 2005.

[86] R. P. Cowburn, D. K. Koltsov, A. O. Adeyeye, M. E. Welland, and D. M. Tricker, "Single-Domain Circular Nanomagnets," *Phys. Rev. Lett.*, vol. 83, no. 5, pp. 1042–1045, Aug. 1999.

[87] W. H. Meiklejohn and C. P. Bean, "New Magnetic Anisotropy," *Phys. Rev.*, vol. 105, no. 3, pp. 904–913, Feb. 1957.

[88] A. E. Berkowitz and K. Takano, "Exchange anisotropy — a review," *J. Magn. Magn. Mater.*, vol. 200, no. 1–3, pp. 552–570, Oct. 1999.

[89] J. Nogués and I. K. Schuller, "Exchange bias," *J. Magn. Magn. Mater.*, vol. 192, no. 2, pp. 203–232, Feb. 1999.

[90] J. Nogués, J. Sort, V. Langlais, V. Skumryev, S. Suriñach, J. S. Muñoz, and M. D. Baró, "Exchange bias in nanostructures," *Phys. Rep.*, vol. 422, no. 3, pp. 65–117, Dec. 2005.

[91] S. Mangin, F. Montaigne, and A. Schuhl, "Interface domain wall and exchange bias phenomena in ferrimagnetic/ferrimagnetic bilayers," *Phys. Rev. B*, vol. 68, no. 14, p. 140404, Oct. 2003.

[92] F. Radu, R. Abrudan, I. Radu, D. Schmitz, and H. Zabel, "Perpendicular exchange bias in ferrimagnetic spin valves," *Nat. Commun.*, vol. 3, p. 715, Mar. 2012.

[93] C. Schubert, B. Hebler, H. Schletter, A. Liebig, M. Daniel, R. Abrudan, F. Radu, and M. Albrecht, "Interfacial exchange coupling in Fe-Tb/[Co/Pt] heterostructures," *Phys. Rev. B*, vol. 87, no. 5, p. 54415, Feb. 2013.

[94] B. Hebler, S. Böttger, D. Nissen, R. Abrudan, F. Radu, and M. Albrecht, "Influence of the Fe-Co ratio on the exchange coupling in TbFeCo/[Co/Pt] heterostructures," *Phys. Rev. B*, vol. 93, no. 18, p. 184423, May 2016.

[95] C. Schubert, "Magnetic order and coupling phenomena in rare-earth-transition-metal based alloys and heterostructures," TU Chemnitz, 2013.

[96] Ching Tsang, R. E. Fontana, Tsann Lin, D. E. Heim, V. S. Speriosu, B. A. Gurney, and M. L. Williams, "Design, fabrication and testing of spin-valve read heads for high density recording," *IEEE Trans. Magn.*, vol. 30, no. 6, pp. 3801–3806, 1994.

[97] C. Chappert, A. Fert, and F. N. Van Dau, "The emergence of spin electronics in data storage," *Nat. Mater.*, vol. 6, no. 11, pp. 813–823, Nov. 2007.

[98] N. A. Spaldin, *Magnetic Materials: Fundamentals and Applications*. Cambridge University Press, 2010.

[99] J. Fassbender, S. Poppe, T. Mewes, J. Juraszek, B. Hillebrands, K.-U. Barholz, R. Mattheis, D. Engel, M. Jung, H. Schmoranzer, and A. Ehresmann, "Ion irradiation of

exchange bias systems for magnetic sensor applications," *Appl. Phys. A Mater. Sci. Process.*, vol. 77, no. 1, pp. 51–56, Jun. 2003.

[100] S. Yuasa, T. Nagahama, A. Fukushima, Y. Suzuki, and K. Ando, "Giant room-temperature magnetoresistance in single-crystal Fe/MgO/Fe magnetic tunnel junctions," *Nat. Mater.*, vol. 3, no. 12, pp. 868–871, Dec. 2004.

[101] D. Paccard, C. Schlenker, O. Massenet, R. Montmory, and A. Yelon, "A New Property of Ferromagnetic-Antiferromagnetic Coupling," *Phys. status solidi*, vol. 16, no. 1, pp. 301–311, 1966.

[102] C. Binek, "Training of the exchange-bias effect: A simple analytic approach," *Phys. Rev. B*, vol. 70, no. 1, p. 14421, Jul. 2004.

[103] S. Brems, D. Buntinx, K. Temst, C. Van Haesendonck, F. Radu, and H. Zabel, "Reversing the Training Effect in Exchange Biased CoO/Co Bilayers," *Phys. Rev. Lett.*, vol. 95, no. 15, p. 157202, Oct. 2005.

[104] J. Keller, P. Miltényi, B. Beschoten, G. Güntherodt, U. Nowak, and K. D. Usadel, "Domain state model for exchange bias. II. Experiments," *Phys. Rev. B*, vol. 66, no. 1, p. 14431, Jul. 2002.

[105] J. Nogués, C. Leighton, and I. K. Schuller, "Correlation between antiferromagnetic interface coupling and positive exchange bias," *Phys. Rev. B*, vol. 61, no. 2, pp. 1315–1317, Jan. 2000.

[106] H. Xu, J. Kolthammer, J. Rudge, E. Girgis, B. C. Choi, Y. K. Hong, G. Abo, T. Speliotis, and D. Niarchos, "Magnetization Process in Vortex-imprinted Ni 80 Fe 20 /Ir 20 Mn 80 Square Elements," *J. Magn.*, vol. 16, no. 2, pp. 83–87, Jun. 2011.

[107] J. Sort, K. S. Buchanan, V. Novosad, A. Hoffmann, G. Salazar-Alvarez, A. Bollero, M. D. Baró, B. Dieny, and J. Nogués, "Imprinting Vortices into Antiferromagnets," *Phys. Rev. Lett.*, vol. 97, no. 6, p. 67201, Aug. 2006.

[108] G. Salazar-Alvarez, J. J. Kavich, J. Sort, A. Mugarza, S. Stepanow, A. Potenza, H. Marchetto, S. S. Dhesi, V. Baltz, B. Dieny, A. Weber, L. J. Heyderman, J. Nogués, and P. Gambardella, "Direct evidence of imprinted vortex states in the antiferromagnet of exchange biased microdisks," *Appl. Phys. Lett.*, vol. 95, no. 1, p. 12510, 2009.

[109] J. Sort, G. Salazar-Alvarez, M. D. Baró, B. Dieny, A. Hoffmann, V. Novosad, and J. Nogués, "Controlling magnetic vortices through exchange bias," *Appl. Phys. Lett.*, vol. 88, no. 4, p. 42502, 2006.

[110] R. Nakatani, T. Yoshida, Y. Endo, Y. Kawamura, M. Yamamoto, T. Takenaga, S. Aya, T. Kuroiwa, S. Beysen, and H. Kobayashi, "Magnetically pinned ring dots for spin valve or magnetic tunnel junction memory cells," *J. Magn. Magn. Mater.*, vol. 286, pp. 31–36, Feb. 2005.

[111] M. Tanase, A. K. Petford-Long, O. Heinonen, K. S. Buchanan, J. Sort, and J. Nogués, "Magnetization reversal in circularly exchange-biased ferromagnetic disks," *Phys. Rev. B*, vol. 79, no. 1, p. 14436, Jan. 2009.

[112] E. Girgis, R. D. Portugal, M. J. Van Bael, K. Temst, and C. Van Haesendonck,

"Asymmetric magnetization reversal in exchange-biased NiFe/CoO submicron-sized structures," *J. Appl. Phys.*, vol. 97, no. 10, p. 103911, 2005.

[113] A. Hoffmann, J. Sort, K. S. Buchanan, and J. Nogues, "Exchange-Biased Magnetic Vortices," *IEEE Trans. Magn.*, vol. 44, no. 7, pp. 1968–1973, Jul. 2008.

[114] J. Sort, A. Hoffmann, S.-H. Chung, K. S. Buchanan, M. Grimsditch, M. D. Baró, B. Dieny, and J. Nogués, "Magnetization Reversal in Submicron Disks: Exchange Biased Vortices," *Phys. Rev. Lett.*, vol. 95, no. 6, p. 67201, Aug. 2005.

[115] K. Y. Guslienko and A. Hoffmann, "Field Evolution of Tilted Vortex Cores in Exchange-Biased Ferromagnetic Dots," *Phys. Rev. Lett.*, vol. 97, no. 10, p. 107203, Sep. 2006.

[116] K. Y. Guslienko and A. Hoffmann, "Vortex magnetization reversal in double-layer ferromagnetic/antiferromagnetic dots," *J. Appl. Phys.*, vol. 101, no. 9, p. 93901, 2007.

[117] D. A. Gilbert, L. Ye, A. Varea, S. Agramunt-Puig, N. del Valle, C. Navau, J. F. López-Barbera, K. S. Buchanan, A. Hoffmann, A. Sánchez, J. Sort, K. Liu, and J. Nogués, "A new reversal mode in exchange coupled antiferromagnetic/ferromagnetic disks: distorted viscous vortex," *Nanoscale*, vol. 7, no. 21, pp. 9878–9885, 2015.

[118] E. a. Dobisz, D. Kercher, M. Grobis, O. Hellwig, E. E. Marinero, D. Weller, and T. R. Albrecht, "Fabrication of 1 Teradot/in.2 CoCrPt bit patterned media and recording performance with a conventional read/write head," *J. Vac. Sci. Technol. B Microelectron. Nanom. Struct.*, vol. 30, no. 6, p. 06FH01, 2012.

[119] B. D. Terris and T. Thomson, "Nanofabricated and self-assembled magnetic structures as data storage media," *J. Phys. D. Appl. Phys.*, vol. 38, no. 12, pp. R199–R222, Jun. 2005.

[120] S. M. Weekes, F. Y. Ogrin, and W. A. Murray, "Fabrication of Large-Area Ferromagnetic Arrays Using Etched Nanosphere Lithography," *Langmuir*, vol. 20, no. 25, pp. 11208–11212, Dec. 2004.

[121] R. Micheletto, H. Fukuda, and M. Ohtsu, "A Simple Method for the Production of a Two-Dimensional, Ordered Array of Small Latex Particles," *Langmuir*, vol. 11, no. 9, pp. 3333–3336, Sep. 1995.

[122] M. Albrecht, G. Hu, I. L. Guhr, T. C. Ulbrich, J. Boneberg, P. Leiderer, and G. Schatz, "Magnetic multilayers on nanospheres," *Nat. Mater.*, vol. 4, no. 3, pp. 203–206, Mar. 2005.

[123] T. C. Ulbrich, D. Makarov, G. Hu, I. L. Guhr, D. Suess, T. Schrefl, and M. Albrecht, "Magnetization Reversal in a Novel Gradient Nanomaterial," *Phys. Rev. Lett.*, vol. 96, no. 7, p. 77202, Feb. 2006.

[124] L. Baraban, D. Makarov, R. Streubel, I. Mönch, D. Grimm, S. Sanchez, and O. G. Schmidt, "Catalytic Janus Motors on Microfluidic Chip: Deterministic Motion for Targeted Cargo Delivery," *ACS Nano*, vol. 6, no. 4, pp. 3383–3389, Apr. 2012.

[125] S. P. Li, W. S. Lew, Y. B. Xu, A. Hirohata, A. Samad, F. Baker, and J. A. C. Bland, "Magnetic nanoscale dots on colloid crystal surfaces," *Appl. Phys. Lett.*, vol. 76, no. 6, p. 748, 2000.

[126] J. H. Yang, S. Y. Yang, M. B. Wei, Y. X. Wang, Y. J. Zhang, N. N. Yang, J. Li, S. S. Liu, W. Li, and X. T. Wu, "Exchange bias of Co/CoO multilayers deposited on nanosphere array," *Appl. Phys. A*, vol. 108, no. 2, pp. 363–368, Aug. 2012.

[127] R. Streubel, D. Makarov, F. Kronast, V. Kravchuk, M. Albrecht, and O. G. Schmidt, "Magnetic vortices on closely packed spherically curved surfaces," *Phys. Rev. B*, vol. 85, no. 17, p. 174429, May 2012.

[128] D. Nissen, D. Mitin, O. Klein, S. S. P. K. Arekapudi, S. Thomas, M.-Y. Im, P. Fischer, and M. Albrecht, "Magnetic coupling of vortices in a two-dimensional lattice," *Nanotechnology*, vol. 26, no. 46, p. 465706, Nov. 2015.

[129] R. Brandt, R. Rückriem, D. A. Gilbert, F. Ganss, T. Senn, K. Liu, M. Albrecht, and H. Schmidt, "Size-dependent magnetization switching characteristics and spin wave modes of FePt nanostructures," *J. Appl. Phys.*, vol. 113, no. 20, p. 203910, 2013.

[130] S. Thomas, D. Nissen, and M. Albrecht, "Temperature dependent magnetization reversal of exchange biased magnetic vortices in IrMn/Fe microcaps," *Appl. Phys. Lett.*, vol. 105, no. 2, p. 22405, Jul. 2014.

[131] Christoph Brombacher, "Herstellung und Untersuchung von magnetischen Schichtsystemen auf sphärischen Nanopartikeln," UNI Konstanz, 2007.

[132] Christoph Brombacher, "Rapid thermal annealing of FePt and FePt/Cu thin films," TU Chemnitz, 2010.

[133] N. Singh, S. Goolaup, and A. O. Adeyeye, "Fabrication of large area nanomagnets," *Nanotechnology*, vol. 15, no. 11, pp. 1539–1544, Nov. 2004.

[134] S. Y. Chou, M. S. Wei, P. R. Krauss, and P. B. Fischer, "Single-domain magnetic pillar array of 35 nm diameter and 65 Gbits/in.2 density for ultrahigh density quantum magnetic storage," *J. Appl. Phys.*, vol. 76, no. 10, p. 6673, 1994.

[135] A. O. Adeyeye, J. A. C. Bland, C. Daboo, D. G. Hasko, and H. Ahmed, "Optimized process for the fabrication of mesoscopic magnetic structures," *J. Appl. Phys.*, vol. 82, no. 1, p. 469, 1997.

[136] J. L. Vossen and W. Kern, *Thin film processes II Vol. 2*. Academic Press, 2012.

[137] M. Ohring, *Materials science of thin films*. San Diego: Academic press, 2001.

[138] M. Knoll and E. Ruska, "Das Elektronenmikroskop," *Zeitschrift für Phys.*, vol. 79, no. 9–10, pp. 699–699, Sep. 1932.

[139] JEOL, "JEM-2100 ELECTRON MICROSCOPE Manual," 2004.

[140] H. Kohl and R. Ludwig, *Transmission Electron Microscopy*, vol. 36. New York, NY: Springer New York, 2008.

[141] H. Alexander, *Physikalische Grundlagen der Elektronenmikroskopie*. Stuttgart: Teubner, 1997.

[142] L. Bergmann, R. Kassing, C. Schaefer, and S. Blügel, *Lehrbuch der Experimentalphysik:*

Festkörper, vol. 6. Walter de Gruyter, 2005.

[143] D. B. Williams and C. B. Carter, "The transmission electron microscope," in *Transmission electron microscopy*, Springer, 1996, pp. 3–17.

[144] D. McMullan, "Scanning electron microscopy 1928-1965," *Scanning*, vol. 17, no. 3, pp. 175–185, Dec. 2006.

[145] L. Spieß, G. Teichert, R. Schwarzer, H. Behnken, and C. Genzel, *Moderne röntgenbeugung: röntgendiffraktometrie für materialwissenschaftler, physiker und chemiker*. Springer-Verlag, 2009.

[146] J. Strähle, "Röntgenbeugung an Kristallen," *Angew. Chemie*, vol. 88, no. 17, pp. 587–587, Sep. 1976.

[147] H. Kiessig, "Interferenz von Röntgenstrahlen an dünnen Schichten," *Ann. Phys.*, vol. 402, no. 7, pp. 769–788, 1931.

[148] R. L. Fagaly, "Superconducting quantum interference device instruments and applications," *Rev. Sci. Instrum.*, vol. 77, no. 10, p. 101101, 2006.

[149] B. D. Josephson, "Possible new effects in superconductive tunnelling," *Phys. Lett.*, vol. 1, no. 7, pp. 251–253, Jul. 1962.

[150] P. W. Anderson and J. M. Rowell, "Probable Observation of the Josephson Superconducting Tunneling Effect," *Phys. Rev. Lett.*, vol. 10, no. 6, pp. 230–232, Mar. 1963.

[151] J. Kerr, "XLIII. On rotation of the plane of polarization by reflection from the pole of a magnet," *Philos. Mag. Ser. 5*, vol. 3, no. 19, pp. 321–343, May 1877.

[152] Z. Q. Qiu and S. D. Bader, "Surface magneto-optic Kerr effect," *Rev. Sci. Instrum.*, vol. 71, no. 3, p. 1243, 2000.

[153] E. Menéndez, A. Martinavicius, M. O. Liedke, G. Abrasonis, J. Fassbender, J. Sommerlatte, K. Nielsch, S. Suriñach, M. D. Baró, J. Nogués, and J. Sort, "Patterning of magnetic structures on austenitic stainless steel by local ion beam nitriding," *Acta Mater.*, vol. 56, no. 17, pp. 4570–4576, Oct. 2008.

[154] M. Grimsditch and P. Vavassori, "The diffracted magneto-optic Kerr effect: what does it tell you?," *J. Phys. Condens. Matter*, vol. 16, no. 9, pp. R275–R294, Mar. 2004.

[155] K. Y. Guslienko, V. Novosad, Y. Otani, H. Shima, and K. Fukamichi, "Field evolution of magnetic vortex state in ferromagnetic disks," *Appl. Phys. Lett.*, vol. 78, no. 24, p. 3848, 2001.

[156] F. A. Ferri, M. A. Pereira-da-Silva, and E. Marega, "Magnetic Force Microscopy: Basic Principles and Applications," in *Atomic Force Microscopy - Imaging, Measuring and Manipulating Surfaces at the Atomic Scale*, InTech, 2012.

[157] P. Fischer, "Studying Nanoscale Magnetism and Its Dynamics With Soft X-Ray Microscopy," *IEEE Trans. Magn.*, vol. 44, no. 7, pp. 1900–1904, Jul. 2008.

[158] J. Stöhr, “X-ray magnetic circular dichroism spectroscopy of transition metal thin films,” *J. Electron Spectros. Relat. Phenomena*, vol. 75, no. C, pp. 253–272, Dec. 1995.

[159] C. T. Chen, F. Sette, Y. Ma, and S. Modesti, “Soft-x-ray magnetic circular dichroism at the L2,3 edges of nickel,” *Phys. Rev. B*, vol. 42, no. 11, pp. 7262–7265, Oct. 1990.

[160] G. Schütz, M. Knülle, R. Wienke, W. Wilhelm, W. Wagner, P. Kienle, and R. Frahm, “Spin-dependent photoabsorption at theL-edges of ferromagnetic Gd and Tb metal,” *Z. Phys. B Condens. Matter*, vol. 73, no. 1, pp. 67–75, Mar. 1988.

[161] G. Schütz, W. Wagner, W. Wilhelm, P. Kienle, R. Zeller, R. Frahm, and G. Materlik, “Absorption of circularly polarized x rays in iron,” *Phys. Rev. Lett.*, vol. 58, no. 7, pp. 737–740, Feb. 1987.

[162] A. S. Schlachter and F. J. Wuilleumier, Eds., *New Directions in Research with Third-Generation Soft X-Ray Synchrotron Radiation Sources*. Dordrecht: Springer Netherlands, 1994.

[163] S.-H. Chung, R. D. McMichael, D. T. Pierce, and J. Unguris, “Phase diagram of magnetic nanodisks measured by scanning electron microscopy with polarization analysis,” *Phys. Rev. B*, vol. 81, no. 2, p. 24410, Jan. 2010.

[164] D. Mitin, D. Nissen, P. Schädlich, S. S. P. K. Arekapudi, and M. Albrecht, “Single vortex core recording in a magnetic vortex lattice,” *J. Appl. Phys.*, vol. 115, no. 6, p. 63906, Feb. 2014.

[165] D. Mitin, M. Grobis, and M. Albrecht, “Scanning magnetoresistive microscopy: An advanced characterization tool for magnetic nanosystems,” *Rev. Sci. Instrum.*, vol. 87, no. 2, p. 23703, Feb. 2016.

[166] A. Moser, D. Weller, M. E. Best, and M. F. Doerner, “Dynamic coercivity measurements in thin film recording media using a contact write/read tester,” *J. Appl. Phys.*, vol. 85, no. 8, p. 5018, 1999.

[167] D. Nissen, S. Thomas, S. S. Arekapudi, and M. Albrecht, “Magnetic vortices in magnetic nano-caps formed on densely packed particle array,” in *2015 IEEE Magnetics Conference (INTERMAG)*, 2015, vol. 2, pp. 1–1.

[168] A. Haldar and A. O. Adeyeye, “Vortex chirality control in circular disks using dipole-coupled nanomagnets,” *Appl. Phys. Lett.*, vol. 106, no. 3, p. 32404, Jan. 2015.

[169] J. Tóbik, V. Cambel, and G. Karapetrov, “Dynamics of vortex nucleation in nanomagnets with broken symmetry,” *Phys. Rev. B*, vol. 86, no. 13, p. 134433, Oct. 2012.

[170] N. Kikuchi, S. Okamoto, O. Kitakami, Y. Shimada, S. G. Kim, Y. Otani, and K. Fukamichi, “Vertical bistable switching of spin vortex in a circular magnetic dot,” *J. Appl. Phys.*, vol. 90, no. 12, p. 6548, 2001.

[171] T. Okuno, K. Shigeto, T. Ono, K. Mibu, and T. Shinjo, “MFM study of magnetic vortex cores in circular permalloy dots: behavior in external field,” *J. Magn. Magn. Mater.*, vol. 240, no. 1–3, pp. 1–6, Feb. 2002.

[172] A. Vogel, A. Drews, M. Weigand, and G. Meier, “Direct imaging of phase relation in a

pair of coupled vortex oscillators," *AIP Adv.*, vol. 2, no. 4, p. 42180, 2012.

[173] A. Vogel, T. Kamionka, M. Martens, A. Drews, K. W. Chou, T. Tyliszczak, H. Stoll, B. Van Waeyenberge, and G. Meier, "Coupled vortex oscillations in spatially separated permalloy squares," *Phys. Rev. Lett.*, vol. 106, no. 13, pp. 1–4, 2011.

[174] J. Mejía-López, D. Altbir, A. H. Romero, X. Batlle, I. V. Roshchin, C.-P. Li, and I. K. Schuller, "Vortex state and effect of anisotropy in sub-100-nm magnetic nanodots," *J. Appl. Phys.*, vol. 100, no. 10, p. 104319, 2006.

[175] G. Mihajlović, M. S. Patrick, J. E. Pearson, V. Novosad, S. D. Bader, M. Field, G. J. Sullivan, and A. Hoffmann, "Temperature dependent nucleation and annihilation of individual magnetic vortices," *Appl. Phys. Lett.*, vol. 96, no. 11, p. 112501, 2010.

[176] V. Novosad, K. Y. Guslienko, H. Shima, Y. Otani, K. Fukamichi, N. Kikuchi, O. Kitakami, and Y. Shimada, "Nucleation and annihilation of magnetic vortices in sub-micron permalloy dots," *IEEE Trans. Magn.*, vol. 37, no. 4, pp. 2088–2090, Jul. 2001.

[177] K. Y. Guslienko, V. Novosad, Y. Otani, H. Shima, and K. Fukamichi, "Magnetization reversal due to vortex nucleation, displacement, and annihilation in submicron ferromagnetic dot arrays," *Phys. Rev. B*, vol. 65, no. 2, p. 24414, Dec. 2001.

[178] M. V. Sapozhnikov, O. L. Ermolaeva, B. G. Gribkov, I. M. Nefedov, I. R. Karetnikova, S. A. Gusev, V. V. Rogov, B. B. Troitskii, and L. V. Khokhlova, "Frustrated magnetic vortices in hexagonal lattice of magnetic nanocaps," *Phys. Rev. B*, vol. 85, no. 5, p. 54402, Feb. 2012.

[179] P. Vavassori, R. Bovolenta, V. Metlushko, and B. Ilic, "Vortex rotation control in Permalloy disks with small circular voids," *J. Appl. Phys.*, vol. 99, no. 5, p. 53902, 2006.

[180] V. Cambel, J. Tóbik, J. Šoltýs, J. Fedor, M. Precner, Š. Gaži, and G. Karapetrov, "The influence of shape anisotropy on vortex nucleation in Pacman-like nanomagnets," *J. Magn. Magn. Mater.*, vol. 336, pp. 29–36, Jun. 2013.

[181] J. Sort, K. S. Buchanan, J. E. Pearson, A. Hoffmann, E. Menéndez, G. Salazar-Alvarez, M. D. Baró, M. Miron, B. Rodmacq, B. Dieny, and J. Nogués, "Tailoring the magnetization reversal of elliptical dots using exchange bias," *J. Appl. Phys.*, vol. 103, no. 7, p. 07C109, 2008.

[182] Z. P. Li, O. Petracic, J. Eisenmenger, and I. K. Schuller, "Reversal behavior of exchange-biased submicron dots," *Appl. Phys. Lett.*, vol. 86, no. 7, pp. 1–3, 2005.

[183] K. M. Lebecki and U. Nowak, "Properties of magnetic vortices at elevated temperatures," *J. Appl. Phys.*, vol. 113, no. 2, p. 23906, 2013.

[184] E. Östman, U. B. Arnalds, E. Melander, V. Kapaklis, G. K. Pálsson, A. Y. Saw, M. A. Verschuuren, F. Kronast, E. T. Papaioannou, C. S. Fadley, and B. Hjörvarsson, "Hysteresis-free switching between vortex and collinear magnetic states," *New J. Phys.*, vol. 16, no. 5, p. 53002, May 2014.

[185] M. S. Lund, W. A. A. Macedo, K. Liu, J. Nogués, I. K. Schuller, and C. Leighton, "Effect of anisotropy on the critical antiferromagnet thickness in exchange-biased bilayers," *Phys. Rev. B*, vol. 66, no. 5, p. 54422, Aug. 2002.

[186] S. C. Hernandez, J. Dou, C. Yu, M. J. Pechan, L. Folks, J. A. Katine, and M. J. Carey, "Exchange-coupled suppression of vortex formation in permalloy nanodot chain arrays," *J. Appl. Phys.*, vol. 105, no. 7, p. 07C125, 2009.

[187] L. E. Fernandez-Outon, G. Vallejo-Fernandez, S. Manzoor, and K. O'Grady, "Thermal instabilities in exchange biased materials," *J. Magn. Magn. Mater.*, vol. 303, no. 2, pp. 296–301, Aug. 2006.

[188] A. G. Biternas, U. Nowak, and R. W. Chantrell, "Training effect of exchange-bias bilayers within the domain state model," *Phys. Rev. B*, vol. 80, no. 13, p. 134419, Oct. 2009.

[189] S. R. Ali, M. R. Ghadimi, M. Fecioru-Morariu, B. Beschoten, and G. Güntherodt, "Training effect of the exchange bias in Co/CoO bilayers originates from the irreversible thermoremanent magnetization of the magnetically diluted antiferromagnet," *Phys. Rev. B*, vol. 85, no. 1, p. 12404, Jan. 2012.

[190] T. Ambrose and C. L. Chien, "Finite-Size Effects and Uncompensated Magnetization in Thin Antiferromagnetic CoO Layers," *Phys. Rev. Lett.*, vol. 76, no. 10, pp. 1743–1746, Mar. 1996.

[191] P. J. van der Zaag, a. R. Ball, L. F. Feiner, R. M. Wolf, and P. a. a. van der Heijden, "Exchange biasing in MBE grown Fe3O4/CoO bilayers: The antiferromagnetic layer thickness dependence," *J. Appl. Phys.*, vol. 79, no. 8, p. 5103, 1996.

[192] T. Ambrose and C. L. Chien, "Dependence of exchange coupling on antiferromagnetic layer thickness in NiFe/CoO bilayers," *J. Appl. Phys.*, vol. 83, no. 11, p. 6822, 1998.

[193] G. Vallejo-Fernandez, L. E. Fernandez-Outon, and K. O'Grady, "Antiferromagnetic grain volume effects in metallic polycrystalline exchange bias systems," *J. Phys. D. Appl. Phys.*, vol. 41, no. 11, p. 112001, Jun. 2008.

[194] A. G. Biternas, R. W. Chantrell, and U. Nowak, "Dependence of training effect on the antiferromagnetic structure of exchange-bias bilayers within the domain-state model," *Phys. Rev. B*, vol. 89, no. 18, p. 184405, May 2014.

[195] A. Bollero, V. Baltz, B. Rodmacq, B. Dieny, S. Landis, and J. Sort, "Out-of-plane exchange bias in [Pt/Co]–IrMn bilayers sputtered on prepatterned nanostructures," *Appl. Phys. Lett.*, vol. 89, no. 15, p. 152502, 2006.

[196] I. L. Guhr, O. Hellwig, C. Brombacher, and M. Albrecht, "Observation of perpendicular exchange bias in [Pd/Co]-CoO nanostructures: Dependence on size, cooling field, and training," *Phys. Rev. B*, vol. 76, no. 6, p. 64434, Aug. 2007.

[197] X. Y. Lang, W. T. Zheng, and Q. Jiang, "Dependence of the blocking temperature in exchange biased ferromagnetic/antiferromagnetic bilayers on the thickness of the antiferromagnetic layer," *Nanotechnology*, vol. 18, no. 15, p. 155701, Apr. 2007.

[198] M. Ali, C. Marrows, M. Al-Jawad, B. Hickey, A. Misra, U. Nowak, and K. Usadel, "Antiferromagnetic layer thickness dependence of the IrMn/Co exchange-bias system," *Phys. Rev. B*, vol. 68, no. 21, pp. 1–7, 2003.

[199] G. Vallejo-Fernandez, N. P. Aley, L. E. Fernandez-Outon, and K. O'Grady, "Control of the setting process in CoFe/IrMn exchange bias systems," *J. Appl. Phys.*, vol. 104, no. 3, p.

33906, 2008.

[200] A. O. Adeyeye and N. Singh, "Large area patterned magnetic nanostructures," *J. Phys. D. Appl. Phys.*, vol. 41, no. 15, p. 153001, Aug. 2008.

[201] F. Radu, M. Etzkorn, R. Siebrecht, T. Schmitte, K. Westerholt, and H. Zabel, "Interfacial domain formation during magnetization reversal in exchange-biased CoO/Co bilayers," *Phys. Rev. B*, vol. 67, no. 13, p. 134409, Apr. 2003.

[202] N. P. Aley and K. O'Grady, "Compositional dependence of antiferromagnetic anisotropy in IrMn/CoFe exchange bias systems," *J. Appl. Phys.*, vol. 109, no. 7, p. 07D719, 2011.

[203] M. D. Stiles and R. D. McMichael, "Temperature dependence of exchange bias in polycrystalline ferromagnet-antiferromagnet bilayers," *Phys. Rev. B*, vol. 60, no. 18, pp. 12950–12956, Nov. 1999.

[204] J. Hu, G. Jin, A. Hu, and Y. Ma, "Temperature dependence of exchange bias and coercivity in ferromagnetic/antiferromagnetic bilayers," *Eur. Phys. J. B*, vol. 40, no. 3, pp. 265–271, Sep. 2004.

[205] F. Radu and H. Zabel, "Exchange Bias Effect of Ferro-/Antiferromagnetic Heterostructures," in *Magnetic Heterostructures*, Berlin, Heidelberg: Springer Berlin Heidelberg, pp. 97–184.

[206] K. O'Grady, L. E. Fernandez-Outon, and G. Vallejo-Fernandez, "A new paradigm for exchange bias in polycrystalline thin films," *J. Magn. Magn. Mater.*, vol. 322, no. 8, pp. 883–899, Apr. 2010.

[207] W. Pan, N. Y. Jih, C. C. Kuo, and M. T. Lin, "Coercivity enhancement near blocking temperature in exchange biased Fe/FexMn1-x films on Cu(001)," *J. Appl. Phys.*, vol. 95, no. 11 II, pp. 7297–7299, 2004.

[208] J. Geshev, L. G. Pereira, and J. E. Schmidt, "Rotatable anisotropy and coercivity in exchange-bias bilayers," *Phys. Rev. B*, vol. 66, no. 13, p. 134432, Oct. 2002.

[209] M. Pajda, J. Kudrnovský, I. Turek, V. Drchal, and P. Bruno, "Ab initio calculations of exchange interactions, spin-wave stiffness constants, and Curie temperatures of Fe, Co, and Ni," *Phys. Rev. B*, vol. 64, no. 17, p. 174402, Oct. 2001.

[210] C. Leighton, M. R. Fitzsimmons, A. Hoffmann, J. Dura, C. F. Majkrzak, M. S. Lund, and I. K. Schuller, "Thickness-dependent coercive mechanisms in exchange-biased bilayers," *Phys. Rev. B*, vol. 65, no. 6, p. 64403, Jan. 2002.

[211] C. Hou, H. Fujiwara, K. Zhang, A. Tanaka, and Y. Shimizu, "Temperature dependence of the exchange-bias field of ferromagnetic layers coupled with antiferromagnetic layers," *Phys. Rev. B*, vol. 63, no. 2, p. 24411, Dec. 2000.

[212] F. Basheer Abdulahad, D.-S. Hung, and S.-F. Lee, "Temperature dependence of static and dynamic magnetic properties in NiFe/IrMn bilayer system," *J. Mater. Res.*, vol. 29, no. 11, pp. 1237–1247, Jun. 2014.

[213] C. Leighton, H. Suhl, M. J. Pechan, R. Compton, J. Nogués, and I. K. Schuller, "Coercivity enhancement above the Néel temperature of an antiferromagnet/ferromagnet

bilayer," *J. Appl. Phys.*, vol. 92, no. 3, p. 1483, 2002.

[214] G. Scholten, K. D. Usadel, and U. Nowak, "Coercivity and exchange bias of ferromagnetic/antiferromagnetic multilayers," *Phys. Rev. B*, vol. 71, no. 6, p. 64413, Feb. 2005.

8 PUBLICATIONS

8.1 Papers

H. Huckfeld, A. Gaul, N. Müglich, D. Holzinger, **D. Nissen**, M. Albrecht, D. Emmrich, A.Beyer, A.Gölzhäuser, and A. Ehresmann, *Structural changes in ion bombarded exchange bias systems and their effect on magnetic properties* (submitted to Phys. Rev. B).

G. Steinbach, M. Schreiber, **D. Nissen**, M. Albrecht, S. Gemming, and A. Erbe, *Stirrers and movers actuated by oscillating fields,* (submitted to Nature Communications).

D. Nissen, O. Klein, P. Matthes, and M. Albrecht, *Exchange-biased Py/CoO vortex structures: Magnetization reversal, cooling field dependence, and training*, Phys. Rev. B (accepted).

B. Hebler, S. Böttger, **D. Nissen**, R. Abrudan, F. Radu, and M. Albrecht*, Influence of the Fe-Co ratio on the exchange coupling in TbFeCo/[Co/Pt] heterostructures,* Phys. Rev. B 93, 184423 (2016).

G. Steinbach, **D. Nissen,** M. Albrecht, E. V. Novak, P. a. Sánchez, S. S. Kantorovich, S. Gemming, and A. Erbe*, Bistable self-assembly in homogeneous colloidal systems for flexible modular architectures*, Soft Matter 12, 2737 (2016).

D. Nissen, D. Mitin, O. Klein, S. S. P. K. Arekapudi, S. Thomas, M.-Y. Im, P. Fischer and M. Albrecht, *Magnetic coupling of vortices in a two-dimensional lattice,* Nanotechnology 26, 465706 (2015).

M. Stärk, F. Schlickeiser, P. Graus, **D. Nissen**, B. Hebler, D. Hinzke, E. Scheer, M. Albrecht, P. Leiderer, U. Nowak, M. Fonin and J. Boneberg, *Controlling the Magnetic Structure of Co/Pd Thin Films by Direct Laser Interference Patterning*, Nanotechnology 26, 205302 (2015).

I. Herrera, Y. Wang, P. Michaux, P. Surendran, S. Juodkazis, S. Whitlock, R. J. McLean, A. Sidorov, **D. Nissen**, M. Albrecht and P. Hannaford, *Sub-micron period lattice structures of magnetic microtraps for ultracold atoms on an atom chip,* J. Phys. D: Appl. Phys. 48, 115002 (2015).

H. Oezelt, A. Kovacs, P. Wohlhueter, E. Kirk, **D. Nissen**, P. Matthes, L.J. Heyderman, M. Albrecht and T. Schrefl, *Micromagnetic simulation of exchange coupled ferri-/ferromagnetic composite in bit patterned media*, J. Appl. Phys. 117, 17E501 (2015).

S. Thomas, **D. Nissen**, and M. Albrecht, *Temperature dependent magnetization reversal of exchange biased magnetic vortices in IrMn/Fe microcaps*, Appl. Phys. Lett. 105, 022405 (2014).

D. Mitin, **D. Nissen**, P. Schädlich, S. S. P. K. Arekapudi, and M. Albrecht, *Single vortex core recording in a magnetic vortex lattice*, J. Appl. Phys. 115, 063906 (2014).

8.2 Presentations

D. Nissen, O. Klein, P. Matthes, and M. Albrecht, *Exchange-Biased Py/CoO Vortex Structures*, MML 2016, Uppsala Sweden.

D. Nissen, D. Mitin, O. Klein, S. S. P. K. Arekapudi, R. Rückriem, S. Thomas, and M. Albrecht, *Magnetic Vortices in Closely Packed Caps Structures,* AIM 2016, Bormio Italy.

D. Nissen, S.Thomas, S.S.Arekpudi, and M.Albrecht, *Magnetic Vortices in Magnetic Nano-Caps formed on Densely Packed Particle Arrays*, IEEE INTERMAG 2015, Beijing China. (10.1109/INTMAG.2015.7157338)

D. Nissen, P. Matthes, D. Mitin, S.S.P.K. Arekapudi, E. Kirk, A. Weber, L. Heyderman, and M. Albrecht, *Exchange Coupled Composite (ECC) GdFe/FePt Heterostructures,* STAR 2015, Kerala India.

D. Nissen, S. Thomas, S.S.Arekpudi, and M.Albrecht, *Investigation of Magnetic Vortices in Cap Structures*, DPG Spring Meeting 2015, Berlin Germany.

D. Nissen, M.-Y. Im, P. Fischer, and M. Albrecht, *Magnetic Vortices in Cap Structures in Confined Geometry*, Zakopane School of Physics 2013, Zakopane Poland.

D. Nissen, M.-Y. Im, P. Fischer, and M. Albrecht, *Magnetic Vortices in Permalloy Cap Structures in Confined Geometry,* DPG Spring Meeting 2013, Regensburg Germany.

ACKNOWLEDGMENT

All the work would not have been possible without the great help of many people. During all the time it was a very pleasant working atmosphere. However, beyond the work, there have been a lot of social activities in the workgroup which made life a little bit easier during the preparation of this thesis. In particular, all the BBQs, the several football games which have been watched, and the various other occasions that have been celebrated.

A special acknowledgment goes to:

- First, I would like to thank my supervisor Prof. Dr. M. Albrecht for giving me the opportunity to work in his group, showing new approaches, and overall supporting me during the thesis.
- Christian Schubert for fruitful discussions, the funny office atmosphere in Chemnitz, and help during a very special beam time at the ALS.
- Patrick Matthes for performing XRR measurements, the funny office atmosphere in Chemnitz, and help during a very special beam time at the ALS.
- Senoy Thomas for many fruitful discussions which helped me a lot, the nice office atmosphere in Chemnitz, and in particular thank you for your hospitality during my trip to India.
- Markus Daniel for performing RBS measurements, the funny office atmosphere in Chemnitz, there is only one real *Mobbingbeauftragter.*
- Dimitriy Mitin for performing SMRM measurements, and many fruitful discussions.
- Sri Sai Phani Kanth Arekapudi for in-field MFM investigations.
- Fabian Ganss and Marc Lindorf for help performing SEM investigations.
- Nataliia Safonova for help during a beam time at the ALS Berkeley.

- Birgit Hebler, Andreas Liebig and Gunter Beddies for many fruitful discussions, and nice conversations, also beyond work.
- Elke Weisse for support in the lab during my time in Chemnitz.
- Ute Vales for providing overall administrative support.
- Alexander Hassdenteufel for many fruitful discussions and the nice friendship which grew in the last years.
- Martin Stiehler for various discussions about physics.
- To all the people who helped me to have a smooth start in Chemnitz, in particular, Grit Rauscher and Katrin Krasselt.
- Philip Schädlich, Gregor Nordheim and Tom Götze for the contributions to this thesis with regard to their Bachelor theses.
- Peter Fischer, Mi-Young Im and Clemens Wuth for supporting me during beam times at the ALS.
- Florian Kronast for beam time support at the SPEEM end station at BESSY II.
- Olga Lik and Wolfgang Reiber for lab support in Augsburg.
- Birgit Knoblich and Oliver Klein for the TEM preparations and investigations.
- All the people who helped me to have a good start in Augsburg.
- Michael Mayr, André Sartori, Martin Fischer, Oana-Tereza Ciubotariu and Alfred Grießer for the friendly office atmosphere in Augsburg.
- My family and friends for their understanding and support during development and research with regard to this thesis in the last years.
- Finally, I thank Steffi. For everything.